Structure and Function of Cytochrome *c* Nitrite Reductase

Dissertation submitted to

Fakultät für Biologie, Universität Konstanz

for the degree of

Doctor of Natural Sciences

by

Dipl.-Biol. Oliver F. Einsle

Max-Planck-Institut für Biochemie

Abteilung Strukturforschung

D-82152 Martinsried

Konstanz, December 1999

Examiner: Prof. Dr. Peter M.H. Kroneck

Coexaminer: Prof. Dr. Robert Huber

Dissertation der Universität Konstanz
Datum der mündlichen Prüfung: 25. 2. 2000
Referenten: Prof. Dr. P. M. H. Kroneck
Prof. Dr. R. Huber

Dedicated to my father,

Dr. Ulrich K. Einsle † 24. 12. 1996

Table of Contents

1 Zusammenfassung

Als ein Schlüsslenzym im biologischen Stickstoffkreislauf katalysiert Cytochrom *c* Nitritreduktase die Sechs-Elektronen-Reduktion von Nitrit zu Ammoniak innerhalb des respiratorischen Stoffwechselwegs der dissimilatorischen Nitratreduktion zu Ammoniak (vgl. 3.2). Ziel der vorliegenden Arbeit war, das bereits durch biochemische und spektroskopische Studien gewonnene Bild des Proteins durch eine detaillierte Analyse von der Primär- bis hin zur Quartärstruktur zu erweitern.

Das für das dissimilatorische Nitritreduktasesystem codierende *nrf*-Operon wurde aus den der ε-Gruppe der Proteobakterien zugehörigen Arten *Sulfurospirillum deleyianum* und *Wolinella succinogenes* kloniert und sequenziert (5.3). Die beiden Operonsequenzen zeigen eine genetische Organisation, welche sich deutlich von bekannten Sequenzen aus Vertretern der γ-Gruppe der Proteobakterien und dem Bacteroiden *Porphyromonas gingivalis* unterscheidet. Dennoch ist das für das Enzym Nitritreduktase codierende *nrfA*-Gen in allen Organismen, für die bislang Sequenzen vorgliegen, hoch konserviert. Die gereinigten Nitritreduktasen aus *S. deleyianum* und *W. succinogenes* wurden im folgenden – als Grundlage zur Strukturaufklärung – kristallisiert.

Da Nitritreduktase fünf Hämgruppen pro Monomer besitzt war es möglich, die Kristallstruktur des Enzyms aus *S. deleyianum* durch *Multiwavelength Anomalous Dispersion* - Phasierung (MAD) zu lösen (5.4.3). Nitritreduktase ist ein dimeres, vorwiegend α-helikales Hämprotein mit einer Reihe struktureller Besonderheiten. Die zehn Hämgruppen des Dimers sind dicht gepackt (5.4.5.3), was direkte und effiziente Elektronenleitung zum Aktivzentrum ermöglicht. Ein Substrat-/Produktkanal durchzieht das gesamte

Protein und sorgt durch sein variierendes elektrostatisches Oberflächenpotential für einen gerichteten Substrat- und Produktfluß zum und vom Aktivzentrum (5.4.5.5). Dort findet sich eine fünffach koordinierte Hämgruppe vom *c*-Typ, als deren proximaler Ligand hier erstmals ein Lysinrest des Proteins beschrieben wird (5.4.5.4). In unmittelbarer Nähe zum Aktivzentrum findet sich ein Calciumion, dessen Rolle vermutlich in der Stabilisierung des Aktivzentrums und der Ausrichtung an der Katalyse beteiligter Reste liegt.

Die Struktur des Enzyms aus *S. deleyianum* wurde im Komplex mit dem Substrat Nitrit und mit dem Inhibitor Sulfat gelöst (5.4.5.6), und zeigte neben einer Reihe neuer Eigenschaften auch unerwartete Ähnlichkeiten zu anderen Multihäm-Cytochromen, insbesondere zu Hydroxylamin-Oxidoreduktase aus *Nitrosomonas europaea* (6.3.1). Ferner war die Struktur Voraussetzung für die kristallographische Analyse des homologen Enzyms aus *W. succinogenes* durch Patterson-Suchmethoden (*Molecular Replacement*). Obwohl das Protein selbst erwartungsgemäß große Ähnlichkeit zu dem aus *S. deleyianum* aufweist, waren die erhaltenen Kristalle von besserer Qualität und lieferten höher aufgelöste Beugungsdaten (5.4.4). Substratkomplexe dieses Enzyms mit Nitrit und Hydroxylamin halfen, entscheidende Schritte im Reaktionsverlauf zu beleuchten und zeigten die an der Substratbindung beteiligten Reste des Proteins auf (5.4.5.7).

Ein Vergleich zwischen Nitritreduktase und dem Elektronentransporter Cytochrom c_3 aus *Desulfovibrio desulfuricans* Essex 6 unterstreicht die unterschiedlichen strukturellen Anforderungen, die an ein Enzym wie Nitritreduktase zu stellen sind (5.5). Mit Ausnahme des photosynthetischen Reaktionszentrums zeigen zudem alle bisher strukturell charakterisierten Multihäm-Cytochrome wiederkehrende Motive in der Anordnung ihrer Hämgruppen. Zwei besondere Motive der Häm-Häm-Wechselwirkung, die in Nitritreduktase und in verschiedenen anderen Cytochromen auftauchen, wurden beschrieben als CC3-Modul und SSC-Motiv (6.3.5). Ihre strukturelle Charakterisierung kann als Grundlage dienen, um Mechanismen der Wechselwirkung zwischen Hämgruppen innerhalb von Proteinen zu verstehen.

2 Summary

Cytochrome *c* nitrite reductase is a key enzyme in the biological nitrogen cycle, as it catalyzes the six-electron reduction of nitrite to ammonia in the energy metabolism referred to as dissimilatory nitrate reduction to ammonia (see 3.2). The topic of the present work was to expand the picture of the enzyme gained through biochemical and spectroscopic examinations by a detailed analysis from primary to quaternary structure.

The *nrf*-operon encoding for the dissimilatory nitrite reductase system has been cloned and sequenced from the two ε-proteobacterial species *Sulfurospirillum deleyianum* and *Wolinella succinogenes* (5.3), revealing a completely different gene organization compared to known sequences from γ-proteobacteria and the bacteroid *Porphyromonas gingivalis*. However, the gene for nitrite reductase itself, *nrfA*, is highly conserved in all organisms sequenced so far. The purified proteins from both *Sulfurospirillum deleyianum* and *Wolinella succinogenes* were thus crystallized as a prerequisite to solve their structures.

With a total of five heme groups per monomer of nitrite reductase it was possible to solve the crystal structure of the *S. deleyianum* enzyme using multiwavelength anomalous dispersion information measured on the K-edge of iron (5.4.3). The structure of nitrite reductase shows a dimeric, mainly α-helical heme protein with several unusual features. Ten heme groups in the dimer are in close packing (5.4.5.3), allowing for direct and fast electron transfer to the active site (5.4.5.4), a five-coordinate *c*-type heme with a lysine residue as proximal ligand. This is a novel type of heme ligation that has not been observed in a protein structure before. Furthermore, a substrate and product channel was detected, which traverses the whole enzyme,

passing the active site and directing substrate influx and product efflux by its electrostatic surface potential (5.4.5.5). Close to the active site, a calcium ion was found in the structure, whose presumed role is to stabilize the active site cavity and orientate residues involved in catalysis.

The crystal structure of the enzyme from *Sulfurospirillum deleyianum* was solved with bound susbtrate nitrite and with an inhibitor, sulfate, revealing novel features as well as unexpected similarities with other multiheme cytochromes, in particular with hydroxylamine oxidoreductase from *Nitrosomonas europaea* (6.3.1). It futhermore provided the basis for solving the structure of *W. succinogenes* nitrite reductase by molecular replacement (5.4.4). Although the protein itself was as expected very similar, the crystals were of better quality diffracting X-rays to higher resolutions. Substrate complexes of this enzyme with nitrite and hydroxylamine helped to illuminate essential steps in the course of the reaction and showed which residues are involved in substrate binding (5.4.5.7).

A comparison with the structure of a more classical electron transfer protein, cytochrome c_3 from *Desulfovibrio desulfuricans* Essex 6, emphasizes the different requirements imposed on an enzyme like nitrite reductase (5.5). With the exception of the photosynthetic reaction centre, all multiheme *c*-type cytochromes that have been structurally characterized to date show certain similar motives. Two special motives of interaction between two heme groups were found in nitrite reductase and in several other structures and were described as the CC3 module and the SSC motif (6.3.5). They might provide a structural basis for understanding general modes of heme-heme interaction in electron-transporting proteins and enzymes.

3 Introduction

3.1 The Biogeochemical Nitrogen Cycle

Nitrogen is an essential constituent part of most biomolecules and cofactors. It is transformed in several metabolic pathways between the oxidation states of nitrogen in nitrate (+V) and in ammonia (–III). In this cycle of pathways, all transformations are catalyzed by metalloenzymes containing copper, molybdenum or iron, the latter predominantly either in the form of iron-sulfur clusters or as iron porphyrins (Berks *et al.*, 1995a; Kroneck *et al.*, 1992).

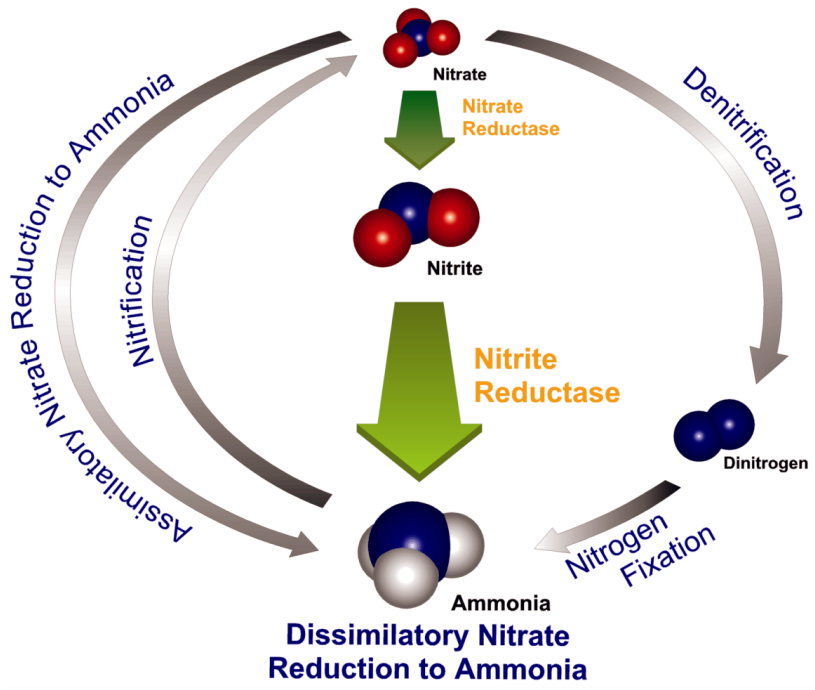

Figure 1: The biogeochemical nitrogen cycle with metabolic pathways connecting the key intermediates nitrate, dinitrogen and ammonia.

Despite of earth's oxidizing atmosphere and contrary to thermodynamical expectations, nitrate is not the globally most abundant modification of nitrogen. With a bond energy of 946 kJ·mol^{-1} at 298 K, the kinetically stable dinitrogen molecule makes up for 70 % of the atmospheric gas. This immense reservoir is only accessible for biosyntheses through the reaction of the procaryotic enzyme nitrogenase, which converts dinitrogen to ammonia in the energetically expensive process of *Nitrogen Fixation*. Ammonia can then be assimilated in anabolic pathways by procaryotes as well as by eucaryotes.

In the chemoautotrophic pathway of *Nitrification*, ammonia is oxidized to nitrate in three steps. Usually the first two are carried out by *Nitrosobacteria*, which form hydroxylamine from ammonia in the two-electron oxidation reaction of ammonia monooxygenase (AMO) and nitrite from hydroxylamine in the four-electron step carried out by hydroxylamine oxidoreductase (HAO). Nitrite is then excreted and taken up by *Nitrobacteria* which possess a nitrite oxidase to convert nitrite to nitrate.

The nitrogen cycle is closed by the reduction of nitrate to dinitrogen in *Denitrification*, a dissimilatory four-step process that proceeds from nitrate via nitrite, nitric oxide and nitrous oxide to dinitrogen. Bacteria utilize positive redox potentials like the ones of nitrate ($E^{o'}(NO_3^-/NO_2^-)$ = + 0.43 V) or nitrite ($E^{o'}(NO_2^-/NO)$ = + 0.35 V) or $E^{o'}(NO_2^-/NH_4^+)$ = + 0.34 V) for energy conservation by chemiosmotic coupling of ATP synthesis and electron transport (Thauer *et al.*, 1977; Zumft, 1997).

3.2 Dissimilatory Nitrate Reduction

In many textbooks and publications, denitrification is still listed as the only dissimilatory pathway of nitrate reduction. However, with the dissimilatory nitrate reduction to ammonia (DNRA) there is a completely independent anaerobic metabolism for nitrate reduction. Moreover, it has even been

shown to quantitatively surpass denitrification in certain habitats, given the appropriate environmental conditions (Jørgensen, 1989; Nishio *et al.*, 1982).

While the terminal oxidases of denitrification obtain electrons through the membraneous quinone pool from NADH or succinate dehydrogenase (Ballard & Ferguson, 1988; Craske & Ferguson, 1986; Ketchum *et al.*, 1991), the predominant electron donors for nitrate-ammonifying bacteria are hydrogen and formate (Abou-Jaoudé *et al.*, 1979a; Abou-Jaoudé *et al.*, 1979b; Enoch & Lester, 1974).

Dissimilatory nitrate reduction to ammonia is a two-step process, with nitrite as the only liberated intermediate. A nitrate reductase carries out the two-electron reduction of nitrate to nitrite, which is then taken up by a nitrite reductase that performs the remaining six-electron step to ammonia.

It should be noted that nitrate is also a potential nitrogen source for assimilatory processes, as it can be reduced to ammonia in the two steps mentioned above and then incorporated into biomolecules. However it has been shown, that the enzyme systems for the assimilatory and dissimilatory nitrate reduction to ammonia are strictly separate (Sias & Ingraham, 1979). The assimilatory enzymes are expressed constitutively at low levels during aerobic as well as during anaerobic growth and their transcription is negatively regulated by ammonium ions (van't Riet *et al.*, 1968; Wimpenny & Cole, 1967).

3.2.1 Physiology

Both denitrification and DNRA commence with a two-electron reduction of nitrate to nitrite. All nitrate reductases characterized so far are molybdo-iron-sulfur proteins, although the presence of a molybdenum-free system has been proposed most recently for *Geobacter metallireducens* (Murillo *et al.*, 1999). They can be located in the cytoplasmic membrane or they can be soluble periplasmic proteins. In both cases, the reduction of nitrate is cou-

pled to the generation of a proton motive force over the cytoplasmic membrane.

At the stage of nitrite the two metabolic pathways split up. Denitrificatory nitrite reductases are either cytochromes cd_1 (Gudat *et al.*, 1973) or trimeric copper proteins (Godden *et al.*, 1991), catalyzing a one-electron reduction of nitrite to nitric oxide. The nitrite reductase of the DNRA pathway reduces nitrite in a six-electron step to ammonia and is the subject of the present work.

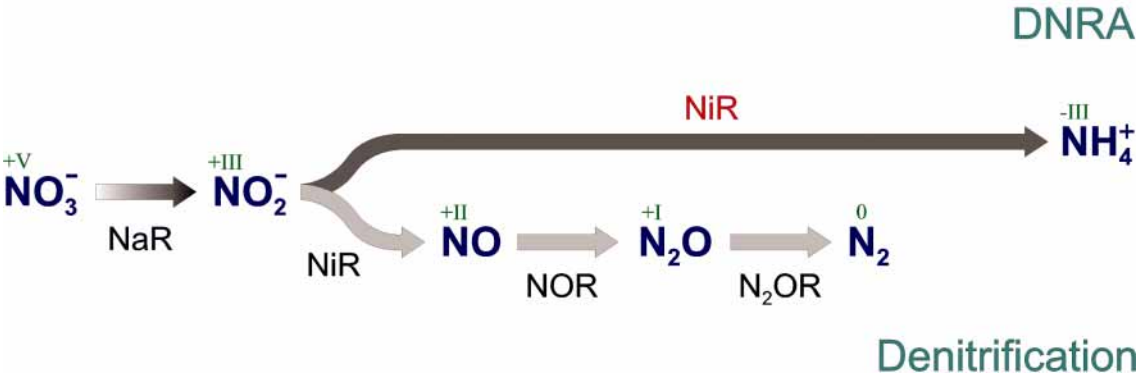

Figure 2: The pathways of dissimilatory nitrite reduction. After the initial two-electron reduction of nitrate to nitrite by nitrate reductase (NaR), the DNRA pathway leads to ammonia in the single six-electron step of nitrite reductase (NiR), while denitrification consists of three subsequent one-electron reductions, catalyzed by nitrite reductases (NiR), a membraneous nitric oxide reductase (NOR) and the periplasmic nitrous oxide reductase (N_2OR).

Several enterobacterial nitrate ammonifiers have been found to possess two independent enzymatic systems for the reduction of nitrite. A cytoplasmatic siroheme nitrite reductase has been described for *Escherichia coli* (Jackson *et al.*, 1981; Zarowny & Sanwal, 1963), which receives electrons from NADH (Coleman *et al.*, 1978) and is homologous to the siroheme sulfite reductase in the same organism (Siegel *et al.*, 1982) as well as to plant type nitrite reductases, where ferredoxin is the physiological electron donor (Lancaster *et al.*, 1979). This enzymatic function is not coupled to energy conservation and its main functions are the regeneration of oxidized pyrimidine nucleotides during anaerobic growth (Cole & Brown, 1980) and the provision of ammonia for assimilatory purposes (see 3.3.3).

The second enzyme, cytochrome *c* nitrite reductase, has first been detected in *E. coli* in the sixties (Cole, 1968; Fujita, 1966). The reduced enzyme could quickly be reoxidized by nitrite and led to the formation of ammonia, but its physiological function remained unclear, until a respiratory formate:nitrite oxidoreductase complex using quinone as an electron carrier was described for *E. coli* (Abou-Jaoudé *et al.*, 1979a; Abou-Jaoudé *et al.*, 1979b) and shortly thereafter for *Desulfovibrio desulfuricans* (Steenkamp & Peck, 1980; Steenkamp & Peck, 1981). The coupling of proton translocation to the reduction of nitrite to ammonia has been shown for *D. desulfuricans* (Steenkamp & Peck, 1981), *Campylobacter sputorum* biovar *bubulus* (de Vries *et al.*, 1982), *E. coli* (Pope & Cole, 1982) and – most recently – *Wolinella succinogenes* (Simon *et al.*, 2000). A direct connection of the reaction to oxidative phosphorylation has been shown for *Desulfovibrio gigas* (Barton *et al.*, 1983) and *Wolinella succinogenes* (Bokranz *et al.*, 1983), establishing cytochrome *c* nitrite reductase as the terminal oxidoreductase in an anaerobic electron transport chain.

In the sulfur-reducing proteobacterium *Sulfurospirillum deleyianum* (formerly "Spirillum" 5175; Schumacher *et al.*, 1992), nitrate ammonification is the main energy source in static anaerobic culture with formate as an electron donor and acetate as a carbon source (Schumacher & Kroneck, 1992). During the reduction of nitrate, nitrite was accumulated quantitatively in the medium. Nitrite reduction to ammonia was only observed after all available nitrate was consumed. This correlates with the finding, that the growth yield of *S. deleyianum* (and thus the rate of ATP synthesis) during growth on nitrate is 20 % higher than the growth rate during growth on nitrite. The same difference was observed for nitrate ammonification in *D. desulfuricans* (Seitz & Cypionka, 1986) and *C. sputorum* biovar *bubulus* (de Vries *et al.*, 1980; de Vries *et al.*, 1982) and seems to be a characteristic feature of this pathway. The attenuation of nitrite reductase activity in the presence of nitrate is an active process that will be discussed in this work.

3.2.2 Occurence

A wide variety of bacterial species have been classified as nitrate ammonifiers (Tiedje, 1988), most of which have a fermentative rather than a respiratory metabolism (Cole, 1988). The presence of a respiratory cytochrome *c* nitrite reductase has so far been confirmed for *E. coli* (Fujita & Sato, 1966; Kaije & Anraku, 1986), *Vibrio fischeri* (Prakhash & Sadana, 1972; Rehr & Klemme, 1986), *D. desulfuricans* (Liu & Peck, 1981) and *D. gigas* (Barton *et al.*, 1983), *C. sputorum* biovar *bubulus* (de Vries *et al.*, 1982), *W. succinogenes* (Blackmore *et al.*, 1986; Liu *et al.*, 1983), *S. deleyianum* (Schumacher & Kroneck, 1991) and *G. metallireducens* (Murillo *et al.*, 1999).

Looking into the phylogenetic tree of eubacteria, all those species belong to the family proteobacteriaceae, but fall into the subdivisions γ (*Escherichia, Vibrio*), δ (*Desulfovibrio, Geobacter*) and ε (*Campylobacter, Wolinella, Sulfurospirillum*). An analysis of available amino acid sequences of cytochrome *c* nitrite reductases seems overdue to better understand the diversity of this pathway.

A comparative estimation of denitrification and nitrate ammonification indicated, that denitrifiers are dominant in reducing and anoxic locations that are rich in nitrate but poor in oxidizable carbon compounds, while nitrate ammonifiers dominate locations that are poor in nitrate and nitrite and rich in carbon sources (Jørgensen, 1989; Tiedje, 1988). A problem in these estimations is the inability to discriminate between respiratory and non-respiratory (NADH-dependent) nitrate ammonification. In sweetwater samples, denitrification has always been found to be dominant (Binnerup *et al.*, 1992), but after $^{15}NO_3^-$ enrichment of sediment layers containing large populations of sulfate reducers and fermenting bacteria, the level of nitrate ammonification was found to be higher than the one of denitrification (Jørgensen, 1989).

3.2.3 Regulation

Dissimilatory nitrate ammonification as an anaerobic metabolism is known to be regulated through the FNR protein (**F**umarate-**N**itrate-**R**egulator), an oxygen-senstive transcription enhancer (Cole, 1990; Page *et al*., 1990). A typical binding site for this protein was described in the putative promoter region of the nitrite reductase operon from *E. coli* (Darwin *et al*., 1993). Thus it seems likely that reports of significant rates of aerobic nitrate reduction to ammonia (Brons & Zehnder, 1990) have to be attributed to the assimilatory pathway. Furthermore, Page *et al.* (1990) could show an involvement of the NarL repressor in the regulation of nitrite reductase and the promoter sequence in the operon also holds a putative operator site for this protein (Darwin *et al.*, 1993).

Studies on growth of *W. succinogenes* with various electron donors indicated, that nitrate ammonification is also inhibited during growth on elemental sulfur as an electron donor (Lorenzen *et al*., 1993). In *S. deleyianum* however, a close relative of *W. succinogenes*, an equally high expression of cytochrome *c* nitrite reductase was observed during growth with elemental sulfur as with nitrate or nitrite as electron donors (Schumacher, 1993).

3.2.4 Dissimilatory Nitrate Reductase

The first reaction step in dissimilatory nitrate ammonification is the two-electron reduction of nitrate to nitrite, catalyzed by the group of enzymes referred to as nitrate reductases. While all nitrate reductases are molybdenum enzymes and can be assumed to share very similar mechanistics as far the reduction of nitrate to nitrite is concerned, they can be subdivided into two structural families (Hille, 1996a; Hille, 1996b). Both of these families form membrane-associated complexes with different ways of electron conduction and membrane insertion.

Assimilatory nitrate reductases (NAD(P)H:Nitrate oxidoreductase, E.C. 1.6.6.x) use NAD(P)H or ferredoxins as electron donors and possess two further subunits, the first containing flavin, the second *b*-type heme groups. The cytochrome subunit is inserted into the periplasmic membrane and obtains electrons from the quinone pool, which are then conducted to the molybdenum site via the flavin- and/or iron-sulfur centers of the second subunit (Blasco *et al.*, 1989). They are not involved in energy conservation and play their part in providing ammonia (via siroheme-containing nitrite reductases, see 3.3.3) for assimilation into biomolecules. Located in the cytoplasm, this class of nitrate reductases is dependent on a transmembraneous nitrate-transporting system, which was found to be inhibited by the presence of oxygen (Hernandez *et al.*, 1991; Hernandez & Rowe, 1988). The mere existence of aerobic denitrification thus already points towards a second system with periplasmic nitrate reductases that do not depend on a nitrate transporter (Siddiqui *et al.*, 1993).

Dissimilatory or respiratory nitrate reductases (Ferrocytochrome:Nitrate oxidoreductase, E.C. 1.7.99.4 and 1.9.6.1) need to be coupled to the generation of a proton potential in order to perform their task. They are periplasmic enzymes which interact with *c*-type instead of *b*-type cytochromes (Costa *et al.*, 1993; Richardson *et al.*, 1990; Siddiqui *et al.*, 1993). An analysis of the *napEDABC* operon of *Thiosphaera pantotropha* (Berks *et al.*, 1995b) examplified the organization of the system: NapA, periplasmic nitrate reductase, is a soluble protein that obtains electrons from NapB, a soluble diheme *c*-type cytochrome. The link to the membraneous quinone pool is provided by NapC, a hydrophobic tetraheme *c*-type cytochrome which is anchored into the membrane through a single N-terminal helix (Roldán *et al.*, 1998).

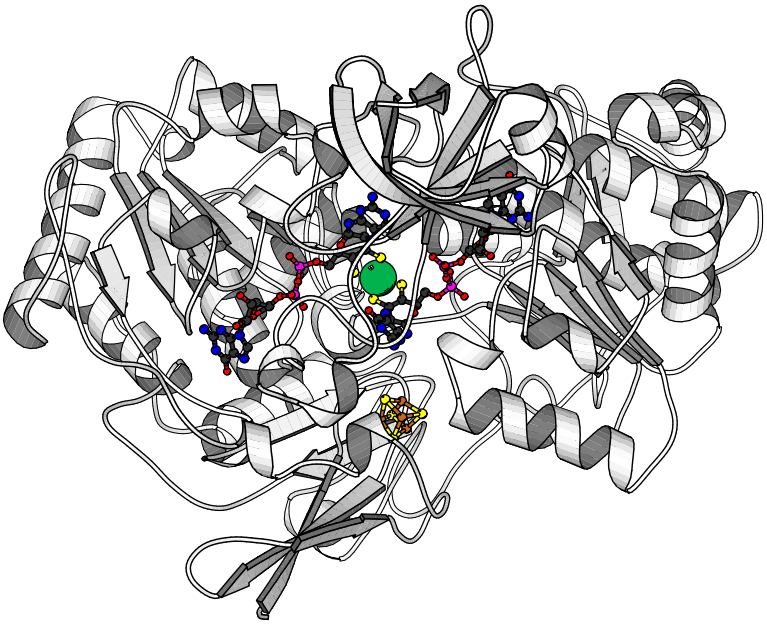

Figure 3: A ribbon plot of the structure of periplasmic nitrate reductase, NapA, from *D. desulfuricans* ATCC 27774 (Dias *et al.*, 1999). The molybdenum atom is shown in green, complexed by two molybdopterin guanidine dinucleotide cofactors (MGD). The molybdenum ion is the site of nitrate reduction, while the Fe_4S_4 cluster depicted below is needed for electron transfer.

The X-ray structure of a periplasmic nitrate reductase, NapA from *D. desulfuricans* ATCC 27774, has been solved most recently (Dias *et al.*, 1999). It shows a mononuclear molybdenum enzyme with high structural homology to formate dehydrogenase H (Boyington *et al.*, 1997). The molybdenum ion is coordinated by two molybdopterin-guanidine-dinucleotide cofactors. It is the active site of nitrate reduction and the crystal structure shows a further oxo-ligand at this centre. The catalyzed reaction consists of the abstraction of an oxygen atom, a typical reaction of molybdenum oxotransferases (Hille, 1996a). A Fe_4S_4 cluster is located close to the molybdenum to transfer electrons from NapB.

3.3 Nitrite Reductases

To this day, four substantially different classes of enzymes capable of the reduction of nitrite have been described, three of which have a respira-

tory function in the bacterial cell. The enzymes involved in the pathway of denitrification, cytochrome cd_1 and the copper-containing nitrite reductase, catalyze the one-electron reduction of nitrite to nitric oxide. Both crystal structures have been solved (Fülöp *et al.*, 1995; Godden *et al.*, 1991) and present two strikingly different solutions for the same task, as it will be discussed below.

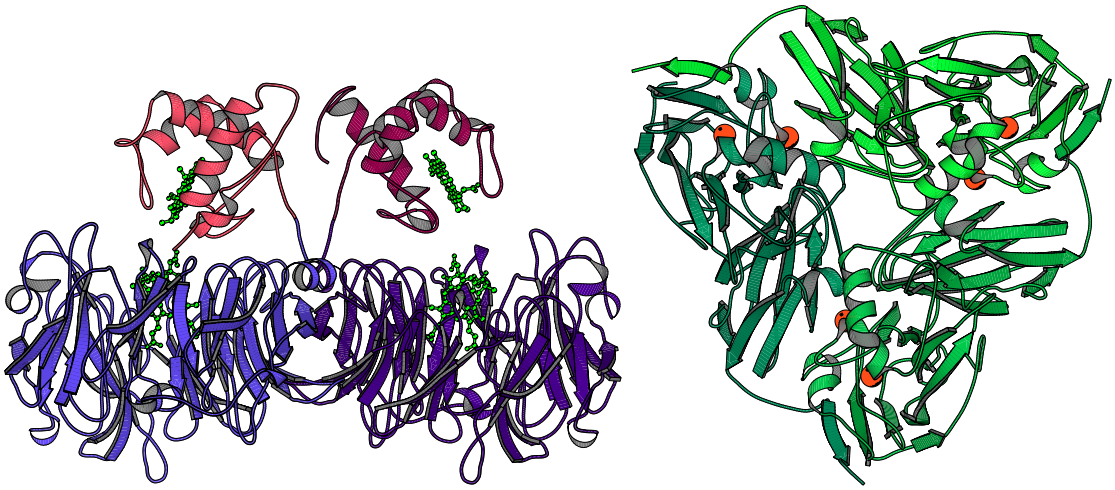

Figure 4: Crystal structures of the two nitrite reductases found in denitrifying bacteria. Cytochrome cd_1 (**left**) is a dimer consisiting of characteristic two-domain monomers (Fülöp *et al.*, 1995). An α-helical cytochrome *c* domain (red) is located above a β-propeller domain (blue) that holds the active site d_1 heme. The copper-containing nitrite reductase (**right**) is a trimer with two mononuclear copper centers per monomer (Godden *et al.*, 1991). The fold of the monomer shows similarities to type I copper proteins, with one copper atom, the electron transfer center, located on the end of a β-barrel. Both proteins catalyze the reduction of nitrite to nitric oxide, but cytochrome cd_1 also functions as a dioxygen reductase.

The third dissimilatory nitrite reductase is cytochrome *c* nitrite reductase, which is again completely unrelated to the enzymes of the denitrification pathway. However, it catalyzes the same reaction as the assimilatory type of nitrite reductases, which is in turn the only one that can also be found in eucaryotes. Although there is no structure of an assimilatory nitrite reductase available to date, amino acid sequence comparisons indicate that the enzyme is homologous to siroheme-containing sulfite reductase, which has been structurally characterized (Crane *et al.*, 1995) and which is even able to catalyze the reduction of nitrite to ammonia (Janick *et al.*, 1983).

Enzyme Class	Architecture	Mass [Da]	Cofactors	Type	Reaction
Cu-containing	trimer	36 000	$2 \times$ Cu	dissim.	$NO_2^- \longrightarrow NO$
cytochrome cd_1	dimer	65 000	1 heme *c*, 1 heme d_1	dissim.	$NO_2^- \longrightarrow NO$
siroheme / Fe_4S_4	monomer	56 000	1 siroheme, 1 Fe_4S_4 cluster	assim.	$NO_2^- \longrightarrow NH_4^+$
cytochrome *c*	dimer	58 000	5 hemes *c*, 1 Ca^{2+}	dissim.	$NO_2^- \longrightarrow NH_4^+$

Table 1: The four different classes of nitrite reductases, their architecture and cofactor composition. For each class, a representative molecular mass is given, not taking into account minor variations between different species. The architecture given is that of the reductase alone. Complex formation with possible electron donors is still a matter of discussion in all four cases.

Obviously all four systems have evolved independently from different families of metalloproteins. The siroheme cofactor of assimilatory nitrite reductase is generally considered as a very ancient member of the tetrapyrrole ligand family, reflecting that the ability to obtain ammonia from nitrate as well as the detoxification of nitrite has emerged early in the history of life.

Subsequently, cytochrome cd_1 might have been the first successful attempt of energy conservation through the reduction of nitrite. It shows a clear domain organization and utilizes the specialized heme d_1 cofactor. Furthermore, prior to the the oxygenation of the atmosphere due to photosynthetic oxygen evolution, copper was mainly bound as insoluble Cu_2S and thus not accessible for biomolecules. With the transition into an oxidizing environment, copper (Cu^{2+}) became available for organisms and iron in turn, now predominantly in the form of $Fe(OH)_3$, was harder to obtain (Williams, 1990). If found to perform similar tasks, copper proteins are thus generally considered more modern than iron proteins.

All this would place the evolution of cytochrome *c* nitrite reductase in a time before that of both reductases from the denitrificatory pathway. In this system however, it seems more promising to investigate the relationships of the enzyme with other multiheme cytochromes and trace their spread and diversity through different species and families of bacteria.

3.3.1 Copper-containing Nitrite Reductase

In 1991, the Cu-dependent nitrite reductase (E.C. 1.7.99.3) from *Achromobacter cycloclastes* was the first to be structurally characterized (Godden *et al.*, 1991). The homotrimer depicted in Figure 4 holds two copper atoms per subunit. One of these centers is a type I copper center with the copper atom ligated by two histidines, a cysteine and a methionine from the same subunit. This part of the protein is a domain with significant homologies to electron transport cupredoxins like azurin or plastocyanin and is presumed to be the entry point for electrons delivered by soluble periplasmic cupredoxins or cytochrome c_6. The second Cu center is of type II, with a square planar ligation geometry, mediated by three histidines from two different subunits and a water molecule that is replaced by nitrite to carry out the enzymatic reaction (Libby & Averill, 1992). When the structure of the substrate complex of the enzme was solved (Murphy *et al.*, 1997) it became clear, that nitrite binds with an oxygen atom to copper and that this oxygen is protonable. After reduction and cleavage of the N-O bond nitric oxide is released, leaving the oxygen atom bound to copper as hydroxide or water.

3.3.2 Cytochrome cd_1 Nitrite Reductase

The second denitrificatory nitrite reductase, cytochrome cd_1 (E.C. 1.9.3.2), has also been the subject of detailed crystallographic studies. It has been described as a bifunctional enzyme, catalyzing not only the reduction of nitrite, but also the reduction of oxygen to water (Yamanaka *et al.*, 1963; Yamanaka & Okunuki, 1963). However, the physiological electron acceptor is nitrite and the structure of the enzyme from *Thiosphaera pantotropha* (Fülöp *et al.*, 1995) revealed the distinct two-domain organization of the enzyme (Figure 4). The smaller, α-helical cytochrome *c* domain showed similarities to soluble cytochromes *c*, but had two histidines as fifth and sixth ligands to the heme iron. The active site of the homodimeric enzyme is located at the d_1 heme, a dioxoisobacteriochlorin moiety that has been observed

here for the first time. It is embedded in the core of a rigid, eight-bladed β-propeller domain and has a histidine from the d_1 domain and a tyrosine from the cytochrome *c* domain as fifth and sixth ligands.

Further insight was obtained from the structures of the oxidized and reduced enzyme with bound substrate and product (Williams *et al.*, 1997). Surprisingly, the ligation of both hemes changes with reduction, along with a major rearrangement of the cytochrome *c* domain. One of the histidine ligands to heme *c* is exchanged for a methionine, and this motion also removes the tyrosine ligand from the d_1 heme, allowing for the binding of substrate. Upon reoxidation, the process is reversed, and the returning tyrosine residue displaces the product, nitric oxide. This mechanism solves the problem of product inhibition by the formation of a highly stable Fe^{II}-NO adduct.

Nitrite is bound to the d_1 heme iron through its nitrogen atom, and one of its oxygens is coordinated by two histidine residues simultaneously (Williams *et al.*, 1997). It has been postulated that this oxygen will leave nitrite as a water after reduction, taking along the protons of the two histidines.

According to stopped-flow experiments (Silvestrini *et al.*, 1990), the rate of nitrite reduction by cytochrome cd_1 is limited by the electron transfer from heme *c* to heme d_1. Heme *c* has a more positive standard redox potential ($E^{0'}(Fe^{III/II})$ = + 0.23 V) than heme d_1 ($E^{0'}(Fe^{III/II})$ = + 0.15 – +0.20 V) and can be assumed to be the entry point for electrons (Meyer & Kamen, 1982). The physiological electron donor of cytochrome cd_1 is presumably cytochrome c_{551} (Yamanaka *et al.*, 1963), encoded by the *nirM* gene on the same operon as the enzyme (Jüngst *et al.*, 1991). However it has been shown, that azurin (Parr *et al.*, 1977) and pseudoazurin (Moir *et al.*, 1993) can also reduce cytochrome cd_1.

3.3.3 Assimilatory Siroheme Nitrite Reductase

Assimilatory nitrite reductases are cytoplasmic enzymes containing the siroheme cofactor. The bacterial enzymes (E.C. 1.6.6.4) use NADH as electron donor, while the closely related eucaryotic and cyanobacterial enzymes (E.C. 1.7.7.1) interact with a ferredoxin. The enzymes from bacteria and plants possess a further flavin-containing subunit, while the cyanobacterial proteins seem to be monomers that interact directly with ferredoxins.

Assimilatory nitrite reductases show clear amino acid sequence homologies to assimilatory sulfite reductase (E.C. 1.8.1.2), the structure of which has been solved to a resolution of 1.6 Å (Crane *et al.*, 1995). This structure of the *E. coli* enzyme missed 74 N-terminal residues which contain the substrate access channel of the protein, but the cofactors were clearly distinguishable. Siroheme is a reduced porphyrin of the isobacteriochlorin class (Murphy & Siegel, 1973), which is coordinated by a cysteine residue that in turn is a bridging ligand to a Fe_4S_4 cluster. The distal position of the siroheme iron atom is the binding site for substrate.

3.3.4 Dissimilatory Cytochrome *c* Nitrite Reductase

Respiratory, ammonia-forming nitrite reductases have been isolated from a series of organisms as listed in 3.2.2. They have been assigned molecular masses between 57 and 69 kDa, while it was generally agreed that heme iron was the sole cofactor. First heme determinations indicated six heme groups per monomer, leading to the long-persisting term *hexaheme* nitrite reductase (Brittain *et al.*, 1992). The first sequence of a *nrfA* gene, the one from *E. coli* (Darwin *et al.*, 1993), then only contained four classical heme-binding motives, Cys-X_1-X_2-Cys-His, resulting in the re-assignment that the enzyme was a tetraheme protein. Only most recently it was established, that the protein actually held five *c*-type heme groups, four binding to the classical motives and one to a novel type, Cys-X_1-X_2-Cys-Lys (Eaves *et al.*, 1998).

Nitrite reductase activity is located on the periplasmic side of the cytoplasmic membrane. Based on the operon structure found in *E. coli*, it has been suggested to form a membrane-associated complex with further proteins encoded downstream on the same operon (Hussain *et al.*, 1994).

3.4 Protein Crystallography

The first protein structures solved to almost atomic resolution by three-dimensional Fourier synthesis of X-ray diffraction patterns of single crystals were the ones of hemoglobin (Perutz *et al.*, 1960) and myoglobin (Kendrew *et al.*, 1960). Seven years before, fibre diffraction studies led to understanding the structure of deoxyribose nucleic acid (Watson & Crick, 1953).

In the almost 40 years that have passed since, protein crystallography has become a well established and reliable technique with a wide range of possible applications. Driven by rapid developments in molecular biology and biochemistry and the triumphant advance of computer hard- and software in the last 20 years, this has led to a total number of more than 11200 protein structures deposited in the Protein Data Bank in the end of 1999. More than 9100 of those structures were solved by X-ray diffraction, around 1800 by multidimensional nuclear magnetic resonance spectroscopy (NMR) and the remaining 200 by computer modeling. This ratio emphasizes the central role of protein crystallography in the field of structural biology.

Structure solution by NMR is at present still limited to small proteins of up to 30 kDa, but it complements protein crystallography in several ways. It provides information on protein dynamics that cannot be obtained from the rather rigid environment of a crystal lattice and it is also not dependent on the availability of protein crystals.

A detailed discussion of protein crystallography is beyond the scope of this work and can be found in relevant textbooks (Blundell & Johnson, 1994; Drenth, 1994; Massa, 1994; McRee, 1993) and in *Meth. Enzymol.* **276**.

3.5 Scope of this Work

Its complex spectroscopic properties and the lack of homologues in structure and sequence made cytochrome *c* nitrite reductase an interesting target for structural analysis. Not only is knowledge of the amino acid sequence needed for building a structural model, but furthermore the comparison of operon sequences of different organisms allows to identify and characterize the enzyme family. The high-resolution X-ray structure of nitrite reductase was expected to help in finding answers to the questions that remained even after detailed biochemical studies, as for example the number and steric arrangement of cofactors, the architecture of the active site, and binding modes of substrate and potential intermediates.

In the present study, the sequences of the *nrf*-operons encoding for cytochrome *c* nitrite reductase from *Sulfurospirillum deleyianum* and *Wolinella succinogenes* were determined and compared to other ones known previously or obtained from databases of genome sequencing projects. With the purified enzyme (Schumacher, 1993; Schumacher & Kroneck, 1991) and the primary sequence at hand, the ongoing objective was to determine the crystal structure of cytochrome *c* nitrite reductase. First crystals had been obtained before (Hammann, 1994; Meininghaus, 1996), but the results of diffraction experiments with those crystals were unsatisfying.

4 Materials and Methods

4.1 Microbiology

4.1.1 Growth of *S. deleyianum* and *W. succinogenes*

Cells of *S. deleyianum* and *W. succinogenes* were grown as described previously (Einsle, 1996; Schumacher, 1993). A basic fresh water medium containing 10 mM KH_2PO_4, 1.5 mM $MgSO_4$, 0.7 mM $CaCl_2$ and 25 mM NH_4Cl was autoclaved for 15 min at 121° C and supplied with 2 $ml \cdot l^{-1}$ of trace element solution SL10a (Einsle, 1996; Widdel, 1986) and 0.4 mM cysteine as a sulfur source.

Compound	[mM]	[$mg \cdot l^{-1}$]
$FeCl_2 \cdot 4\ H_2O$	15.0	1901.3
$ZnCl_2 \cdot 7\ H_2O$	0.5	144.1
$MnSO_4 \cdot 2\ H_2O$	0.5	99.0
H_3BO_3	0.1	6.2
$CoCl_2 \cdot 6\ H_2O$	0.5	119.3
$CuCl_2 \cdot 2\ H_2O$	0.1	17.0
$NiCl_2 \cdot 6\ H_2O$	0.1	23.8
$Na_2MoO_4 \cdot 2\ H_2O$	0.15	36.3

Table 2: Trace element solultion SL10a, modified and supplemented after Widdel (1986). The salts were dissolved in 7 ml of 25% HCl, the volume adjusted to 1 l and autoclaved for 15 min at 121°C.

The pH was adjusted to 7.2 with 2 M Na_2CO_3 or 2 M HCl. The best protein yields were obtained when 40 mM of formate as electron donor, 10mM of nitrate as electron acceptor and 10 mM of acetate as a carbon source were supplied. The medium was inoculated with 10% of its volume from a stock culture and grown to early stationary phase at 30° C within 25 to 40 h. As *S.*

deleyianum tolerates up tp 0.2% of oxygen, autoclaving the media was sufficient to create the desired microaerobic environment.

Genomic DNA was prepared from cells grown for protein purification. During the course of the crystallization experiments, further batches of nitrite reductase were used that were kindly supplied by Petra Stach, Klaus Sulger and Mark Meininghaus.

4.1.2 Growth of *Escherichia coli*

Derivative strains of *Escherichia coli* K12 were used for cloning purposes during the sequencing of the *nrf* operons. The relevant genotypes were:

- **INV αF'** (Hanahan, 1983): *recA1 supE44 endAI hsdR17* ($r_k^- m_k^+$) *gyrA96 relA1 thi-1 Φ80 lacZαΔM15*(*lacZYA-argF*) *deoR*$^+$ *F'*
- **XL1-Blue** (Bullock *et al.*, 1987):]: *recA1 supE44 endAI hsdR17 gyrA96 relA1 thi-1* (*lac-proAB*) [*F' proAB lacI*$_q$ *lacZ M15 Tn10* (*Tet*$^+$)]

Bacteria were grown at 37° C in Luria-Bertani medium (1% NaCl, 0.5% yeast extract, 1% tryptone, pH 7.5), which was supplemented with ampicillin (100 mg·l^{-1}) for selection of transformands. Transformation was carried out by heat shock or electroporation (Ausubel *et al.*, 1990; Sambrook *et al.*, 1989). For antibiotic resistance selection, ampicillin was added to a concentration of 100 mg·l^{-1}.

4.2 Molecular Biology

4.2.1 Preparation of Bacterial Genomic DNA

Preparation of genomic DNA from *S. deleyianum* and *W. succinogenes* was carried out following protocols established for *E. coli* (Ausubel *et al.*, 1990). Cells were harvested from 5 ml of medium and resuspended in 600 µl

of 0.5% SDS, 1 mM EDTA and 10 mM Tris/HCl pH 8. Proteinase K (United States Biochemicals, Cleveland, USA) was added to 100 $mg \cdot l^{-1}$ and after incubation for 1 h at 37° C the cells were broken by osmotic shock by addition of 100 µl 5 M NaCl. This lysis procedure proved to be practicable for all species that were tried.

80 µl of a solution containing 10% CTAB and 0.7 M NaCl was added and incubated for 10 min at 65° C to precipitate proteins and lipids, follwed by four extraction steps with a 25:24:1 mixture of phenol/chloroform/isoamyl alcohol. DNA was precipitated by addition of 0.7 volume parts of chilled isopropanol, centrifuged at 14000 rpm for 30 min and the pellet washed with 70% ethanol. Purified DNA was then resuspended in 10 mM Tris/HCl pH 8.5. To determine DNA by UV/vis spectroscopy, a molar extinction coefficient was calculated from the GC content (Schumacher, 1993) as described previously (Einsle, 1996).

4.2.2 Preparation of Plasmid DNA

Plasmid DNA was isolated from *E. coli* using the QiaPlasmid Kits (Qiagen, Hilden, Germany) or following a modified boiling lysis procedure (Ausubel *et al.*, 1990). Cells of *E. coli* were harvested and resuspended in 8% sucrose, 5% Triton X-100, 50 mM EDTA and 50 mM Tris/HCl pH 8.0. Lysozyme was added to 0.2 $mg \cdot ml^{-1}$ to labilize the cell walls and the cells were incubated in boiling water for 1 min. After centrifugation at 14000 rpm for 15 min, the pellet containig cellular debris, chromosomal DNA and denatured proteins could be removed and a 30 min RNAse digest was carried out.

Plasmid DNA was precipitated with 0.7 volume parts of chilled isopropanol, centrifuged at 14000 rpm for 10 min and the pellet was washed with 70% ethanol. Purified DNA was then resuspended in 10 mM Tris/HCl pH 8.5. DNA was determined at 260 nm.

4.2.3 Sequencing Strategy

Starting point for the sequencing of the *nrf* operons from *S. deleyianum* and *W. succinogenes* was a partial sequence of *S. deleyianum nrfA* that was obtained in an earlier study (Einsle, 1996). This sequence covered the amino acids 1 to 317 of NrfA plus a 120 bp 5'-overhang.

4.2.3.1 Polymerase Chain Reaction

Polymerase Chain Reaction (Innis *et al.*, 1988; Saiki *et al.*, 1988) was carried out with *Taq* polymerase (Perkin Elmer, Vaterstetten, Germany) or *Pfu* polymerase (Stratagene, Heidelberg, Germany) on a Stratagene Robocycler Gradient 96 (Stratagene, Heidelberg, Germany).

4.2.3.2 Design of PCR Primers

Oligonucleotide primers for PCR and sequencing reactions were designed under the following preconditions: With a total length of 20 to 27 bp the GC content should not exceed 50%. Among the last five basepairs should be no less than three G≡C pairs, which have a stronger interaction than A=T pairs. Primers were ordered from MWG Biotech (Ebersberg, Germany) or the Genzentrum der Ludwig-Maximilian-Universität (München, Germany).

4.2.3.3 Inverse PCR

Inverse PCR was the first method used for sequencing of unknown regions of DNA flanking a known fragment. Genomic DNA was treated with a restriction endonuclease which, after digestion, was inactivated by heat. The digest was then diluted and incubated with DNA ligase. This led to a religation of the restriction fragments, while the dilution step increased the possibility of self-ligation. PCR on such a religated DNA ring with primers pointing out of the known region would then amplify the unknown region between the primers and the next restriction site of the enzyme chosen. Digests with different enzymes allowed for reliable genome walking with fragments averaging between 300 and 700 bp.

4.2.3.4 Anchor-ligated Genome Walking

In order to overcome the practial size limitations for new fragments obtained through inverse PCR, an anchor-ligated PCR approach in combination with nested PCR was applied using the Universal Genome Walker Kit (Clontech, Heidelberg, Germany).

4.3 Protein Biochemistry

Unless mentioned specifically, standard techniques and materials were used. Protein solutions were handled on ice and frozen in liquid nitrogen for long-time storage. Buffer exchange was carried out on NAP gravity flow columns (Pharmacia, Uppsala, Sweden). Buffers of low ionic strength were used for crystallization experiments, most commonly 5 mM HEPES/NaOH pH 7.0 or 5 mM MES/NaOH pH 6.0.

Dicontinuous SDS polyacrylamide gel electrophoresis was done according to Laemmli (1970), and gels were stained with Coomassie brillant blue or with silver (Heukeshoven & Dernick, 1985). Protein concentration was determined using bicinchoninic acid (Smith *et al.*, 1985). For *S. deleyianum* nitrite reductase, the molar extinction coefficients for the predominant heme absorption maxima have been described (Schumacher, 1993) and were used for concentration determinations. Protein solutions were concentrated using MicroSep or MacroSep concentrators (Pall Gelman Sciences, Roßdorf, Germany).

4.3.1 Purification of Nitrite Reductase

Although the purification protocols for nitrite reductase from *S. deleyianum* were well established (Schumacher, 1993; Schumacher & Kroneck, 1991), crystals were hard to reproduce in batches from different purifications. To overcome this problem, an optimization of the purification proce-

dure was attempted. For small-scale experiments with different columns and buffers, the SMART system (Pharmacia, Uppsala, Sweden) was used.

4.3.2 Sequencing of cytochrome c_3

To obtain the peptide sequence of cytochrome c_3 from *D. desulfuricans* Essex 6 that was needed for building the molecular replacement model, an N-terminal sequence of 35 residues was determined. Then the protein was cleaved by addition of a small crystal of cyanogen bromide. The two resulting fragments were separated on a Superdex Peptide HR 10/30 column in 0.1% trifluoracetic acid containing 25% acetonitrile.

Enzymatic cleavages were carried out with endopeptidase Lys-C and Asp-N. In the first case, the peptides were separated by reversed phase HPLC (Vydac C18) with a linear gradient of 3-42% acetonitrile in 0.1% trifluoracetic acid, while in the case of the cleavage with endopeptidase Asp-N the small C-terminal peptide was separated from an uncleaved large N-terminal fragment by size exclusion chromatography on the Superdex Peptide column as above.

Subsequently, the covalently attached heme groups were cut off with nitrosulphenyl chloride (Fontana *et al.*, 1973). Then the apoprotein chain was digested with chymotrypsin. The complex mixture of fragments generated due to partial cleavages and cleavage at unusual sites was separated by size exclusion HPLC.

Pools of fractions containing peptides needed for sequence alignment as identified by N-terminal sequence analysis were further separated by reversed-phase HPLC as above. Sequencing was done by Dr. Karlheinz Mann on an Applied Biosystems sequencer model 492.

4.4 Crystallography

4.4.1 Theoretical Background

The maximum achievable resolution of any microscopic technique is limited by the applied wavelength. The radiation needed to analyze atomic distances (e.g. 1.54 Å for a carbon-carbon σ-bond) lies within the spectral range of X-rays. However, while light or electron microscopy uses lenses to merge the waves diffracted by an object into an enlarged image, there are no such lenses available for X-rays.

Max von Laue realized in 1912, that the three-dimensionally ordered lattice arrangement of a crystal will cause interference of the diffracted photons resulting in discrete maxima whose intensity can be measured in an appropriate experimental setup.

4.4.1.1 Crystal Growth

The process of crystal formation is in principle energetically favoured, driven by the gain of entropy through the loss of the proteins' ordered hydratation shell. A solution of the protein is slowly brought into a state of supersaturation – usually by evaporation of water – until ordered crystals are formed. Mechanistically, crystal growth can be divided into two stages, *seed formation* and *crystal growth*. Supersaturation of the system – defined as the difference of the chemical potentials of solution and crystal – is a prerequisite for both stages. Seed formation occurs in an equilibrium of formation and dissolving of small aggregates, determined by the free energy ΔG:

$$\Delta G = -k_B T \frac{4\pi r^3}{V \ln \beta} + 4\pi\gamma r^2$$

V is the volume of a molecule within the aggregate, $\beta = c/c_S$ is the supersaturation (protein concentration c, protein solubility c_S) of the solution, k_B is the Boltzmann constant, γ the free surface energy in between the aggrega-

te and the solution and r is the aggregates' radius. The first term describes the gain of energy due to the decrease of free energy in the system and the second term is the energy needed to overcome surface tension during aggregate formation. ΔG will have a maximum at a critical radius r_c, meaning that aggregates with a radius smaller than r_c will redissolve, while for those bigger than r_c further crystal growth means a decrease of ΔG. The critical cluster size for protein crystals is between 10 and 200 molecules.

Solubility of the protein, C, can be described as a function of the ionic strength I in the precipitant solution:

$$\ln C = \ln C_0 + \underbrace{\frac{AZ^2\sqrt{I}}{1 + aB\sqrt{I}}}_{\text{„Salting in“}} \underbrace{- K_S I}_{\text{„Salting out“}}$$

Herein, C_0 is the solubility of the protein in water, I is the ionic strength (I = ½ Σ_i $c_i z_i^2$ with concentration c and charge z of the ion), Z is the total charge of the protein, a is the sum of radii of protein and salt ion, K_S is an empirical salting-out constant and A and B are constants depending on temperature and dielectricity.

For high salt concentrations, the salting-out term will be dominant, and it can be derived that ions with a high charge density will have stronger influence on the solubility, as described in the Hofmeister series in 1888:

K_S for anions: citrate > tartrate > sulfate > acetate > chloride > nitrate

K_S for cations: $Li^+ > K^+ > NH_4^+ > Ca^{2+} > Sr^{2+} > Ba^{2+} > Al^{3+}$

In addition to salts, commonly used precipitants are polyethylene glycoles or organic solvents like ethanol, isopropanol or methylpentane diol.

4.4.1.2 Crystals

A crystal can be regarded as a three-dimensional repetition of a single building block, the *unit cell*. Within the unit cell, a crystal can contain further symmetry elements, dividing it into several *asymmetric units* which

form the most basic structural element within the crystal. The geometry of the unit cell together with the possible symmetry operations defines the *space group* of the crystal. Although there are 230 space groups in seven crystal systems (*triclinic*, *monoclinic*, *orthorhombic*, *tetragonal*, *trigonal*, *hexagonal* and *cubic*), only 65 are enantiomorphic and are thus feasible for chiral molecules such as proteins. Identification of the correct space group is essential for correct indexing of diffraction patterns and therefore the first step of understanding a crystal structure.

4.4.1.3 X-ray Diffraction by Crystals

Upon interaction with the atoms in a crystal, the oscillating electrical field of an X-ray photon induces an oscillation of equal frequency in the electron hull of the atom. The electrons act as oscillating dipoles emitting secondary radiation of the same frequency as the incident radiation, but with a phase difference of 180°. In this elastic or coherent diffraction, the phase shifts between single waves originating from any point of finite electron density sum up to a total intensity of the secondary radiation of zero (destructive interference), except if the path difference between the waves is an integer multiple of their wavelength (constructive interference). Given the correct orientation of the crystal, this condition is fulfilled for corresponding positions in all unit cells. Diffraction of X-rays on the real lattice of a crystal thus creates another three-dimensional lattice of diffraction maxima. As the geometric properties of this lattice are inverse to those of the real crystal, it is referred to as the *reciprocal lattice*.

A convenient way to describe diffraction by a crystal lattice is to imagine every single diffraction spot to be a reflection of the incident beam on an imaginary lattice plane which is identified by the *Miller indices* (*h*,*k*,*l*) (Figure 5A). The normal vectors $\vec{S}$ of those lattice planes then build up the reciprocal lattice, their length reflecting the reciprocal distance of the planes.

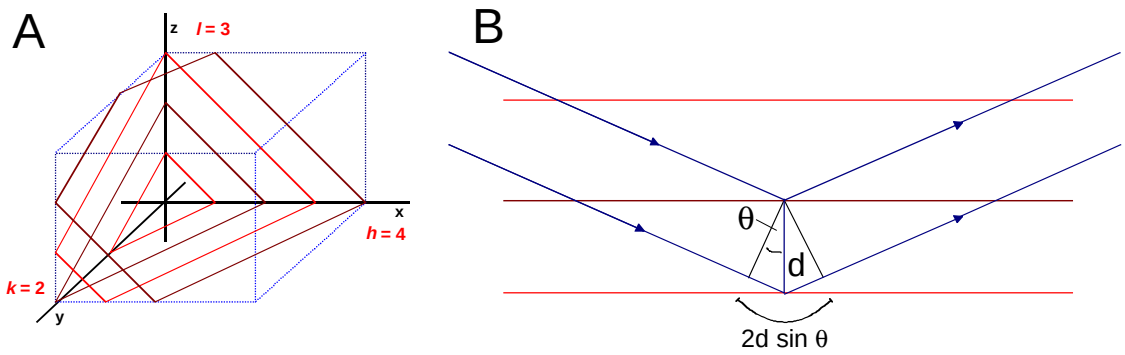

Figure 5: Reciprocal lattice planes and Bragg's law. **A**) Lattice planes that allow for constructive interference of diffracted waves are those that divide the unit cell sides into integer fractions. The number of those fractions is used to index the plane. The group of lattice planes shown would have the Miller indices (4 2 3). **B**) Two waves that are reflected by two adjacent lattice planes with distance *d* have a difference in path length that is equal to 2d sin θ, as it can easily be derived from the scheme. A prerequisite for constructive interference is, that this difference in path is an integer multiple of the wavelength used: 2d sin θ = nλ (Bragg's law).

Regarding elastic diffraction on a set of lattice planes with distance d, constructive interference will occur at an angle θ, if the path difference between the diffracted waves is an integer multiple of the wavelength λ. This relation between reflection angle and lattice plane distance is known as *Bragg's law* (Figure 5B):

$$2\, d_{hkl} \sin \theta = n\, \lambda$$

The *Ewald sphere* (Figure 6) is a tool for constructing reciprocal lattice points on the basis of Bragg's law. It is a sphere of radius $1/\lambda$ with the crystal in its centre. The point where the incident beam $\vec{s}_0$ enters the sphere and the origin O of the reciprocal lattice are on opposite sides of the centre. Bragg's law is fulfilled for every reciprocal lattice point that lies on the Ewald sphere. A rotation of the crystal rotates the reciprocal lattice in the same way, allowing different reciprocal lattice points to intersect with the sphere. For the given orientation of the crystal, those points are the ones that can be recorded on an X-ray detector.

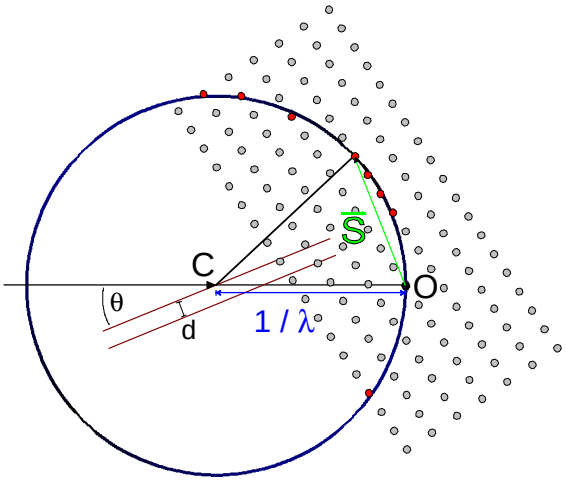

Figure 6: The Ewald construction. In reciprocal space, the crystal (C) is placed in the center of a sphere (here, in two dimensions, a circle) with radius 1/λ, called the Ewald sphere. The origin of the reciprocal lattice, i.e. reflection (0 0 0), is placed in (O). The reciprocal lattice (grey dots) will rotate as the crystal does and only those reciprocal lattice points that intersect with the Ewald sphere will be in diffraction condition (red dots) and will be recorded on an image plate detector in real space.

As every recorded diffraction spot represents one lattice plane (*h*,*k*,*l*), the measurement of the positions of the spots is sufficient to deduce the geometry of the crystal and in most cases also the space group, as additional symmetry elements can manifest in the form of systematic extinctions of reflections. On the other hand, the content of the unit cell influences the intensity of the diffraction spots. A crystal is described as the convolution of the unit cell content with the three-dimensional lattice. As the diffraction image is the result of multiplying these molecular transformations with the discrete reciprocal lattice, the intensity of a diffraction spot will be high if the intensity of the underlying convolution is high and vice versa.

The result of a data collection on a crystal will primarily be the knowledge about space group and unit cell dimensions, and – based on this – an intensity measurement $I(h,k,l)$ for every reflection (h,k,l).

4.4.1.4 The Electron Density Function

The goal of a crystallographic experiment is to calculate the distribution of electron density in the asymmetric unit of the crystal in order to be able to place an atomic model of the crystallized molecule therein.

If the electron hull of an atom is considered spherical, its diffraction contribution, the *atomic scattering factor,* does not depend on the direction of the incident beam. However, because of the finite extent of the atom, the phase difference for photons diffracted at different positions in the electron hull will increase with the diffraction angle θ which corresponds to $\left|\vec{S}\right|$ and thus to resolution:

$$f_0 = \int_{x,y,z} \rho(x,y,z)\exp(2\pi i(hx+ky+lz))dxdydz$$

A further decrease of diffraction power with increasing angle is caused by thermal movement of the atoms, by statistic disorders, absorption or scaling errors. To compensate for this, the mean square displacement $\overline{u}^2$ of the atomic vibration is modeled as the isotropic *Debye-Waller temperature factor* $B = 8\pi^2\overline{u}^2$ and added to the atomic scattering factor as an additional exponential decay term:

$$f = f_0 \exp\left(-B\frac{\sin^2\theta}{\lambda^2}\right)$$

With this, the scattering of all atoms in the asymmetric unit is the sum of all atomic scattering factors, taking in account individual phase shifts. For every single reflection (h,k,l) this summation leads to a *structure factor* $F(h,k,l)$:

$$F(h,k,l) = \sum_i f_i \exp(2\pi i(hx+ky+lz))$$

The reciprocal lattice is the Fourier transform of the electron distribution in the crystal, split up in the form of the structure factors. This means that the electron density $\rho(x,y,z)$ for every point in real space can be calculated as a Fourier summation over all structure factors:

$$\rho(x,y,z) = \frac{1}{V}\sum_{h,k,l} F(h,k,l)\exp(2\pi i(hx+ky+lz))$$

4.4.1.5 The Phase Problem

Approaching from the side of the diffraction experiment, each structure factor $F(h,k,l)$ also represents a reflection by one lattice plane. It is described by a wave function with an amplitude and a phase angle:

$$F(h,k,l) = \underbrace{|F(h,k,l)|}_{Amplitude} \underbrace{\exp i\alpha(h,k,l)}_{Phase\ angle}$$

The structure factor amplitude can be obtained experimentally, as it is in principle the square root of the measured intensity:

$$I(h,k,l) \approx |F(h,k,l)|^2$$

The total energy $E(h,k,l)$ in a diffracted beam for a mosaic crystal rotating with uniform angular velocity ω through the reflecting position is given by Darwin's equation (Darwin, 1914):

$$E(h,k,l) = \frac{I_0}{\omega}\lambda^3 \frac{e^4}{m_e^2 c^4} \frac{1+\cos^2 2\theta}{2} \frac{LAV_x}{V^2} |F(h,k,l)|^2$$

Herein, I_0 is the intensity of the incident beam, λ is the wavelength, e and m_e are charge and mass of the electron and c is the velocity of light. The term $(1+\cos^2 2\theta)/2$ is a polarization factor that originates from the fact that an electron does not scatter along its direction of vibration. The Lorentz factor L depends on the data acquisition technique and the absorption factor A takes into account the intensity loss through photoelectric absorption and Rayleigh scattering. V_x is the crystal volume and V is the volume of the unit cell.

While the structure factor amplitude can be derived from the measured intensity as described above, information about the phase angle is lost. Without correct phase angles, the calculation of an interpretable electron density is impossible, a dilemma commonly referred to as the *phase problem* of crystallography.

Four approaches to overcome this problem are applicable today:

- Molecular Replacement (MR)
- Multiple Isomorphous Replacement (MIR)
- Multiple-wavelength Anomalous Dispersion (MAD)
- Direct Methods

The method of Molecular Replacement depends on the availability of a sufficiently homologous model structure which is oriented by Patterson search techniques and then used for initial phase calculations (Hoppe, 1957; Huber, 1965; Rossmann & Blow, 1962). Without any previous knowledge of the structure, Multiple Isomorphous Replacement is still the most commonly used method. Herein it is attempted to place heavy atoms on specific sites in the protein – either by soaking or by cocrystallization – and to identify their positions by comparing the data collected from a native crystal with that of a derived one (Green *et al*., 1954). MAD, which was applied for nitrite reductase and will be described in the following paragraph, depends on precisely tunable synchrotron radiation which has only been available for the last years, but is becoming more and more standard (Hendrickson *et al*., 1988).

Direct methods are the common way to determine phases in small molecule crystallography, but due to the high number of atoms per asymmetric unit and the limited resolution that is obtained from most protein crystals, this approach has rarely been successful for large biomolecules. Most recently the number of protein structures solved by direct methods is increasing and the development is promising, but small molecule size, high resolution and good data quality are still a prerequisite.

4.4.1.6 MAD and Metalloproteins

If the atomic absorption coefficient of an element is plotted as a function of X-ray wavelength, a curve with several sharp edge features is obtained. On these absorption edges, the photon energy of the X-rays is sufficient to

eject an electron from the atom and so the absorbed energy will not contribute to the scattering of the atom at this wavelength (see also Figure 16).

A frequently encountered problem in MIR is the derivation of crystals with heavy atoms without destroying the morphology that is essential for comparing derived and native data sets. Metalloproteins *per se* contain heavy atoms, and measurements around the absorption edge of a specific metal can produce data in which the contribution of this metal is significantly different depending on the exact wavelength, in analogy to a native and a derivative data set.

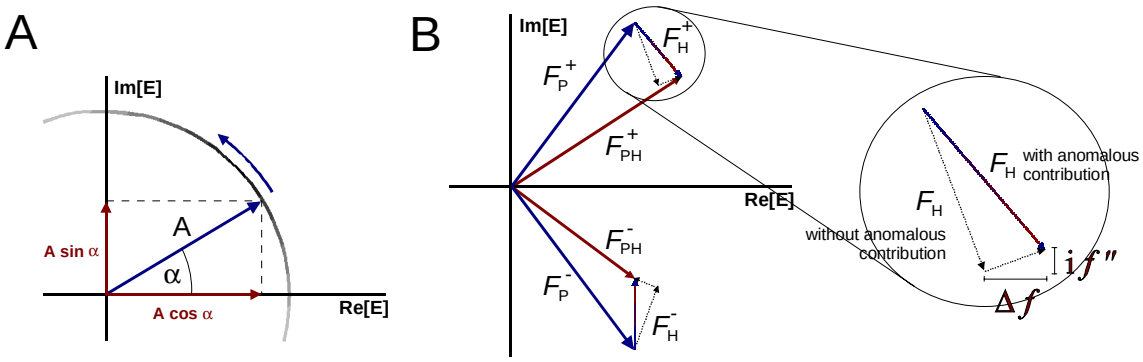

Figure 7: A) An Argand diagram of the Gaussian plane. A complex wave function can be described by a rotating vector with a length ***A*** (amplitude) and an angle α (phase) with the real axis. **B**) The difference between MIR and MAD. In MIR, the structure factor F_H^+ of a heavy atom adds to the one of the protein (F_P^+) producing the combined structure factor F_{PH}^+ that can be measured. The same is true for the Friedel mates, which are identical except for the sign of the phase angle. If anomalous contribution is considered, an additional shift is added to he heavy atom contribution, that can be separated into a real part (Δ*f*) and an imaginary part (i *f* "), and the Friedel pairs will no longer be equal. In MAD on metalloproteins, only this shift can be used, because protein and heavy atom can not be separated. Although the anomalous contribution is small compared to F_H^+ it can be used for phasing because the data are measured on a single crystal and there is no anisomorphy problem.

In addition, it is no longer correct to consider electrons as free electrons when measuring close to an absorption edge. Inner electrons interact with the nucleus, even more so in heavy elements, and the result is a phase shift of the diffracted beam that differs from the regular 180° and is called *anomalous scattering*. In an Argand diagram of the Gaussian plane (Figure 7A), the atomic scattering vector is rotated counterclockwise, modified by a

real contribution $f' = f + \Delta f$ and an imaginary contribution f'' (Figure 7B). These two components are related through the Kramers-Kronig equation

$$f'(\omega) = \frac{2}{\pi} \int_0^\infty \frac{\omega' f''(\omega')}{\omega^2 - \omega'^2} d\omega'$$

with the respective X-ray frequencies ω and ω'.

As a consequence, the structure factors of Friedel pairs, $F_{PH}(h,k,l) = F_{PH}^+$ and $F_{PH}(\overline{h},\overline{k},\overline{l}) = F_{PH}^-$, are no longer equal and their difference

$$\Delta|F|_{ano} = \left(|F_{PH}^+| - |F_{PH}^-|\right)\frac{f'}{2f''}$$

can be used separately or in combination with isomorphous replacement to search for the anomalous scatterers' positions. While the dispersive f' contribution of the absorption edge in MAD is not unequivocal (as in the case of a single derivative in MIR), the anomalous scattering information can compensate this ambiguity, such that all the information needed to solve an unknown structure can be obtained from a single crystal containing anomalous scatterers.

The first step then is to localize the atomic positions of the anomalous scatterers. While it is not possible to calculate an electron density map without phase information, the intensities $I = |F|^2$ themselves can be used to calculate a *Patterson function* (Patterson, 1934), whose maxima are interatomic distance vectors rather than real-space atomic positions:

$$P(u,v,w) = \frac{1}{V} \sum_{h,k,l} |F(h,k,l)|^2 \cos 2\pi(hu + kv + lw)$$

If an *anomalous difference Patterson map* is calculated with $\left(\Delta|F|_{ano}\right)^2$ as coefficients, it will only show maxima at the positions of distance vectors between the anomalous scatterers.

Once their positions have been determined and refined, the structure factors of the protein can be derived according to

$$F_P = F_{PH} - F_H$$

with the help of the Harker construction (Harker, 1956).

In addition to the dispersive difference of the scattering of the metal near the absorption edge compared to the remote data set, the anomalous contribution can be used to compensate the phase ambiguity for every single reflection that a single derivative will give (Figure 8).

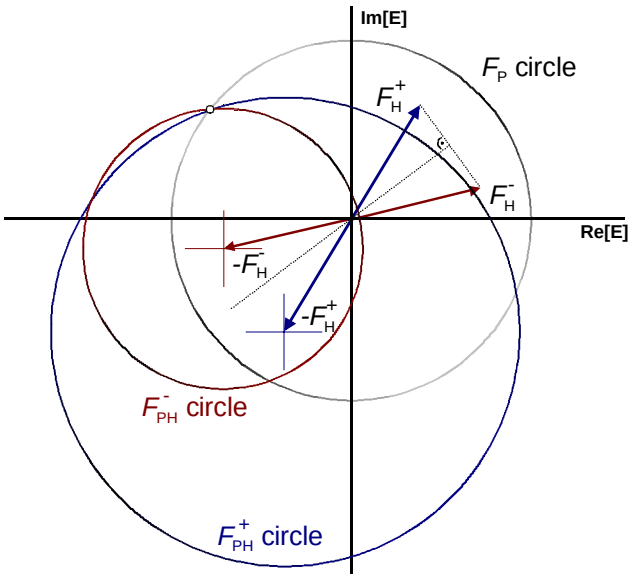

Figure 8: A Harker diagram for the deduction of protein phase angles by anomalous scattering (after Drenth, 1994). $|F_P|$ is the structure factor amplitude for the reference (remote) dataset and $|F_{PH}^+|$ and $|F_{PH}^-|$ for the Friedel mates of the dataset with maximized anomalous contribution (f "). The contribution of the metal to the structure factor is F_H^+ for one member of the Friedel pair and F_H^- for the other member. Due to the anomalous scattering component, these two structure factors are not symmetric to the horizontal axis. For clarification, the F_H^- vectors have been drawn with opposite phase angles such that the three circles intersect in a single point. The dashed line then indicates the direction of the nonanomalous scattering part of the heavy atoms.

Although the anomalous contribution of a metal corresponds only to a small fraction of the electrons in the heavy atom, the problem of nonisomorphy, which is always present in MIR, does not occur in MAD. All data sets can be measured from a single crystal in its native form.

4.4.2 Crystal Growth and Data Collection

Cytochrome *c* nitrite reductase from *S. deleyianum* has first been crystallized in 1994 (Hammann, 1994). These crystals grew without seeding and were assigned to a primitive orthorhombic lattice, with cell constants of **a** = 93.5 Å, **b** = 109.7 Å and **c** = 187.0 Å, but no complete dataset was obtained because of crystal degradation.

In 1996, the crystallization experiments were repeated with new protein material, but the crystals could never be reproduced. Only with the help of microseeding it was possible to find a new crystal form belonging to space group P $2_12_12_1$, but with significantly larger cell constants of **a** = 136.4 Å, **b** = 145.6 Å and **c** = 228.1 Å (Meininghaus, 1996). Consequently, the first attempts within this work were aimed at improving these crystals. Reproducibility and diffraction quality were poor and the best data set ever measured from this crystal form had a limiting resolution of 3.8 Å. The key to solving the structure was thus to find new conditions for a crystal form with better diffraction properties.

4.4.2.1 Crystallization Experiments

Protein crystals were grown by the method of vapour diffusion, where the protein solution was mixed with a precipitant solution and equilibrated against a higher concentrated precipitant reservoir in a closed environment. Under regular conditions, using non-volatile precipitants such as polyethylene glycol or salts, equilibrium is reached by diffusion of water from the protein drop to the reservoir, thus slowly increasing the concentration of all components in the drop (McPherson, 1982).

Sitting drop experiments were carried out in Cryschem plates (Charles Supper Company, Natick, USA), hanging drop setups in Linbro tissue culture plates with siliconized cover slides (Hampton Research, Laguna Hills, USA).

Initial crystallization experiments included a screening of single precipitants at different pH values. The precipitant concentration was raised in small steps over several weeks until the protein crystallized, aggregated or denatured. In order to screen large numbers of more complex precipitant solutions, the method of *sparse matrix sampling* was applied (Carter Jr. & Carter, 1979; Jancarik & Kim, 1991) to obtain promising starting conditions which could then be refined further.

4.4.2.2 Crystal Seeding

While the sparse matrix sampling method produced good quality crystals of cytochrome c_3 from *D. desulfuricans* Essex 6, it was not successful for nitrite reductase. However it was possible to grow small rhombic crystal plates when the protein concentration was raised to 40 $mg \cdot ml^{-1}$ from a solution of 2% PEG 6000 and 0.1 M HEPES/NaOH pH 7.5 within four to six weeks.

If the protein concentration needed for seed formation is substantially higher than the one needed for crystal growth, it might be useful to add reagents like salts or detergents that increase the protein solubility and help to push it across the seed formation threshold. However, crystals obtained in this way will usually be small and badly ordered, as growth will continue very fast once a seed is formed.

To overcome this problem, small crystals can be transferred into crystallization setups with lower precipitant and protein concentrations. The introduced seeds can then grow at a lower and more ordered rate without facing the problem of further seed formation. Crystal seeding can be carried out as *microseeding*, by transferring only fragments of crushed seed crystals, or as *macroseeding*, where it is attempted to bring a whole crystal to a new environment and let it grow bigger.

Microseeding proved to be a crucial step in obtaining reproducible good-quality crystals of nitrite reductase. Seed transfer to a variety of conditions produced crystals in different sizes and shapes, the best of which were ob-

tained using 9% PEG 8000, 130 mM $(NH_4)_2SO_4$ and 100 mM MES/NaOH at pH 6.8.

Crystal platelets of *W. succinogenes* nitrite reductase grew within two to three days from 12% PEG 4000, 200 mM $(NH_4)_2SO_4$ and 100 mM sodium acetate pH 5.7. With the addition of 15 mM YCl_3 the plates were improved into reproducible, large single crystals.

4.4.2.3 Cryocrystallography

A commonly observed problem in protein crystallography is damaging of crystals in the X-ray beam, especially if intense synchrotron radiation is used. This damage is mainly caused by the formation of water radicals by the X-ray photons which in turn react with the protein molecules, destroying the order of the crystal lattice. To minimize crystal degradation, crystals were cooled to 100 K with a nitrogen stream cooling system (Oxford Cryosystems, Oxford, UK), reducing the mobility of solvent radicals significantly.

Protein crystals are not supposed to be frozen in the nitrogen stream, as formation of ice crystals in the solvent leads to strong powder diffraction rings in the diffraction pattern. Addition of cryoprotectants helps to avoid ice formation, but as such reagents are often strongly hygroscopic, they can dehydrate and thus destroy the crystal.

To successfully cool nitrite reductase crystals for MAD data collection, 2-methyl-2,4-pentanediol (MPD) was applied. Crystals were transferred from the mother liquor into a harvesting buffer containing 5% MPD and incubated for 15 minutes. The concentration of MPD was raised in steps of 5%, with 15 minutes equilibration time each, until 20% of MPD were reached and the crystals showed no ice rings in the diffraction pattern.

In later experiments with substrate complexes of nitrite reductase, a protocol was developed which used (2-*R*,3-*R*)-Butane-2,3-diol as a cryoprotectant. This compound is known to work at concentrations of only 8% (*v*/*v*)

(Rodgers, 1994) and was simply added to the harvesting buffer in a 1:10 ratio immediately before the crystal was transferred from the mother liquor.

4.4.2.4 Substrate Complexes

In order to examine the binding of different substrates and intermediates to the active site of nitrite reductase, crystals were transferred into a harvesting buffer where the original compound ammonium sulfate was replaced by the respective substrate. After incubation for a sufficient time to allow for binding, the crystals were cooled and measured. Successful substrate binding could usually be monitored at resolutions of around 2.5 Å in *S. deleyianum* and up to 2.0 Å in the *W. succinogenes* enzyme, both of which could be obtained with $Cu_{K\alpha}$ radiation. All data sets with higher resolutions were measured with synchrotron radiation.

4.4.2.5 Data Collection

The datasets used to solve the crystal structure of *S. deleyianum* nitrite reductase were collected from a single crystal of approximately 150 × 150 × 50 µm in size, which was cooled as described above. Measurements were taken on wiggler beamline 6 (BW6) of the German Electron Synchrotron DESY, Hamburg, on a Mar Research CCD detector.

An X-ray fluorescence scan was carried out around the K-shell absorption edge of iron to determine the optimal wavelengths for data collection. This procedure is neccessary, because although element-specific absorption edges can be calculated according to the theory of Cromer and Liberman (Cromer & Liberman, 1970), the interaction of the scattering atom with its chemical neighbours influences the scattering behaviour considerably. The absorption edge itself is shifted mainly by the oxidation state of the iron atoms, while the local chemical environment introduces a fine structure (EXAFS) to the absorption edge, caused by the interference of the emitted photoelectron with the electron hulls of the surrounding atoms (backscattering). Thus the maximum achievable f'' can be significantly larger than the

theoretical edge jump. On the other hand, the maximum achievable $|f'|$ is smaller than the theoretical value due to limitations of the bandwidth of the X-ray source.

Measurements for some substrate complexes of nitrite reductase and for cytochrome c_3 were taken on a Rigaku Rotaflex rotating anode X-ray generator with $Cu_{K\alpha}$ radiation at a wavelength of λ_{Cu} = 1.5418 Å with Mar Research 2000 or Mar345 image plate detectors, ususally with rotation angles of 1° per image.

All data sets were indexed, integrated and scaled using the programs DENZO and SCALEPACK (Otwinowski & Minor, 1996). For all further steps of structure solution, data sets were converted with S2MTZ, TRUNCATE and MTZ2VARIOUS (Collaborative Computational Project No. 4, 1994) from intensities to structure factor amplitudes and to suitable file formats.

4.4.3 Graphical Representation

Illustrations of structures were prepared using Molscript (Kraulis, 1991) or Bobscript (Esnouf, 1997) and in some cases rendered with Raster3D (Merritt & Bacon, 1997). Surface illustrations were prepared with GRASP (Nicholls *et al.*, 1993) or Swiss-PdbViewer (Guex & Peitsch, 1996). Sequence alignments of *nrfA* and *nrfH* were made using the Wisconsin GCG Package and plotted with Alscript (Barton, 1993).

4.4.4 Database Searches

Preliminary sequence data of the *nrf* operons of *Shewanella putrefaciens* and *Porphyromonas gingivalis* were obtained from The Institute for Genomic Research website at ***http://www.tigr.org***. The preliminary sequence of the *Salmonella typhi nrf* operon stems from The Sanger Centre's website at

http://www.sanger.ac.uk/Projects/S_typhi. In both cases the nucleotide sequence of *S. deleyianum nrfA* was used for the searches.

Sequence-based secondary structure predictions were carried out through the PHDsec service at the European Molecular Biology Laboratoy (***http://www.embl-heidelberg.de***) (Rost, 1996; Rost & Sander, 1993; Rost & Sander, 1994).

5 Results

The system of dissimilatory nitrite reduction to ammonia has been analyzed on several levels: The DNA sequence of the *nrf*-operon shows, that the enzyme and its regulation are highly conserved through several families of eubacteria while the ways on which electrons are transported to it are remarkably different. Secondary structure predictions indicate a fold that is virtually identical for all known NrfA sequences. The tertiary structures of *S. deleyianum* and *W. succinogenes* nitrite reductase show a novel fold with an atypical active site heme group and the quaternary structure reveals that the previous assumptions that nitrite reductase forms a tetramer will have to be reconsidered.

5.1 A Probe for *nrfA*

After a partial sequence of *S. deleyianum nrfA* was obtained (Einsle, 1996), primers were derived from three parts of the sequence that were most highly conserved in the three *nrfA* sequences known then, *E. coli*, *H. influenzae* and *S. deleyianum*. Those primers were used to screen for *nrfA* in other bacterial genomes and two of them were successful for *W. succinogenes* as well as for *D. desulfuricans* ATCC 27774 (data not shown):

CHVEYYF-1-N: 5‘ – TGY CAY GTN GAR TAY TAY TT – 3‘

PMLKAQHP-2-C: 5‘ – GGG TGY TGY GCT TTY ARC ATT GG – 3‘

Later, the structure showed that both stretches of sequence encode for residues in direct vicinity to the active site and it seems very likely that they will be highly conserved in the *nrfA* genes of most organisms. Hence the above primers might be useful probes for the presence of the gene in unknown species. From fragments of *nrfA* from *S. deleyianum* and *W. succinogenes* it was then possible to obtain the full operon sequences gradually by inverse PCR and anchor-ligated genome walking.

5.2 Further *nrf* Operon Sequences

Homology searches were not only carried out in the EMBL nucleotide database, where the sequence of *H. influenzae* was found, but also in preliminary sequences of genome projects currently in progress in The Sanger Centre and The Institue for Genomic Research.

Three more sequences were found in currently sequenced genomes, from the γ-proteobacteria *Salmonella typhi* and *Shewanella putrefaciens* and from the bacteroid *Porphyromonas gingivalis*. The seven operons divide into at least two groups, the *nrfABCDEFG* type found in γ-proteobacteria and the *nrfHAIJ* type of the ε-proteobacteria. *P. gingivalis* shows a third form of operon organization, but as it will be discussed below it can easily be related to the ε-proteobacterial operon type.

Species	Family	Reference	Gene structure
Escherichia coli	γ-proteobacteria	(Hussain *et al.*, 1994)	*nrfABCDEFG*
Haemophilus influenzae Rd	γ-proteobacteria	(Fleischmann *et al.*, 1995)	*nrfABCDEFG*
Sulfurospirillum deleyianum	ε-proteobacteria	this work	*nrfHAIJ*
Wolinella succinogenes	ε-proteobacteria	this work	*nrfHAIJ*
Salmonella typhi	γ-proteobacteria	The Sanger Centre	*nrfABCDEFG*
Shewanella putrefaciens	γ-proteobacteria	TIGR	*nrfABCDEFG*
Porphyromonas gingivalis	bacteroides	TIGR	*nrfHAKLM*

Table 3: Overview of the seven *nrf* operon sequences available at present.

The *nrfHAIJ* type has a novel operon organization that implies significant differences in the functionality of the nitrite reductase system and will thus be discussed in detail below.

5.3 Organization of the *nrf* Operon

The *nrf* operon (*n*itrite *r*eduction with *f*ormate) has been sequenced from *S. deleyianum* and *W. succinogenes*. In both species it consists of four structural genes which have been assigned *nrfH*, *nrfA*, *nrfI* and *nrfJ*. *NrfA* is the gene encoding dissimilatory nitrite reductase and *nrfH* codes for a small tetraheme cytochrome which is presumed to be its physiological electron donor. The other two genes show similarities to type II cytochrome *c* biogenesis proteins and have been assigned *nrfI* and *nrfJ*.

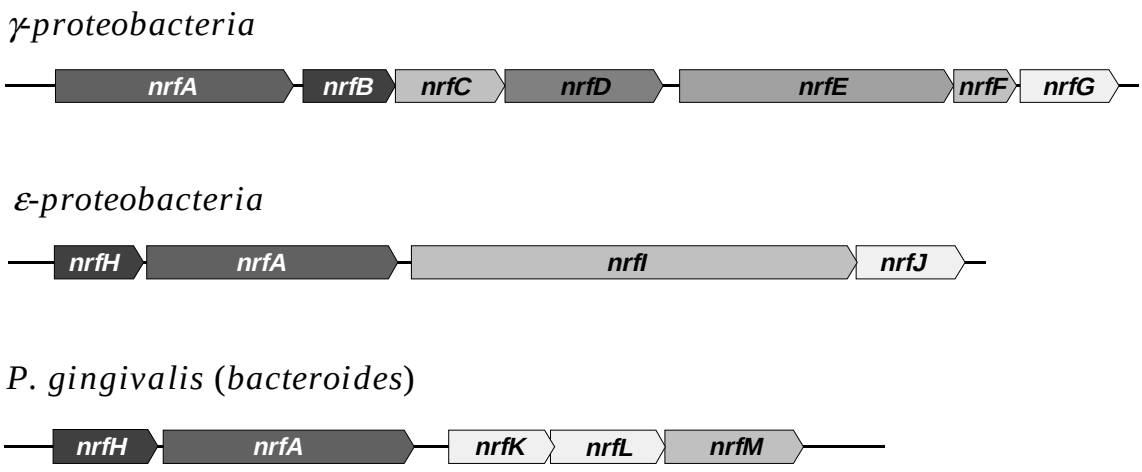

Figure 9: Schematic organization of the different *nrf* operon organization types. The *nrfHAIJ* type of ε-proteobacteria differs distinctly from the *nrfABCDEFG* type of γ-proteobacteria, and the bacteroid *P. gingivalis* shows a futher variation of the *nrfHAIJ* type.

As the two closely related species show a high degree of homology in all four genes, the boundaries of the operon can be reliably assigned simply by the fact that the genes following upstream and downstream of the operon are not the same. The gene upstream and on the counter strand of *nrfH* is a

cell-division regulating gene in *W. succinogenes*, assigned *mreB* by its ca. 40% homolgy to the rod-shape determining protein of several other bacterial species, including *Thermotoga maritima*, *E. coli* and *H. influenzae*. In the *S. deleyianum* genome however, the next gene encodes for a typical histidine kinase protein of a two-component regulatory system.

Downstream of *nrfJ*, both operon sequences are followed by a region containing putative open reading frames that have not been assigned to any known protein and the high similarity between the DNA sequences ends (data not shown). A nucleotide sequence is present that suggests a hairpin structure typical for a transcription terminator.

From the preliminary genomic DNA sequence of *Porphyromonas gingivalis* (Bacteria, Cytophagales, Bacteroidaceae), a third type of the *nrf* operon was identified, which is related to the nrfHAIJ type with variations in the last genes.

5.3.1 The *nrf* Promoter

The promoter region of the *nrf* operon is located in the gap between *nrfH* and the gene following further upstream on the opposite strand. In both *S. deleyianum* and *W. succinogenes* this gap is around 350 bp wide and contains apart from a Pribnow box, the binding site for RNA polymerase, operator sequences for positive and negative regulation of the transcription of the operon.

It has been shown that expression of the *nrf* operon in *E. coli* is subject to positive regulation by the anaerobic transcription control factor FNR and that it is repressed by the presence of nitrate, mediated through the NarL protein (Page *et al.*, 1990). Binding sites for both regulators have been proposed for the *nrf* promoter of *E.coli* (Darwin *et al.*, 1993). This assumption is confirmed by the presence of the same sites not only in *S. deleyianum* and *W. succinogenes*, but also in the three other *nrf* operon sequences from *S. typhi*, *S. putrefaciens* and *P. gingivalis*. Regulation of an operon through

both FNR and NarL is not observed for the first time in this case and has been investigated most thoroughly for the *nirB* promoter of *E. coli* (Bell *et al.*, 1990; Tyson *et al.*, 1993).

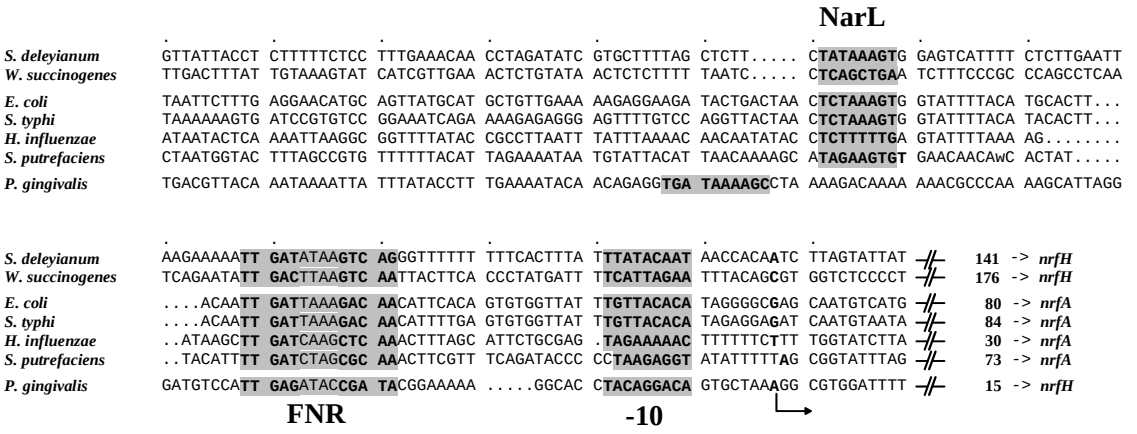

Figure 10: Alignment of the promoter regions of the seven *nrf*-operon sequences. Binding sites for the transcription regulator FNR could be clearly identified, together with a putative Pribnow box motif and a transcription starting point. The negative regulator NarL binds to a motif further upstream.

The transcription factor FNR binds to a characteristic palindromic site around 41 bp upstream of the transciption start which has been described in *E. coli* to have the consensus sequence 5‘-TTGAT-N_4-ATCAA-3‘ (Eiglmeier *et al.*, 1989; Jayaraman *et al.*, 1989). A similar sequence can be found in the *nrf* promoter of *S. deleyianum* (5‘-TTGAT-N_4-GTCAG-3‘) as well as in the one of *W. succinogenes* (5‘-TTGAC-N_4-GTCAA-3‘), and also in *S. typhi*, *S. putrefaciens* and *P. gingivalis* (Figure 10). The sequence of *S. putrefaciens* seems to show even more than one FNR binding site upstream of the *nrfH* gene, but the significance of the other sites is unclear. Interestingly, the amino acid sequence of FNR is similar to that of another transcription factor, CRP (Shaw *et al.*, 1983), which also binds as a dimer to a similar binding sequence (Bell *et al.*, 1989; Spiro & Guest, 1987; Spiro & Guest, 1990)

Relative to the FNR binding site the start of transcription can be located approximately 41 bp downstream, where all seven sequences show a possible Pribnow box motif around position -10. While the binding of FNR to its

operator is close enough to the Pribnow box to function by via direct interaction with RNA polymerase, the NarL repressor binds further upstream.

NarL, whose crystal structure has been solved recently (Baikalov *et al.*, 1996), has also been suggested to recognize specific bindig motives (Eiglmeier *et al.*, 1989; Page *et al.*, 1990), but those are not as characteristic as the ones for FNR. Nevertheless, the assignment made for the NarL operator sequence in the *E. coli nrf* promoter (Darwin *et al.*, 1993) seems to be consistent with similar motives in the promoter regions of the other organisms that contain the *nrf* operon (Figure 10). As a repressor, NarL binds probably too far upstream of the transcription start to interact directly with RNA polymerase, but it might be able to impair the binding of FNR, which seems to be essential for transcription.

5.3.2 *NrfH*; Electron Carrier and Membrane Anchor

In the *nrfABCDEFG* operon type, *nrfB* encodes for a hydrophilic 22 kDa pentaheme *c*-type cytochrome which was assumed to be the physiological electron donor of nitrite reductase (Hussain *et al.*, 1994), mediating between NrfA and NrfCD, which form a membraneous quinol oxidase (Hussain *et al.*, 1994). In the *nrfHAIJ* operon type, this function is adopted by *nrfH*, a membrane-anchored tetraheme *c*-type cytochrome of 19 kDa, while *nrfC* and *nrfD* or any homologues are missing completely. Note however, that two homologues of *nrfC* and *nrfD* have been found in the genome of *W. succinogenes*. Actually the highest scores in databases searches using *nrfC* and *nrfD* of *E. coli* as a query sequence are obtained for *psrB* and *psrC*, which belong to the *psrABC* operon coding for the periplasmic polysulfide reductase system of *Wolinella* (Klimmek *et al.*, 1991; Krafft *et al.*, 1992; Krafft *et al.*, 1995). It can be expected that the PsrBC complex is in complete analogy the *E. coli* NrfCD complex and that its function is to oxidize menaquinone and deliver electrons to a periplasmic reductase.

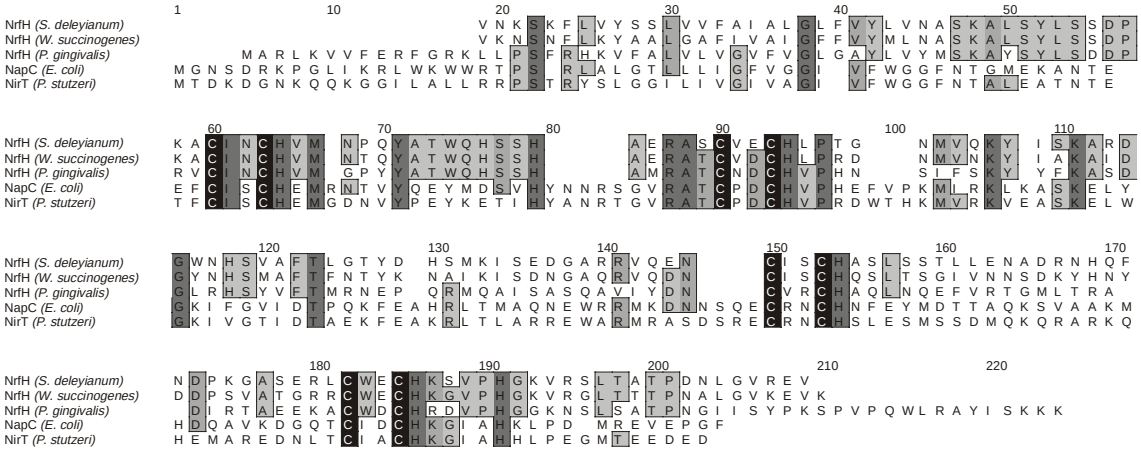

Figure 11: An alignment of the amino acid sequences of NrfH from *S. deleyianum*, *W. succinogenes* and *P. gingivalis* with two of the classical members of the NirT/NapC family of multiheme cytochromes, NapC from *E. coli* and NirT from *Pseudomonas stutzeri*. The cysteine residues of the four conserved heme-binding motives are marked in black.

In the genomes of *S. deleyianum*, *W. succinogenes* and *P. gingivalis*, *nrfH* is located directly upstream of *nrfA*. In contrast to the latter, *nrfH* is hardly homologous to its counterpart from the γ-subdivision of proteobacteria (*nrfB*). Database sequence comparisons show that NrfH belongs to the NirT/NapC family (Berks *et al.*, 1995b; Roldán *et al.*, 1998) of multiheme *c* cytochromes. Located in the periplasm, these globular proteins are supposedly anchored in the cytoplasmic membrane by a single transmembrane α-helix, as replacement of the N-terminal part of NapC by a cleavable export sequence produced a soluble form of the protein (Roldán *et al.*, 1998).

Cytochromes of this family are widely distributed in the bacterial kingdom. They are found in the operons encoding for the systems of periplasmic nitrate reductase (*napC*, (Berks *et al.*, 1995b; Blattner *et al.*, 1997)), dimethylsulfoxide reductase (*dorC*, (Shaw *et al.*, 1996)), trimethylamine-N-oxide reductase (*torC*, (Méjean *et al.*, 1994)), fumarate reductase (*fccC*, (Simon *et al.*, 1998)), cytochrome cd_1 nitrite reductase (*nirT*, (Jüngst *et al.*, 1991)), hydroxylamine oxidoreductase (*cycB*, (Bergmann *et al.*, 1994)) and others. *TorC* and *dorC* are pentaheme proteins (Méjean *et al.*, 1994), but their first four heme-binding motives align well to the other members of the familiy while the fifth is separated from the first four and close to the car-

boxyterminal end of the chain. It has been proposed that these proteins are able to directly mediate electron transport between the membraneous quinone pool and periplasmic reductases and oxidases (Roldán *et al.*, 1998).

Based on the sequence, NrfH could be identified as the small subunit in the M4 form (Schumacher & Kroneck, 1991) of *W. succinogenes* nitrite reductase. Although the N-terminal seemed to be blocked to protein sequencing (Edman & Henschen, 1975), cleavage of the β subunit with cyanogen bromide resulted in a fragment which corresponded to residues 104-109 (KISEDG) in the sequence predicted for NrfH (Simon *et al.*, 2000).

In the same work, the NrfHA complex was reconstituted in liposomes together with the membraneous formate dehydrogenase and menaquinone. These liposomes were found to catalyze electron transport from formate to nitrite, coupled to the generation of an electrochemical proton potential across the liposomal membrane. The obvious conclusion is that in bacteria with the *nrfHAIJ* operon type, the dissimilatory nitrite reductase NrfA forms a membrane-associated complex with its electron donor, NrfH.

5.3.3 *NrfA*; Cytochrome *c* Nitrite Reductase

The first published sequence of a gene for cytochrome *c* nitrite reductase was the one from *E. coli* (Darwin *et al.*, 1993). It was a surprise in so far, as it contained only 10 cysteines, thus ruling out the possiblity for the enzyme to be a hexaheme *c* protein. Subsequently, a discussion started whether or not the NrfA orthologues of different organisms might contain different numbers of heme groups, with suggestions ranging between four (Darwin *et al.*, 1993; Schumacher *et al.*, 1994) and six (Costa *et al.*, 1996). With the sequences obtained in the course of this work and from ongoing genome sequencing projects, we are now able to align a total of seven NrfA sequences from three different groups of bacteria. The result is what seems a highly homologous family of enzymes, conserved in all key features, including the number of heme binding sites, which is five.

All proteins show sequence homologies in the range of 50-60% to each of the others, with the exception of the closely related *S. deleyianum* and *W. succinogenes*, which share a homology of 78% and of *S. typhi* and *E. coli* with a homology of 90%. Sequence-based secondary structure predictions indicate, that all NrfA proteins will share a very similar fold, especially concerning the long α-helical segments in the carboxyterminal part of the gene (Figure 12). A comparison of this secondary structure predictions with the actually observed secondary structural elements in the *S. deleyianum* enzyme shows, that the claimed accuracy of higher than 70 % is actually reached (Rost & Sander, 1993).

All the sequences also share the novel heme binding motif Cys-X_1-X_2-Cys-Lys, which holds the active site heme group of nitrite reductase. Several regions of the protein sequence show a very high amount of conserved residues, the most prominent of which are the ones where the primers described in 5.1 will bind. All residues which were later found to play essential roles in the structure are conserved throughout all sequences. Among them are the active site residues (5.4.5.4), the ones lining the substrate/product channel (5.4.5.5) and the aminoterminal leader sequences for periplasmic export. The obvious consequence is to predict, that cytochrome *c* nitrite reductases are a protein family with a unique and conserved cofactor composition, fold and functionality.

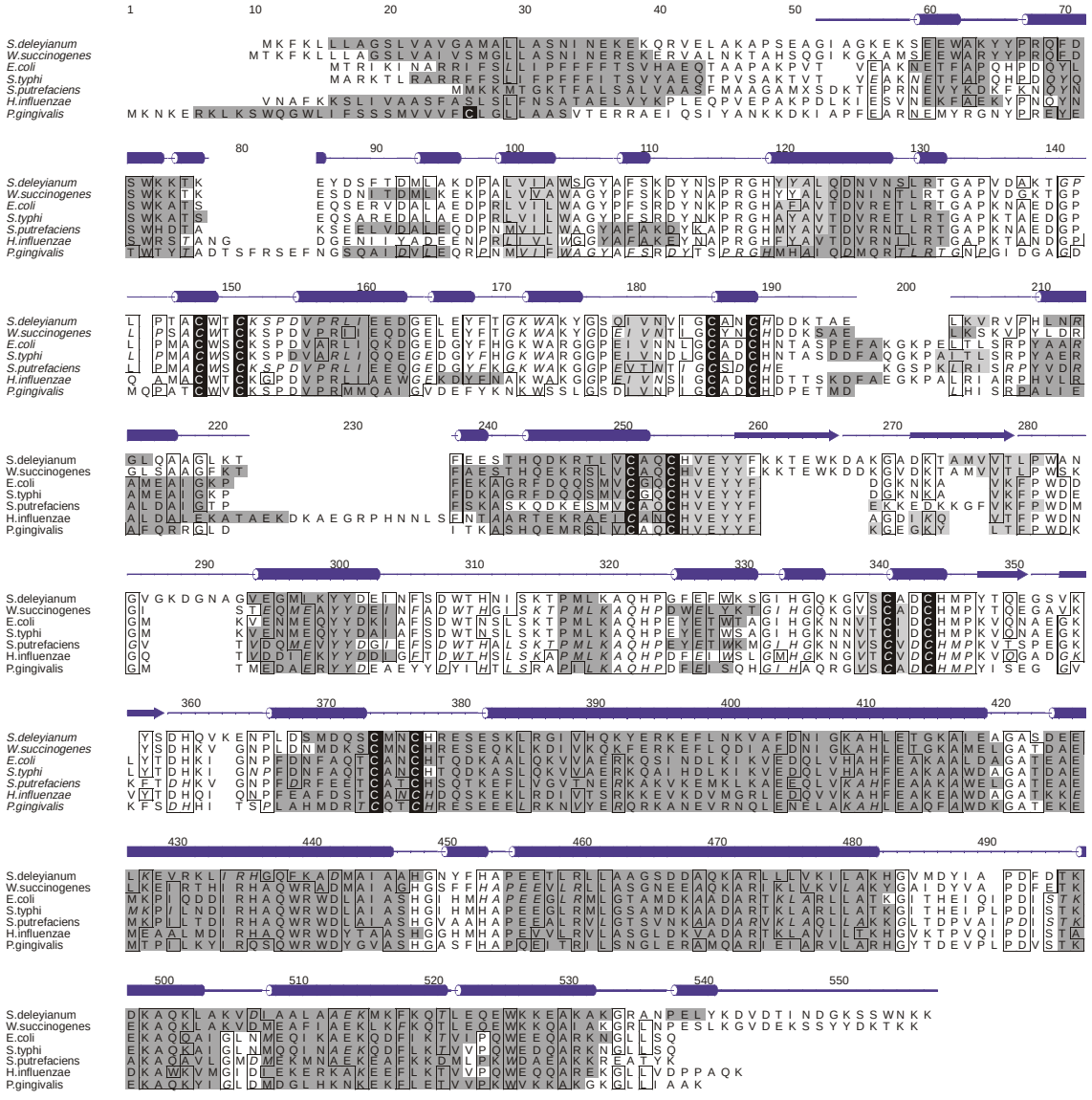

Figure 12: Alignment of the seven known amino acid sequences of NrfA. The secondary structure scheme given is derived from the *S. deleyianum* crystal structure (Figure 20). Conserved residues are boxed and shading is according to PHDSec secondary structure predictions, dark grey for helices and light grey for sheets, emphasizing that those proteins form a familiy with a high degree of structural homology.

5.3.4 *NrfI*; Heme Transport

The last two genes in the *nrfHAIJ* operon are not part of the membrane-associated nitrite reductase complex. *NrfI* encodes for an integral membrane protein of 902 amino acids (*W. succinogenes*). Database searches yield the highest homology to the predicted *ccsA* gene from *Helicobacter pylori* (936 aa, 36% sequence identity). The C-terminal part of *nrfI* is similar to CcsA

proteins of chloroplasts and Gram-positive bacteria, which usually have a size of 300-350 residues and show a sequence identity to *nrfI* in the range of 25-30%. The N-terminal part of *nrfI* shows a weak resemblance to Ccs1 proteins, suggesting that the *nrfI* gene (as well as *H. pylori ccsA*) is the result of a gene fusion.

CcsA and Ccs1 are the essential transmembrane proteins of the cytochrome *c* biogenesis system of ε-proteobacteria, Gram-positive bacteria, chloroplasts and cyanobacteria (Kranz *et al.*, 1998). They supposedly form a heme transporter that carries the free, reduced protoheme IX group across the cytoplasmic membrane to be attached to the unfolded apocytochrome which is independently exported via the *sec* system (Duong *et al.*, 1997; Pohlschröder *et al.*, 1997). Characteristically, CcsA-like proteins contain a tryptophan-rich motif with the core consensus sequence **WG**x**W**x**WD** and at least two conserved histidines (Goldman *et al.*, 1998; Xie & Merchant, 1996). These elements are essential for heme delivery, as the tryptophans might provide a hydrophobic environment for the porphyrin, while the histidines ligate the ferrous iron to avoid its oxidation, as only ferrous heme seems to be attached to apocytochromes by this system (Nicholson & Neupert, 1989). In the sequence of NrfI from *W. succinogenes*, the sequence **WG**RY**W**A**WD** is found at position 796.

5.3.5 *NrfJ*; A Crippled Thioredoxin?

Apart from CcsA and Ccs1, the cytochrome *c* maturation system of ε-proteobacteria consists of at least two further genes, *resA* and *ccd1*, the function of which is not yet fully understood. ResA encodes for a thiol-disulphide oxidoreductase that is located in the periplasm or plastid intermembrane space and anchored in the membrane with a single N-terminal helix. The analogy of this to the more closely studied Ccl2 (CcmH) protein of the γ-proteobacterial cytochrome *c* maturation system (Monika *et al.*, 1997)

suggests, that its role is the reduction of cysteinyl residues of the apocytochrome *c* while it is presented to the heme group.

In the Gram-positive *Bacillus subtilis*, the orthologues of Ccs1 and CcsA were called ResB and ResC, respectively, and are organized in an operon together with ResA (Sun *et al*., 1996). A fourth gene, *ccdA*, which is not linked to the *res* operon in *B. subtilis* (but is in several other species), is required at a late stage in cytochrome *c* maturation (Schiött *et al*., 1997). CcdA is related to the disulphide isomerase protein DipZ from *E. coli*, which has been hypothesized as being involved in the transfer of reducing equivalents across the membrane (Crooke & Cole, 1995).

The *nrfJ* gene poduct, consisting of 217 residues in *W. succinogenes*, shows similarities to ResA of *B. subtilis* as well as to its presumed orthologues in the genomes of *Mycobacterium* sp., *Synechocystis* sp. 6803 and *Aquifex aeolicus*. Like those typical ResA proteins, *nrfJ* is predicted to carry an N-terminal transmembrane helix, but it does not contain any cysteine residues and therefore lacks the typical Cys-X_1-X_2-Cys motif that is believed to be essential to actually reduce apocytochromes. Interestingly, *nrfJ* also shares 20% sequence identity and 43% homology to ORF HP0377 of the *H. pylori* genome sequence, which is located directly upstream of the *ccs1*/*ccsA* fusion protein.

Based on the sequence, mutants of *W. succinogenes* were constructed to investigate the function of the novel genes *nrfI* and *nrfJ* (Simon *et al.*, 2000). While a Δ*nrfIJ* mutant lost its ability to reduce nitrite to ammonia, the mutant Δ*nrfJ* showed a phenotype that could not be distinguished from the wild type. Furthermore, it was found that while NrfH was seemingly unchanged in the Δ*nrfIJ* mutant, NrfA was still synthesized, but its heme content was reduced compared to the active enzyme obtained from both wild type strain and Δ*nrfJ* mutant. While this observation confirms the presumed involvement of NrfI in the attachment of the active site heme group of NrfA, it also indicates that *nrfJ* might be a pseudogene, derived from a *resA*

orthologue, but with no essential function in the nitrite ammonification system.

5.3.6 The *nrf* Operon of *Porphyromonas gingivalis*

When checking databases of unfinished genome sequencing projects, it was a surprise to find a highly conserved *nrfA* gene outside of the Proteobacteria group for the first time. *Porphyromonas gingivalis*, a Gram-negative anaerobe, is associated with chronic and severe periodontitis and is a member of the Cytophagales/Flavobacter/Bacteroides phylum of Eubacteria (Paster *et al*., 1994; Woese, 1987). The *nrf* operon of this organism starts with a promoter region that can be well aligned to the other known *nrf* promoters (Figure 10). The first gene that follows is *nrfH*, supposedly coding for a tetraheme *c*-type cytochrome of 204 amino acids, which is homologous to the *nrfH* gene products of *S. deleyianum* (49%, with 43% sequence identity) and *W. succinogenes* (53% with 45% sequence identity). *NrfA*, the following gene is a typical member of the family, with sequence similarities of 50-60% to the other *nrfA* genes.

As expected, the following genes are related to cytochrome *c* maturation, but at this point the *P. gingivalis* operon differs from the two known types. Three further genes are following *nrfA* after a gap of 74 residues, and as their open reading frames are overlapping they can be assumed to form a transcriptional unit. In continuation of the established nomenclature, those three genes have been named *nrfK*, *nrfL* and *nrfM*. The easiest gene to identify is *nrfM*, which is a typical homologue of *ccsA*, including the tryptophan-rich motif **WG**TY**W**N**WD** at position 200. It aligns with other *ccsA* genes as well as with the C-terminal part of *nrfI* with a similarity of 43% and an identity of 31% in a 203 aa overlap. Thus, *nrfM* can be assumed to be a special heme transporter for the active site heme of NrfA, analogous to *nrfI* and *nrfE*.

The case is more difficult for *nrfK* and *nrfL*, both of which do not produce any clear matches in database searches. However, there is a low similari-

ty between *nrfL* and Ccs1 proteins and it does align to the Ccs1-like region of NrfI with a homology of 23% over a stretch of 114 residues. The C-terminal part of *nrfK* can be aligned to the N-terminus of *nrfI*, but this mapping of *nrfK*, *nrfL* and *nrfM* on *nrfI* leads to an overlap of *nrfK* and *nrfL* and a gap of 300 residues between *nrfL* and *nrfK*. Obviously, a simple fragmentation of *nrfI* is not sufficient to explain the existence of *nrfKLM* in the *P. gingivalis* operon, but the function of the three genes can be expected to correspond to *nrfI*.

Note that a search in the preliminary genome sequence of *P. gingivalis* did not produce any other CcsA-like proteins so far. Most likely, the genes in the *nrf* operon do not represent the only heme transporting sytem in the genome. This is indicated by the presence of *c*-type cytochromes in a Δ*nrfIJ* mutant of *W. succinogenes*, but the corresponding genes remain to be identified.

5.4 The Crystal Structure of NrfA

5.4.1 Purification of Nitrite Reductase for Crystallization

Different preparations of nitrite reductase showed a remarkable variance in crystallization properties, ranging from large single crystals grown under different conditions without seeding (Hammann, 1994) to no crystal growth at all, even with the help of microseeding. The regular purification procedure included polyethylene imine precipitation, followed by DE52 anion exchange and hydroxyl apatite column chromatography. The resulting protein was usually purified further by a gel filtration step, but a minor amount of impurities remained. To improve purity of the protein, different buffer conditions for this gel filtration were tested on a SMART system before a large-scale preparation on a Pharmacia FPLC system.

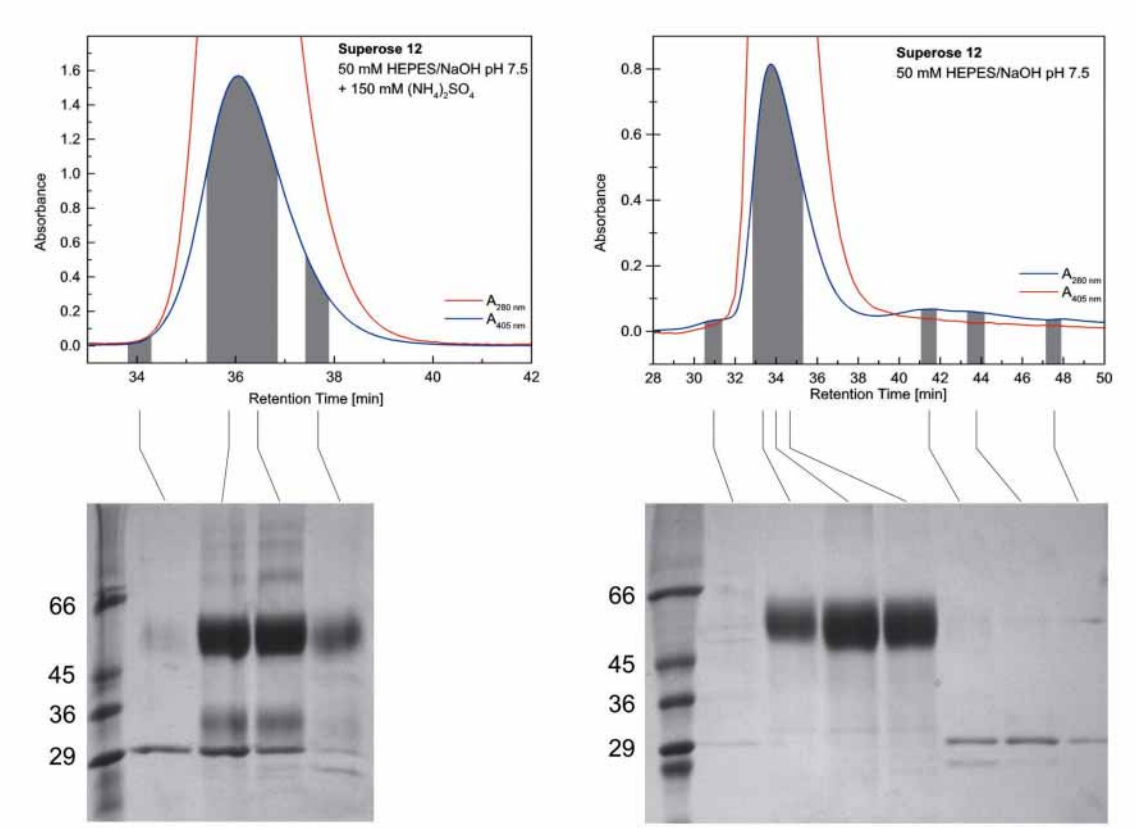

Figure 13: Optimization of the final gel filtration step to increase purity of nitrite reductase. While the enzyme and impurities adhere on a gel column run with a buffer containing ammonium sulfate (**left**), nitrite reductase separates from the smaller proteins when run without salt (**right**). Note that, according to the A_{405} line in the right spectrum, these impurities do not show any heme absorption and can thus not be accounted to small amounts of NrfH in nitrite reductase preparations from the soluble fraction.

Under the established conditions (Schumacher & Kroneck, 1991) using a buffer containing ammonium sulfate, it was not possible to separate the remaining impurities from the enzyme. This was only achieved after using a salt-free buffer (Figure 13, left). The procedure could be scaled up on a Superdex 200 gel filtration column and produced more than 60% of the applied protein in a central pool that did not show additional bands on silver-stained SDS-PAGE gels.

As the use of salt in gel filtration buffers is intended to weaken ionic interactions between proteins and in turn favour hydrophobic interactions, this finding indicates that the impurities in nitrite reductase preparations interact in the latter way. As the structure showed (see 5.4.5.9), crystal pak-

king is dependent on nitrite reductase dimers interacting via their hydrophobic "underside". It seems likely, that impurities binding to nitrite reductase at this place will have a negative effect on crystal growth. The purified protein was used for crystallization experiments, which were successful and produced bigger crystals than without this additional step, but the increased purity was not sufficient to overcome the need for microseeding.

The gel filtration experiments furthermore demonstrated, that the 20 kDa band, which frequently appeared in preparations of nitrite reductase from the soluble fraction, shows no absorption at 405 nm and can thus not be NrfH, the electron donor of nitrite reductase, which is a tetraheme *c*-type cytochrome.

5.4.2 Crystallization

Crystals of spacegroup $P2_12_12_1$, as described by Meininghaus (1996), were used for microseeding. Although this led to several new conditions with large crystals, it was not possible to cool them in a nitrogen stream. The best data set collected thus had a limiting resolution of only 3.8 Å due to crystal degradation. One possible explanation for the lower diffraction quality might be the higher solvent content, 69 %, at a Matthews parameter V_M of 3.17 $Å^3$/Da (Matthews, 1968) for six monomers in the asymmetric unit.

As it turned out, the key to obtaining good crystals of nitrite reductase required concentrating of the protein solution to concentrations higher than 20 $mg \cdot ml^{-1}$. It can be assumed that nitrite reductase isolated from the soluble fraction, which has been described as an active monomer (Schumacher & Kroneck, 1991), needs high concentrations to quantitatively form the dimer that can be observed in all crystal forms known so far. This effect could also be observed in *W. succinogenes* nitrite reductase, where no crystals grew unless the protein solution was concentrated.

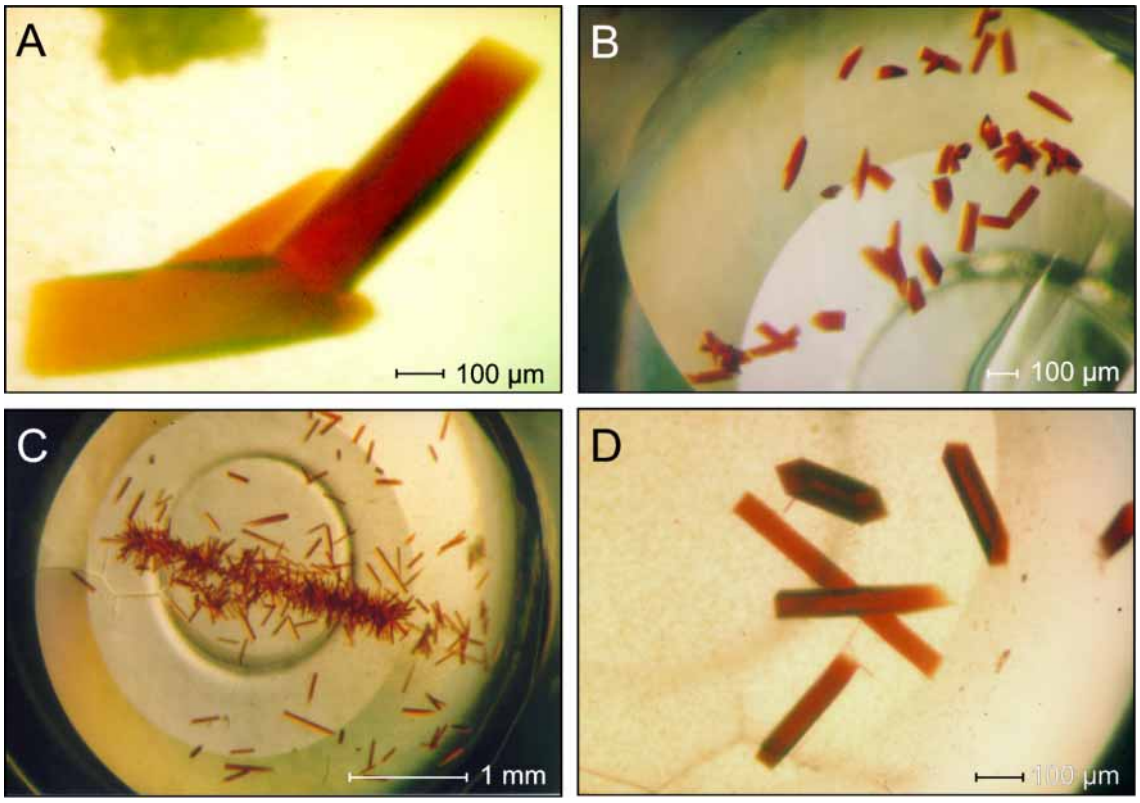

Figure 14: Crystals of cytochrome *c* nitrite reductase from *S. deleyianum* obtained by microseeding. **A**) Large crystals of the $P2_12_12_1$ crystal form with 6 monomers per asymmetric unit. From these crystals, data was collected to 3.8 Å. **B, C, D)** Crystals of the $P2_12_12$ form with 3 monomers per asymmetric unit. Small crystals (B) were optimized by several seeding steps to get large, well-diffracting single crystals (D). When too many seeds were transferred, a large number of small crystals grew where the rabbit whisker was streaked through the drop (C).

Well-diffracting crystals of *S. deleyianum* nitrite reductase were obtained through microseeding and belonged to spacegroup $P2_12_12$ with unit cell dimensions of **a** = 107.5 Å, **b** = 185.3 Å and **c** = 92.2 Å. This crystal form was used to solve the structure of the protein as well as for soaking experiments. With three monomers of 58.6 kDa in the asymmetric unit, the Matthews parameter for this crystal form was V_M = 2.61 Å^3/Da (Matthews, 1968), corresponding to a solvent content of 53 %.

Organism	Space Group		a [Å]	b [Å]	c [Å]	d_{min} [Å]	V_M [Å^3/Da]	mol. / a.u.
S. deleyianum	$P2_12_12_1$	(19)	136.4	145.6	228.1	3.8	3.17	6
S. deleyianum	$P2_12_12$	(18)	107.5	185.3	92.2	1.9	2.61	3
W. succinogenes	$I\,4_122$	(98)	119.1	119.1	186.5	1.6	2.83	1

Table 4: An overview of the nitrite reductase crystal forms obtained and characterized in the course of in this work. Crystal packing of these cells is discussed in 5.4.5.9.

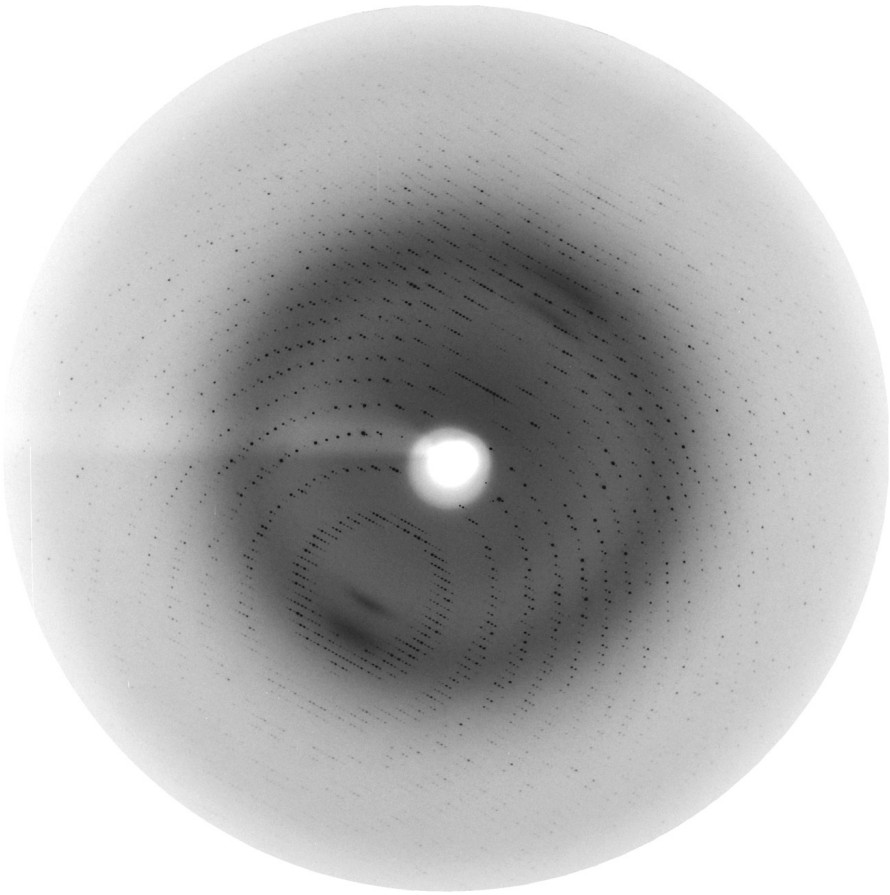

Figure 15: Diffraction image of the *S. deleyianum* nitrite reductase crystal which was used for the MAD experiment. The image was recorded on a MarCCD detector on beamline BW6 at DESY, Hamburg with a rotation of 0.5° during exposure and a crystal mosaicity of approximately 0.3°. The detector edge corresponds to a limiting resolution of 1.85 Å at an X-ray wavelength of 1.05 Å.

Crystallization experiments with *W. succinogenes* nitrite reductase were carried out with protein prepared from the soluble fraction of the cells as well as from the membrane extract. The two distinct preparations both showed a strong 20 kDa band on SDS-PAGE, which was not present in preparations of *S. deleyianum* nitrite reductase purified from the soluble fraction. However, the crystals obtained only had the NrfA protein. They belonged to space group $I4_122$, containing a single monomer per asymmetric unit in a cell of **a** = **b** = 119.1 Å and **c** = 186.5 Å. In spite of a Matthews parameter of V_M = 2.83 Å^3/Da – corresponding to a rather high solvent content of 57% – the crystals were stable and well ordered and diffracted to resolutions better than 2.0 Å on a rotating anode X-ray source.

5.4.3 Nitrite Reductase from *S. deleyianum*

5.4.3.1 MAD Data Collection

As a prerequisite for MAD data collection, an X-ray fluorescence scan was carried out to determine the exact position of the K-shell iron absorption edge of *S. deleyianum* nitrite reductase. The observed edge was shifted compared to the theoretical expectations for free iron (as derived from the equation of Kramers and Kronig) by approximately +18 eV and showed a distinct EXAFS feature.

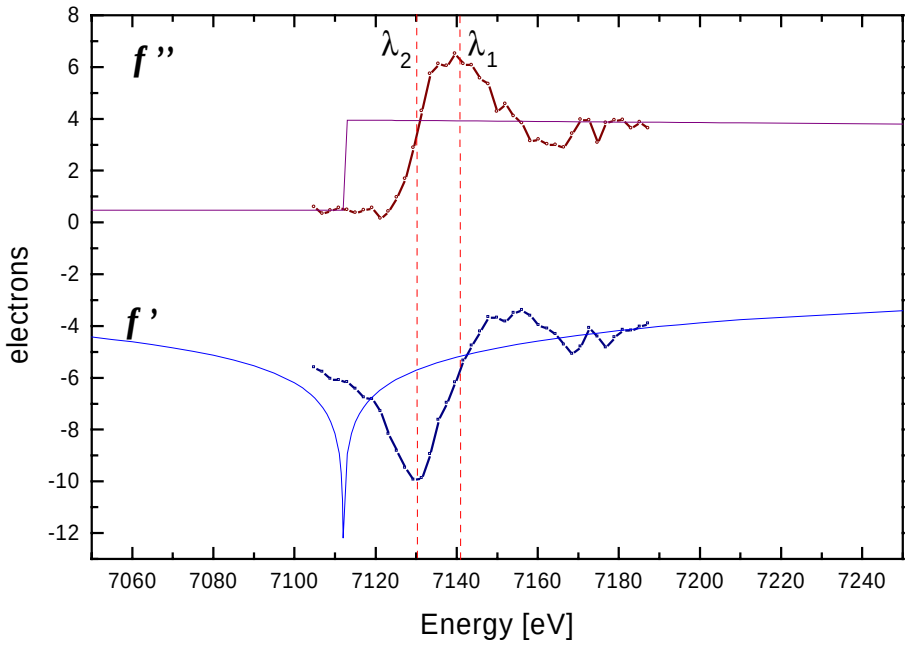

Figure 16: Choice of wavelengths for the MAD experiment. The theoretical values for the iron absorption edge as obtained from the equation of Kramers and Kronig and the actual X-ray fluorescence scan of the nitrite reductase crystal show a shift of 18 eV. Wavelengths for data collection were chosen to maximize the anomalous *f''* contribution and the dispersive *f'* inflection, respectively.

According to this scan, the wavelengths for MAD data collection were chosen, λ_1 = 1.7362 Å to maximize the anomalous f'' contribution of the iron atoms and λ_2 = 1.7390 Å at the peak of the f' inflection. A third, remote, dataset was collected at the intensity maximum of the synchrotron radiation

at λ_3 = 1.0500 Å. In order to optimize completeness of Friedel pairs, two 90° oscillation sets were measured at each λ_1 and λ_2 with a difference of 180°. The rotation angle for every single image was 0.5° to avoid spot overlap.

5.4.3.2 Self-rotation Function

A self-rotation function of the remote data set of *S. deleyianum* nitrite reductase was calculated with the program GLRF (Tong & Rossman, 1990). It shows a non-crystallographic twofold symmetry axis almost perpendicular to the **a**-axis of the unit cell. To accomodate three molecules in the asymmetric unit, two of which form a non-crystallographic dimer, it was likely to assume that the third monomer forms a dimer using a crystallographic twofold axis.

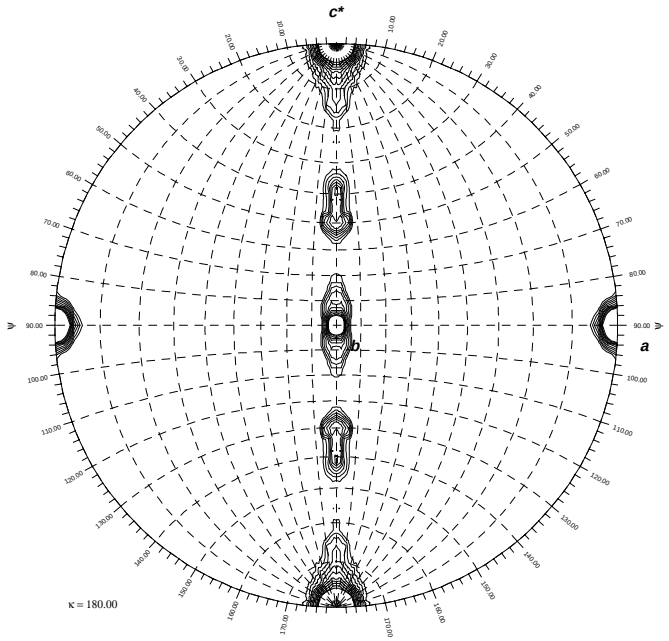

Figure 17: Polar plot of a self-rotation function for a twofold correlation (κ = 180°) of *S. deleyianum* nitrite reductase. In the orthogonalization convention used, the real space **a** axis coincides with the Cartesian **x** axis, **b** coincides with **y** and **c*** with **z**.

5.4.3.3 Location of the Iron Positions

Difference Patterson maps were calculated for the dispersive differences of the (f' – remote) datasets as well as for the anomalous differences in all three datasets using the program FFT (Collaborative Computational Project

No. 4, 1994). As expected, the anomalous difference Patterson maps of the f'' dataset showed the most favorable signal-to-noise ratio.

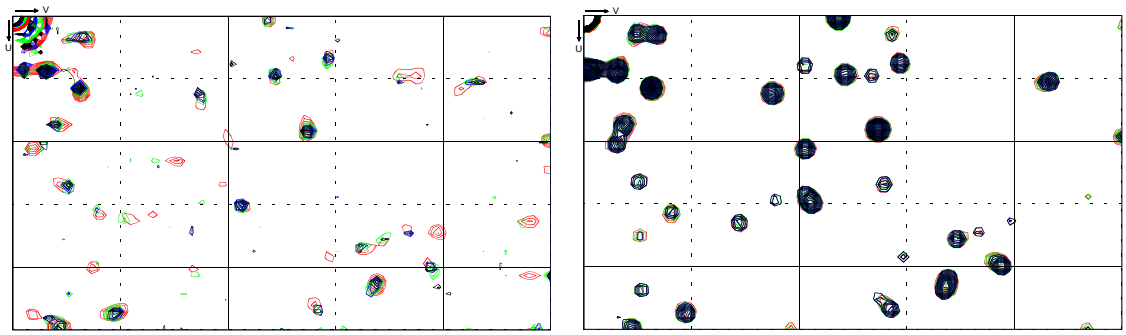

Figure 18: Plots of the **w** = 0 Harker section of the anomalous difference Patterson map for the f'' dataset of *S. deleyianum* nitrite reductase, calculated with different high resolution limits (red: 5.0 Å, green: 4.0 Å, blue: 3.0 Å, black: 2.3 Å). The left side shows the experimental map, the right side is a theoretical map calculated from the correct iron positions. The origin of the maps is in the upper left corner. Note the low noise in the experimental map. Structure factors were calculated with SFALL and Patterson maps with FFT. The plots were done with NPO (all programs from CCP4 (Collaborative Computational Project No. 4, 1994)).

Resolution-independent peaks were present in all three Harker sections of space group $P2_12_12$, **u** = ½, **v** = ½ and **w** = 0. Cross-vector verification, manually as well as with the program RSPS (Collaborative Computational Project No. 4, 1994), helped to find a first set of four putative iron positions which were then used for phasing with MLPHARE (Collaborative Computational Project No. 4, 1994). The highest peaks from the resulting Fourier map were analyzed for consistency with the anomalous difference Patterson map and, if correct, used for a new cycle of phase calculations. Thus it was possible to successively find 15 iron positions which divided into three groups of five and produced a sensible packing when the spacegroup's symmetry operations were applied.

5.4.3.4 Phase Calculations

When trying to obtain phases for model building, MLPHARE did not produce interpretable electron density maps, so the program SHARP (La Fortelle *et al.*, 1997) was used, resulting in a phasing power of 3.0 and a figure of merit of 0.54 over the whole resolution range of anomalous data

(Table 5). The according values obtained with MLPHARE were 1.6 and 0.42, respectively.

Wavelength [Å]	Resolution limits [Å]	Completeness [%]	R_{merge} [%]*	*f'*	*f''*	Phasing power$_{iso}$†	Phasing power$_{ano}$‡	R_{Cullis}‖	R_{Kraut}¶
1.0500	1.9	98.9	10.5	0.2	1.7		0.95		21.9
1.7362	2.3	99.9	11.8	-5.8	6.0	2.71	0.65	59.6	66.7
1.7390	2.3	98.5	10.0	-10.0	3.5	3.00	1.12	55.8	52.0

Table 5: MAD phasing statistics. * $\boldsymbol{R}_{\text{merge}} = \sum_{hkl}\left|\langle I\rangle - I\right| / \sum_{hkl}|I|$; † isomorphous phasing power = $\sum_n |F_H| / \sum_n |E|$ where $|F_H|$ is the calculated structure factor amplitude of the heavy atom structure and E is the residual lack of closure error; ‡ anomalous phasing power = $2\sum_n |F_H''| / \sum_n |E|$ where $|F_H''|$ is the anomalous contribution amplitude; ‖ $\boldsymbol{R}_{\text{cullis}} = \sum_{hkl}\left\|F_{PH} \pm F_P| - |F_{H(calc)}\right| / \sum_{hkl}|F_{PH} \pm F_P|$ for centric reflections and isomorphous contributions; ¶ $R_{\text{Kraut}} = \sum_{hkl}\left\|F_{PH}| - |F_P^{\pm} + F_{H(calc)}^{\pm}\right\| / \sum_{hkl}|F_{PH}|$ for anomalous scattering contributions.

At this stage, the electron density maps were clearly interpretable, characteristic features such as α-helices and the planar heme groups could be distinguished.

5.4.3.5 Electron Density Modifications

To facilitate model building, a bulk solvent correction was carried out with SOLOMON (Abrahams & Leslie, 1996). A single round of electron density averaging between the monomers was done using the program AVE (Kleywegt, 1996). This led to an electron density map of sufficient quality to build a complete model including all sidechains before any further refinement.

5.4.3.6 Model Building and Refinement

For crystallographic refinement and electron density map calculations, X-PLOR (Brünger, 1992) was used with Engh and Huber parameters (Engh & Huber, 1991). In addition, a molecular dynamics torsion angle refinement based on maximum likelihood algorithms was carried out with the develop-

ment version 0.3 of the Crystallography and NMR System CNS (Brünger *et al.*, 1998).

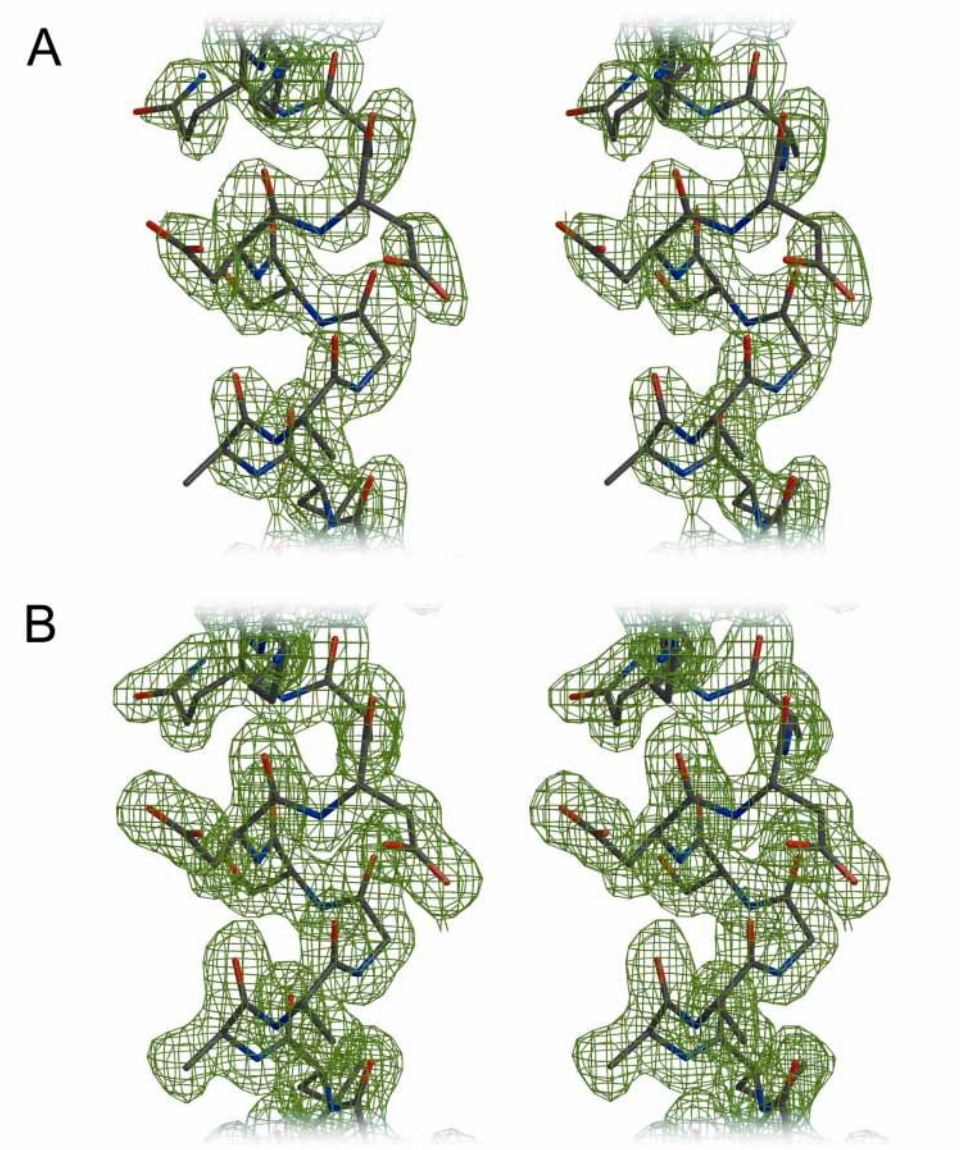

Figure 19: Exemplary electron densities. **A**) The experimental density of *S. deleyianum* nitrite reductase after MAD phasing, solvent flattening and threefold real-space averaging. This density was used to build the complete model including all sidechains. **B**) The same region of the protein with the final, refined $2F_o–F_c$ electron density contoured at 1.0 σ. The pictures show the central region of helix *h*25, which is crucial for dimer formation.

After building the complete model, the structure refined to a crystallographic *R*-Factor (R_{free}) of 0.281 (0.328). 1485 water molecules and 9 sulfate ions were built and the *R*-Factor (R_{free}) was refined to its final value of 0.184

(0.220) at a resolution of 1.9 Å. Non-crystallographic symmetry restraints were only applied in the first refinement cycles.

5.4.3.7 A Second Crystal Form

Once the structure of *S. deleyianum* nitrite reductase was solved it could be used to find a molecular replacement solution in the data of the crystal form described by Meininghaus (1996). The program AMoRe produced a solution with six monomers per asymmetric unit.

Although the resolution of 3.8 Å limits the amount of information that can be obtained from the structure, it should be noted that the hexamer which builds up the asymmetric unit is the same as the one found in the better diffracting $P2_12_12$ crystals. There the hexamer is built by the three monomers in the asymmetric unit and a crystallographic twofold axis.

5.4.4 Nitrite Reductase from *W. succinogenes*

Crystallization of *W. succinogenes* nitrite reductase depended on two factors: (i) on protein concentration as in the case of the *S. deleyianum* enzyme, and (ii) on the presence of yttrium ions. As it can be seen from the crystal packing (5.4.5.7), yttrium plays a crucial role in mediating crystal contacts.

5.4.4.1 Data Collection and Molecular Replacement

Crystals proved to be of sufficient quality to collect data to a limiting resolution of better than 2 Å on a rotating anode X-ray source. Molecular replacement with the nitrite reductase model from *S. deleyianum* produced a clear solution with a correlation of 69.6 % and an *R*-factor of 30.6 % for one monomer per asymmetric unit.

In most cases soaking of small molecules into these crystals did not alter the diffraction properties. Thus it was possible to analyze the binding of

different substrates or potential reaction intermediates to the active site of the enzyme.

Compound		Conc. used [mM]	Soaking time [h]	d_{min} [Å]	Reflections	Completeness [%]	R_{merge} [%]
sulfate*	(native)	–	–	1.6	83 904	95.1	8.4
nitrite*	($NaNO_2$)	100	12	1.7	68 553	93.4	7.3
azide*	(NaN_3)	100	2	1.6	81 570	92.2	7.6
hydroxylamine	(H_2NOH)	50	2	2.0	45 781	99.5	8.3

Table 6: Substrate complexes of *W. succinogenes* nitrite reductase that were prepared and analyzed in this work. * synchrotron data measured in DESY/Hamburg on beamline BW6.

Nitrite, as the physiological substrate of nitrite reductase and hydroxylamine as a postulated reaction intermediate were chosen to monitor the reaction pathway and elucidate the protein residues involved in substrate binding. Azide was known to inhibit the activity of nitrite reductase.

5.4.4.2 Model Building and Refinement

After replacing the amino acids in which the *S. deleyianum* model differed from the *W. succinogenes* structure and a first round of positional refinement, six additional residues, 37 – 41, could be built at the N-terminal of the peptide chain. This is most likely due to His 39 in the *W. succinogenes* sequence, which is hydrogen-bonded to O_η of Tyr 65 with its $N_{\varepsilon 2}$ and to the backbone oxygen of Asp 173 with its $N_{\delta 1}$, thus fixing this part of the sequence to the protein. Residue 39 is a serine in the *S. deleyianum* sequence and is not ordered in the crystal. Refinement of the structure was carried out with the development version 0.9 of CNS (Brünger *et al.*, 1998), using torsion angle molecular dynamics and conjugate gradient positional methods. Secondary structure calculations and quality assessments were done with PROCHECK (Laskowski *et al.*, 1993).

5.4.5 Description of the Structure

5.4.5.1 Overall Structure

Cytochrome *c* nitrite reductase is a dimeric enzyme of ~ 100 Å × 80 Å × 50 Å, with ten heme groups in remarkably close packing (Figure 20). The protein folds into one compact domain, with α-helices as the predominant secondary structural motif, ranging from short helical turns to four long helices near the C-terminal end of the peptide chain. Eight 3_{10} helices of three or four residues in length are observed, seven of which occur within the first 200 residues. β-sheet structures are found only in short, antiparallel strands, where one is part of a funnel-like cavity leading to the active site.

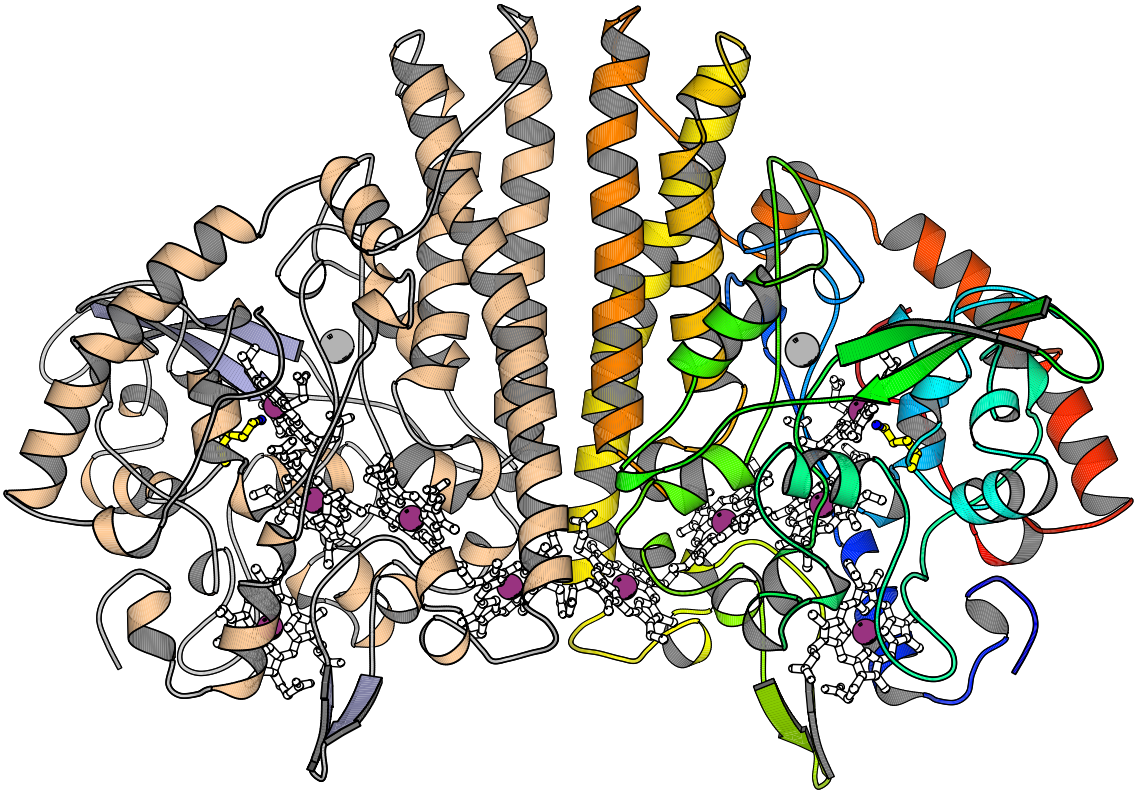

Figure 20: The nitrite reductase dimer. A front view of the enzyme from *S. deleyianum* with the dimer axis oriented vertically, the five hemes in each monomer (white), the Ca^{2+} ions (grey) and Lys 133 which coordinates the active-site iron atom (yellow). In the right monomer, the protein chain is coloured blue from the amino-terminal end to red at the carboxy-terminal end, in the left monomer according to secondary structure. The dimer interface is dominated by three long α-helices per monomer. All hemes in the dimer are covalently attached to the protein and their iron atoms are arranged almost in a plane parallel to the plane of the paper.

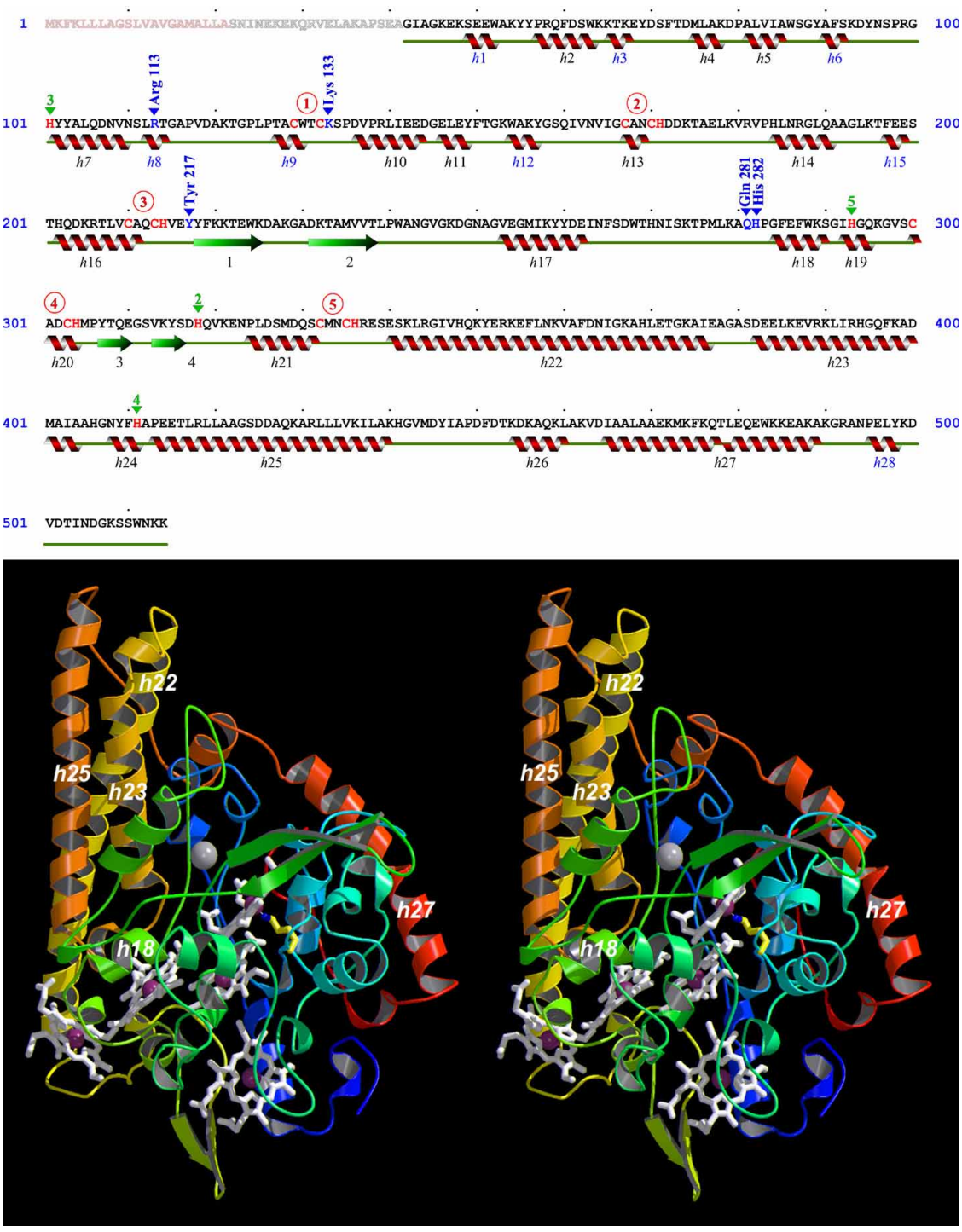

Figure 21: Primary, secondary and tertiary structure of *S. deleyianum* nitrite reductase. The five hemes are attached to the cysteine motives which are numbered according to their occurence in the sequence in red circles. The sixth histidine ligands of hemes 2 to 5 are indicated by green letters. The sequence outlined in red at the aminoterminal end of the chain is the leader peptide for periplasmic export. In the crystal structure the chain is visible from residue 42 onward. The residues in blue are active site residues. The secondary structure depicted below the sequence was derived from the crystal structure. Type 3_{10} helices are in blue, while α-helices are labelled in black. The stereo image represents a nitrite reductase monomer in an orientation identical to the right monomer in Figure 20.

Dimer formation is mediated by helices *h*22 and *h*25 with helix *h*25 as the key element, as it interacts with its counterpart in the other monomer over its full length of 28 residues corresponding to 42 Å. The contact surface has an area of 1674 $Å^2$ or 8.5% of the total accessible surface area of a monomer.

5.4.5.2 Differences between *S. deleyianum* and *W. succinogenes*

As expected from amino acid sequence comparisons, the structures of nitrite reductase from both organisms are very similar. A root mean square displacement of 1.19 Å for the C_α atoms has to be considered in the light that the three 'identical' monomers in the asymmetric unit of the *S. deleyianum* crystals themselves have a root mean square displacement of the C_α atoms of 0.37 Å among each other. The main differences in the peptide chain are two insertions in the *S. deleyianum* protein, one of 5 residues (245 to 251) and another one of one residue (321), both of which are unique to the *S. deleyianum* sequence and do not occur in either one of the other six NrfA sequences (Figure 12).

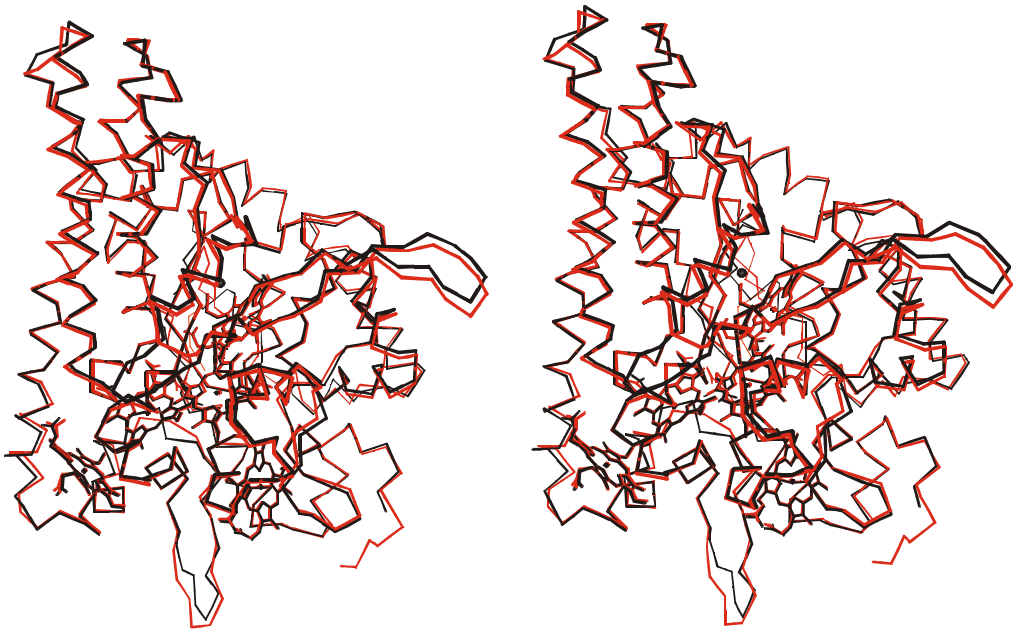

Figure 22: C_α-trace superposition of *S. deleyianum* (black) and *W. succinogenes* (red) nitrite reductases. The overall RMSD of the C_α atoms is 1.19 Å.

Apart from these insertions and the additional residues at the N-terminus of the *W. succinogenes* polypeptide chain, a further major difference is the C-terminus of the chain, which forms an α-helix in *S. deleyianum* and a short two-stranded β-sheet in *W. succinogenes*. The residues that surround the active site and form the substrate/product channel are completely conserved.

5.4.5.3 Heme Cofactor Arrangement

The five hemes in the monomer of cytochrome *c* nitrite reductase are in close contact, with Fe-Fe distances between 9 and 12.7 Å (Figure 23). They are arranged as a group of three almost coplanar hemes (1, 3, 4), with heme 1 forming the active site. Hemes 2 and 5 are further apart and are not coplanar with heme 1, 3 and 4. All hemes except heme 1 are bis-histidinyl-coordinated and are linked to the peptide backbone via thioether bonds to the cysteine residues of a classical heme-binding motif for periplasmic proteins, Cys-X_1-X_2-Cys-His.

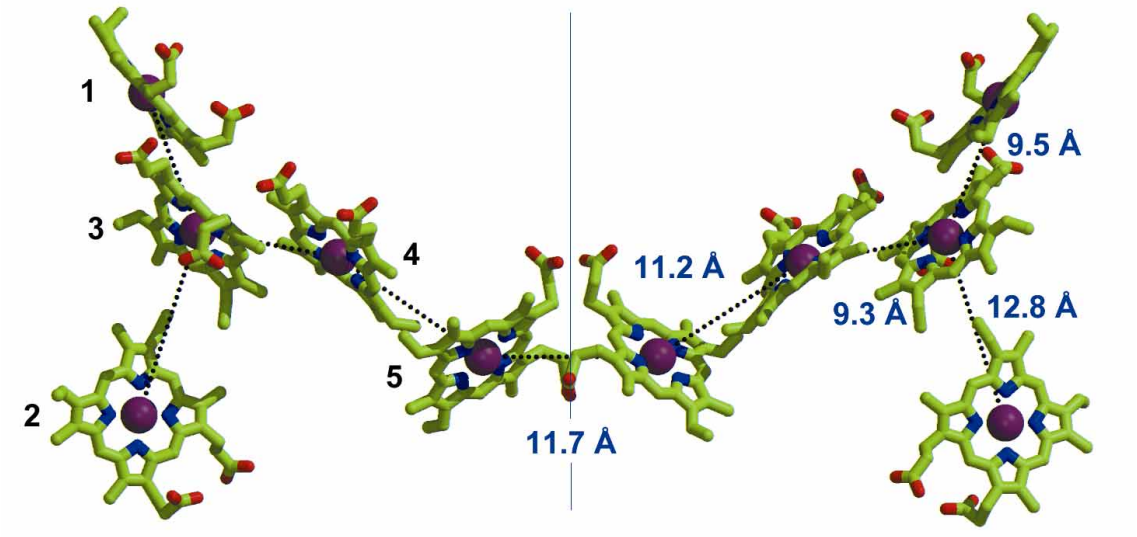

Figure 23: Heme arrangement. The overall orientation corresponds to Figure 20, with the active site located at heme 1 and the line indicating the dimer interface. Hemes in the left monomer are numbered according to their attachment to the protein chain. In the right monomer, the Fe-Fe distances between the hemes are given. Hemes 5 interact across the dimer interface with a distance closer than hemes 2 and 3 within each monomer.

With edge-to-edge distances below 4 Å, hemes 1, 3 and 4 are close enough to allow direct π-electron interaction of the porphyrin rings. The propionate sidechains of heme 4 are exposed to the solvent, while those of heme 3 are hydrogen-bonded inside the protein and those of heme 1 take part in forming the active site cavity. All heme groups show a slight distortion from ideal planarity in the porphyrin plane, most strongly in heme 2 and least in the only slightly saddled active site heme 1.

The five heme groups of *W. succinogenes* nitrite reductase align with the ones of the *S. deleyianum* enzyme within a root mean square displacement of 0.12 Å for all atoms. They will thus be considered identical in all subsequent discussions and comparisons. Residues are given in the numbering of the *S. deleyianum* sequence, with the *W. succinogenes* numbers in brackets if different.

5.4.5.4 The Active Site

The site of nitrite reduction is clearly heme 1, with the Nζ atom of lysine 133 (134) coordinating the iron atom, replacing a histidine in the classical binding motif (Figure 24), and a sulfate anion from the crystallization buffer bound in the sixth coordination position. This novel type of heme iron coordination is observed here for the first time and nitrite reductase is the only case known so far where a lysine appears as part of an otherwise classical heme binding motif.

A lysine-coordination had been proposed for cytochrome *f* of the photosynthetic cytochrome b_6f complex (Davis *et al.*, 1988), but the structure solution showed, that the spectroscopically observed amine nitrogen stems from the N-terminal end of the peptide chain and not from a lysine (Martinez *et al.*, 1994). Furthermore, a M100K mutant of the monohemic *Thiobacillus versutus* cytochrome c_{550} has been described, where the heme-ligating methionine has been engineered into a lysine (Ubbink *et al.*, 1994), postulating a heme-lysine coordination that shifts the heme's redox potential by –329 mV. However, a structure of the mutant is not available.

On the distal side of the heme group, three protein residues surrounding the active site heme are in a position to interact with bound substrate: Arg 113 (114), Tyr 217 (218) and His 282 (277).

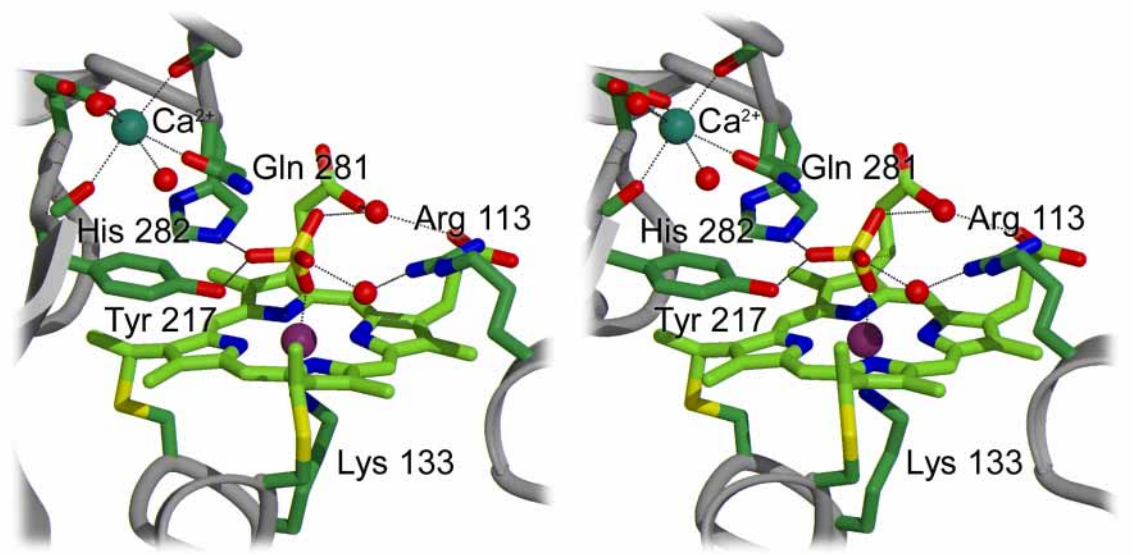

Figure 24: Stereo view of the active site of *S. deleyianum* nitrite reductase. A view is given from the protein surface down the active site channel. Tyr 217 and His 282 bind sulfate, an inhibitor of nitrite reductase activity. A Ca^{2+} ion close by bridges stretches of protein which hold these two residues.

An additional electron density maximum was detected close to the active site which was – due to bond distances and coordination geometry – assigned to Ca^{2+}. This was confirmed by ICP mass spectroscopy, which yielded 1.0 ± 0.1 atoms of Ca^{2+} per monomer of nitrite reductase.

The Ca^{2+} ion is coordinated by the carboxy group of Glu 216 (217) in a bidentate manner, by Gln 281 (276), by two peptide carbonyl oxygens and by two water molecules. Sulfate binds to the iron with an oxygen atom at a bond length of 2.0 Å. It is further coordinated to both His 282 (in *S. deleyianum* only) and Tyr 217 (218) with a single oxygen atom and to a water molecule which in turn is coordinated to the two propionate sidechains of heme 1. Arg 113 (114) also forms a hydrogen bond to one of the propionates and is bonded to the sulfate via another water molecule. The roof of the active site cavity is formed by Phe 91 (92), Lys 279 (274), Tyr 95 (96), Ala 404 (398) and Gln 281 (276), which coordinates the Ca^{2+} by its carboxamide oxygen such

that the amino group faces the active site. This contributes significantly to the positive electrostatic surface potential surrounding the active site (Figure 25).

5.4.5.5 The Substrate/Product Channel

S. deleyianum nitrite reductase does not only reduce nitrite to ammonia, but also the potential intermediates NO and hydroxylamine. No intermediates are released during turnover of nitrite. Obviously, the active site accommodates anions and uncharged molecules and releases the ammonium cation only after the full six-electron reduction. The preference for anions is reflected by a positive electrostatic potential around and inside of the active site cavity. This is induced by the residues building up the cavity: Tyr 217 (218), His 282 (277), Arg 113 (114), Gln 281 (276) and Lys 279 (274). These residues will serve as stores and donors for protons required for the reduction of nitrite to ammonia and can be resupplied by water molecules. Considering the good accessibility of the active site for water molecules and the presumably lowered pH on the periplasmic side of the cytoplasmic membrane where nitrite reductase is located, the product of nitrite reduction will be the positively charged ammonium ion rather than uncharged ammonia.

The cationic product might make use of a second channel leading to the protein surface opposite to the entry channel. This second channel is lined by His 406 (400) and Tyr 95 (96) and is filled with coordinated water molecules (Figure 25). It branches before reaching the protein surface and ends with both arms in areas with a significantly negative electrostatic surface potential. The existence of separate pathways for substrate and product with matched electrostatic potential could also contribute to the high specific activity of nitrite reductase compared to the siroheme-containing nitrite reductases which catalyze the same reaction (see 3.3.3).

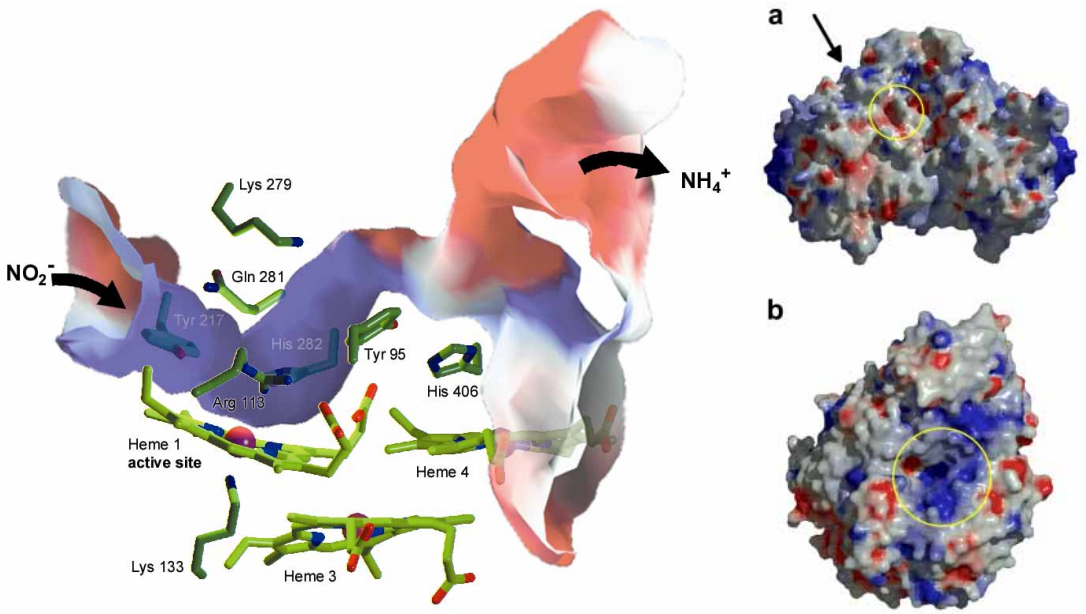

Figure 25: The Active Site Channel of *S. deleyianum*. Apart from the channel leading from the protein surface to the catalytic site, a second channel has been detected that reaches the protein surface on the opposite side of the molecule. The whole channel is rendered as a semitransparent surface and colored according to the electrostatic surface potential; blue for a positive and red for a negative potential (cutoff +10 and -10, respectively). The right side shows the electrostatic surface potential of (a) the dimer and (b) the monomer looking into the active site channel (arrow in (a)). The circles indicate entrance and exit of the channel.

The same substrate channel can as well be located in the structure of the *W. succinogenes* enzyme and is formed by the same set of residues. As these residues are strictly conserved throughout all *nrfA* sequences known, it can be assumed that this channel and the directed flow of substrate and product are an essential feature of the enzyme, representing an optimization of substrate specificity and reaction efficiency.

5.4.5.6 Substrate binding

Nitrite reductases of both *S. deleyianum* and *W. succinogenes* have first been structurally characterized with a sulfate ion bound to the active site iron of the oxidized enzyme. Sulfate could be clearly oriented in the observed difference electron densities.

The binding of sulfate by the protein ligands surrounding the active site heme group differs significantly in the structures of both organisms. Most

obvious is a torsion around the χ_1 angle of Tyr 218 of 5° away from the bound substrate in the case of the *W. succinogenes* enzyme.

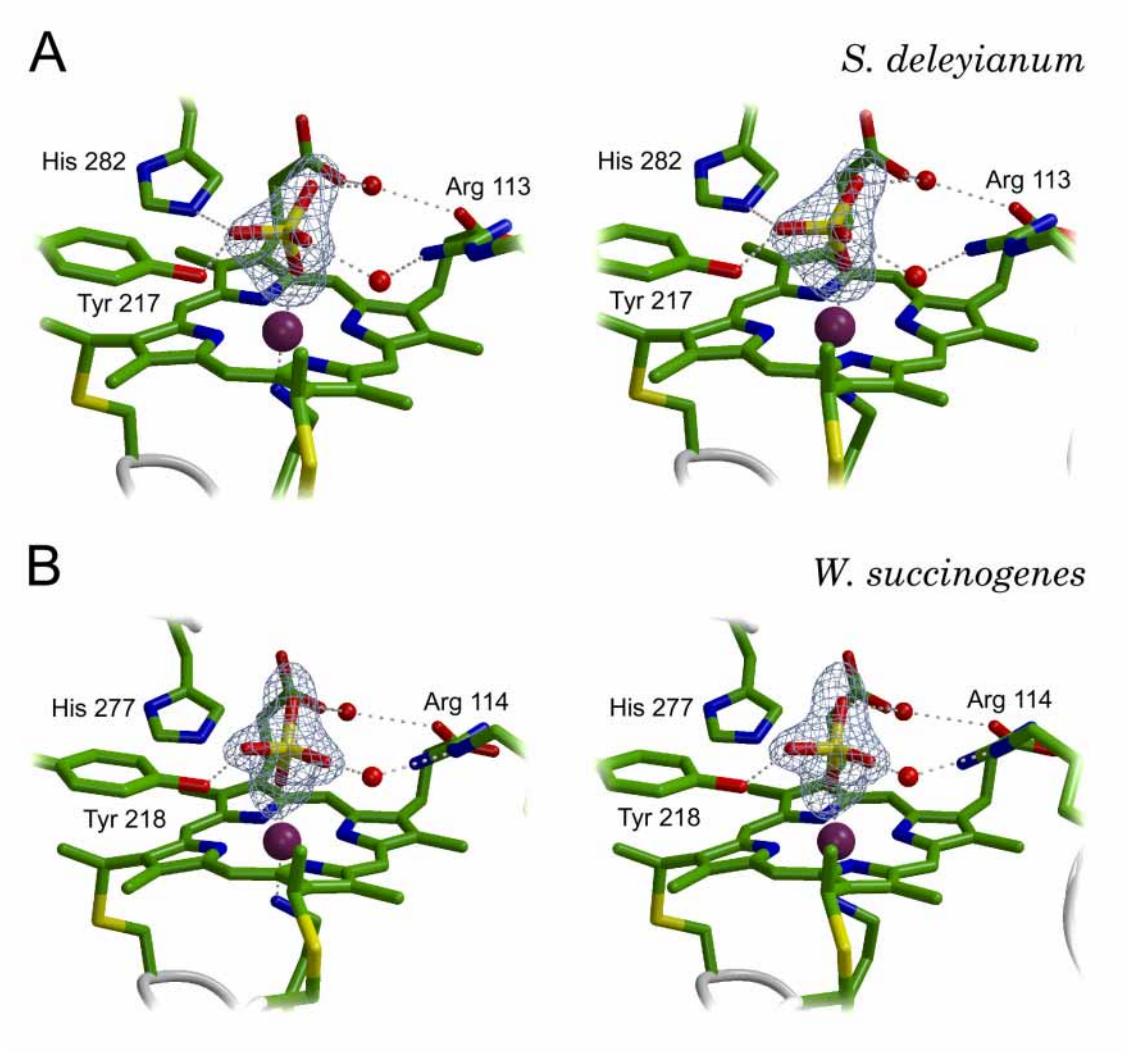

Figure 26: The active site heme groups of both organisms with bound sulfate anions. **A)** Nitrite reductase from *S. deleyianum*. The F_o–F_c difference electron density at 1.90 Å shows the sulfate with one oxygen bound to both His 282 and Tyr 217. In **B)**, the *W. succinogenes* enzyme at 1.60 Å resolution, the sulfate anion is twisted and does not bind to His 277. The main difference between both crystals is a shift of 2 pH units.

For the sulfate ion, this difference causes a rotation such that its O_1 atom is bound to both His 282 (at 2.6 Å) and Tyr 217 (at 2.8 Å) in the *S. deleyianum* structure, but only to Tyr 218 (2.6 Å) in the *W. succinogenes* enzyme, where the distance to $N_{\varepsilon 2}$ of His 277 has increased to 3.3 Å. Of the two other oxygen atoms of sulfate, one is bound to Arg 113 in *S. deleyianum* at a distance of 3.6 Å, and to Arg 114 in *W. succinogenes* at 2.8 Å. The remaining

oxygen is bound to a water molecule within the active site cavity, which, regardless of a small shift, retains its position and bonding pattern in both organisms. The distance between the fourth oxygen of sulfate and the heme iron is around 2.05 Å in both structures.

5.4.5.7 Tracing the reaction pathway

In order to elucidate the course of the reaction of nitrite reductase, the substrate nitrite as well as the key intermediate hydroxylamine were soaked into oxidized crystals of *W.succinogenes* nitrite reductase. Additionally, a dataset of a nitrite-bound form of *S. deleyianum* nitrite reductase was obtained, but in this case the resolution was limited to 2.5 Å.

Even at this resolution it becomes evident, that a similar situation is observed for the nitrite-bound structures as for the ones with sulfate. As expected, nitrite binds to the active site ferric iron through its nitrogen atom. In analogy to the sulfate-containing structures, Tyr 217 is closer to the ligand in *S. deleyianum* than Tyr 218 is in *W. succinogenes*. As a result of this, nitrite is bound in the *S. deleyianum* structure with one oxygen to both His 282 (2.9 Å) and Tyr 217 (2.9 Å) and to a water molecule with the other oxygen. In *W. succinogenes* however, there is no interaction with Tyr 218 (4.1 Å), but a rather close hydrogen bond of 2.6 Å to His 277. Due to this, the nitrite ion's O-N-O plane is twisted by 45° in respect to the *S. deleyianum* enzyme and the other oxygen atom is in hydrogen bond distance (2.9 Å) to Arg 114. The difference electron density for nitrite was well-defined in this structure and allowed for refining the substrate complex without introducing artificial distances by applying patches. This way, the refinement resulted in a rather short iron-to-nitrite bond length. However, the difference in this between the two determined structures – 1.6 Å in the structure measured on a rotating-anode generator (resolution 2.0 Å) versus 1.84 Å in the synchrotron structure (resolution 1.7 Å) – shows the limitations of a crystallographic analysis in this resolution range.

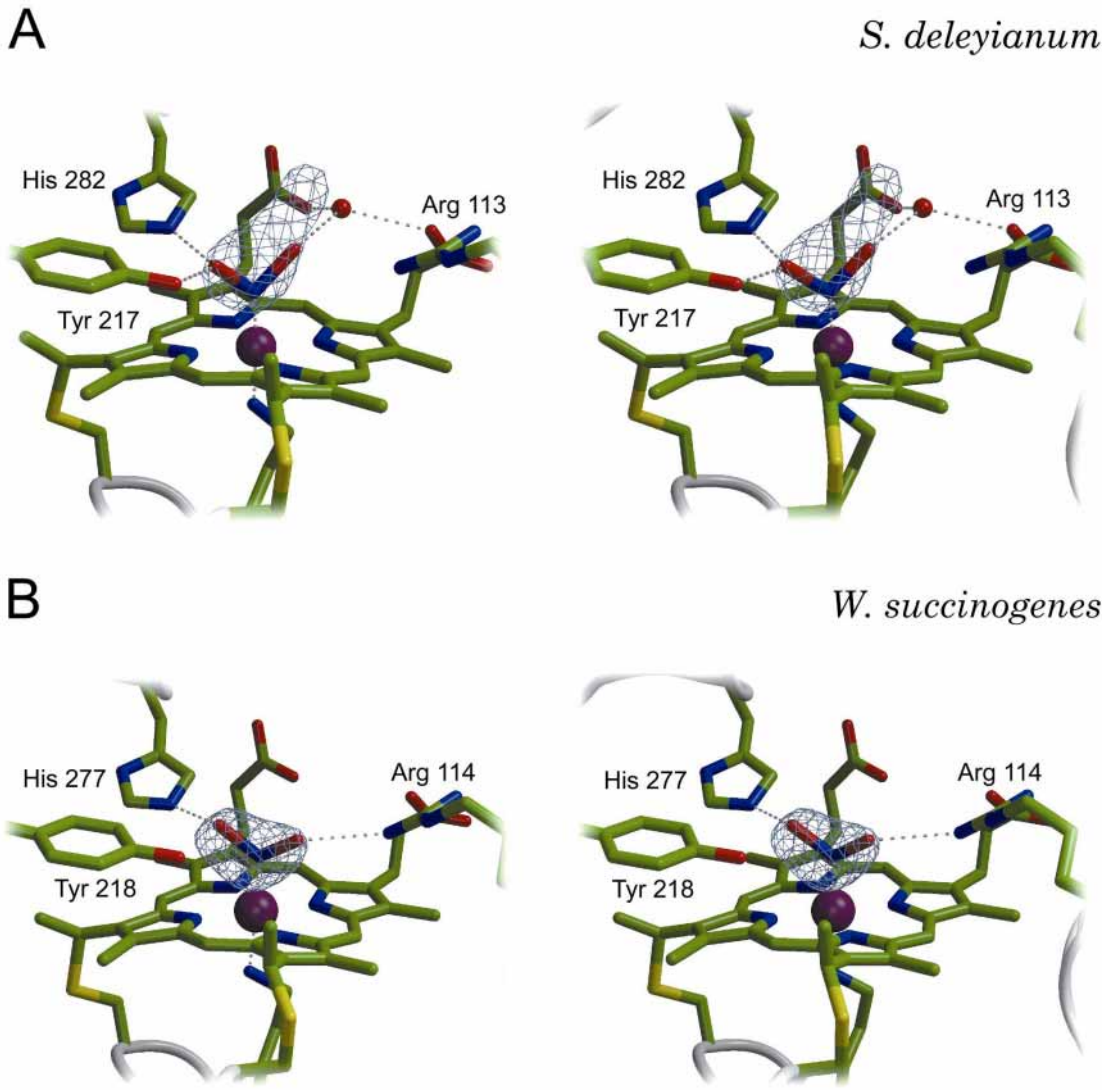

Figure 27: Binding of nitrite to the oxidized nitrite reductases from **A)** *S. deleyianum* at 2.5 Å resolution and **B**) *W. succinogenes* at 1.7 Å. Like in the case of the sulfate adducts (Figure 26), the substrate is twisted in the *S. delyianum* structure by approximately 45°.

Soaking crystals of nitrite reductase with hydroxylamine proved to be more difficult, as this compound – in contrast to nitrite – seemed to have a harmful effect on crystal quality. An optimization of soaking time and hydroxylamine concentration in the soaking solution finally made it possible to collect data to a resolution of 2.0 Å.

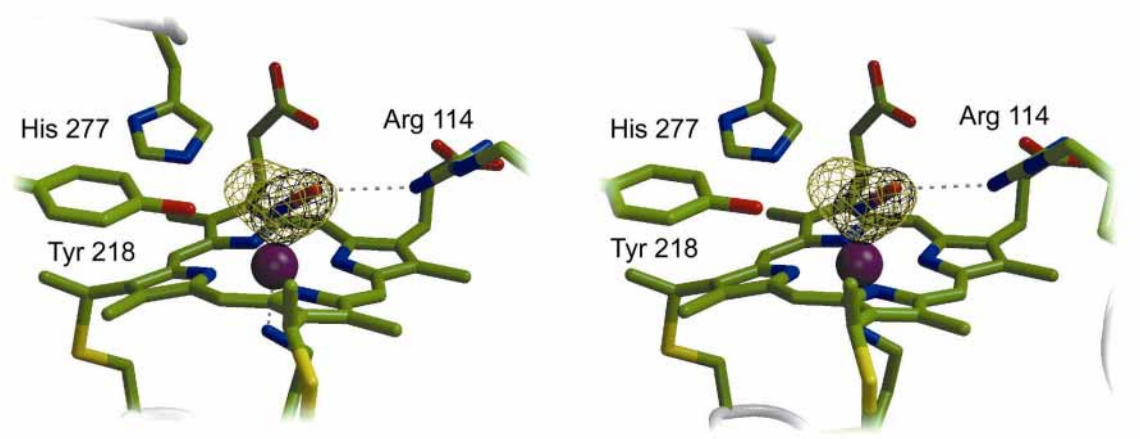

Figure 28: The active site of *W. succinogenes* nitrite reductase with the difference electron density observed in the hydroxylamine soak at 2.0 Å in black. Hydroxylamine is modelled into this density, and the superimposed difference electron density of the 1.7 Å nitrite soak (yellow) indicates, that the first part of the reduction of nitrite is the abstraction of the oxygen atom that is bound to His 277.

Only the nitrogen and the oxygen atom of hydroxylamine can be seen at this resolution, and it is not possible to distinguish between both atoms. However, the resulting difference density of the hydroxylamine soak turned out to be in excellent agreement with the one of the nitrite soak (Figure 28). Assuming that it is the nitrogen atom that binds to heme iron, the resulting position of hydroxylamine coincides with the nitrogen and one of the oxygen atoms of nitrite. This would indicate that in the course of the reaction sequence of nitrite reductase, the oxygen atom that binds to His 277 is the one that leaves the nitrite molecule first. Bond distances in the structure are 1.7 Å for the Fe-N bond to the heme iron and 2.9 Å for the hydrogen bond to Arg 114, but due to the limited resolution these values are as uncertain as the ones for nitrite.

5.4.5.8 Mechanism of Inhibition by Azide

The azide anion has been described as an inhibitor of nitrite reductase activity for the enzyme from *S. deleyianum* (Schumacher, 1993). It was expected to bind to the active site of the enzyme in an end-on manner similar to the binding of hydroxylamine. As azide is more elongated (2.30 Å for the whole molecule) than hydroxylamine (1.40 Å for the N-O bond), a complex of

azide bound to the active site should provide better information about the binding angle to iron than the one of hydroxylamine.

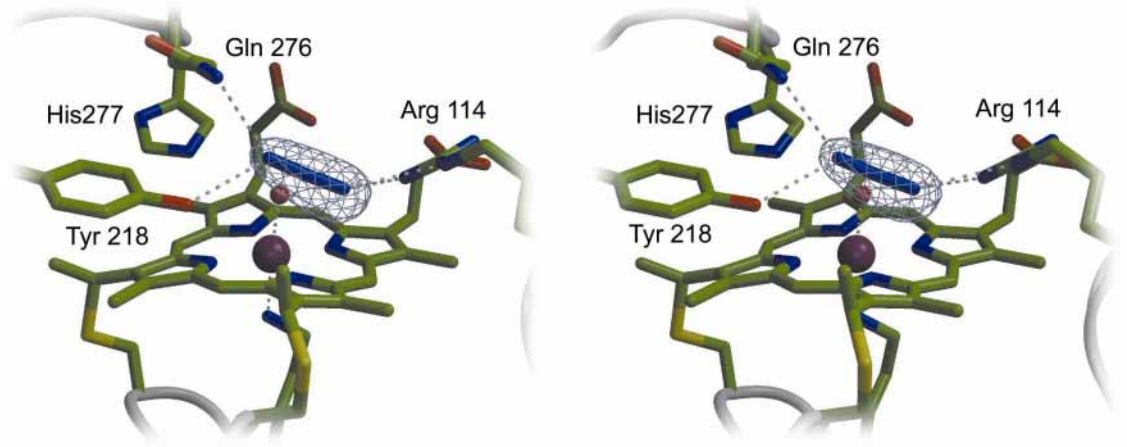

Figure 29: Binding of the azide anion in the substrate channel of *W. succinogenes* nitrite reductase. The depicted electron density is a F_o–F_c difference density, contoured at 3.0 σ. A water molecule is bound to the active site iron.

Azide was soaked into crystals of *W. succinogenes* nitrite reductase and was found to bind without impairing the diffraction quality of the crystals, even at concentrations as high as 100 mM. However it was surprising to find that the anion did obviously not bind to the active site. Instead it bound to residues lining the active site entrance, with hydrogen bonds to Gln 276 (3.0 Å), Tyr 218 (2.8 Å) and to N_ε (3.0 Å) and $N_{\eta 1}$ (2.9 Å) of Arg 114. This interaction is strong enough to quantitatively replace the sulfate ion which bound to the active site before soaking. The remaining difference electron density at the active site was interpreted with a water molecule at a Fe-O bond distance of 2.1 Å. Datasets were collected to 2.0 Å resolution on a rotating anode generator and to 1.7 Å using synchrotron radiation. At lower contour levels, the more highly resolved data set showed some positive difference density between the heme-bound water and the O_η atom of Tyr 217. This indicates that binding of azide to heme iron might occur to a minor degree (< 5 %), but considering the high concentations of azide used in the soak this is not assumed to be of physiological significance.

5.4.5.9 Crystal Packing

Three different crystal forms of cytochrome *c* nitrite reductase have been characterized, two for the enzyme of *S. deleyianum* and one for *W. succinogenes* (Table 4). These crystal forms belong to different space groups and in all cases the protein is subject to very dissimilar crystal packing interactions. This offers the possibility to recognize possible crystallization artifacts.

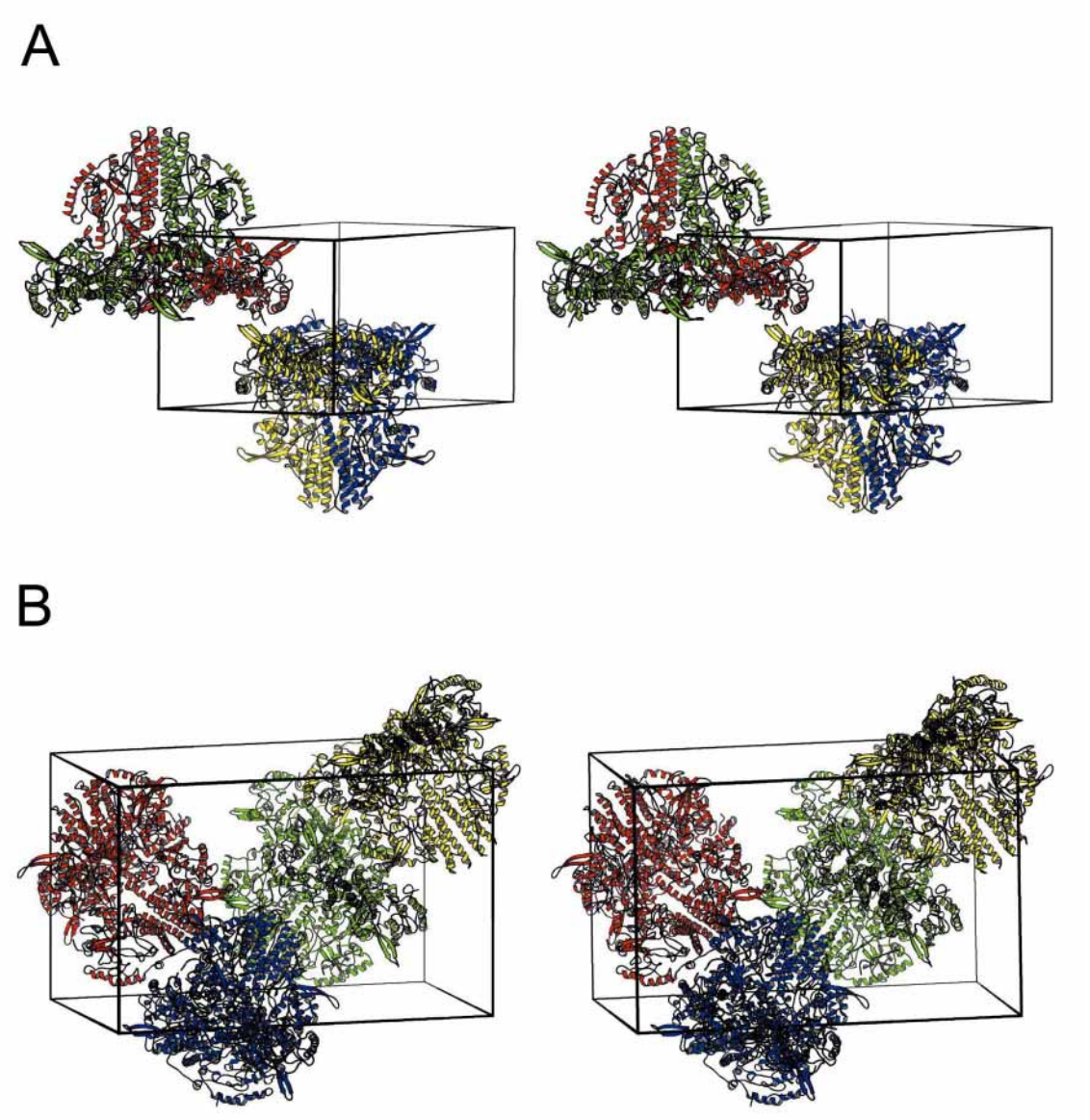

Figure 30: Crystal packing in the two crystal forms of *S. deleyianum* nitrite reductase, with different colous representing asymmetric units. **A**) The unit cell of the $P2_12_12$ crystal. Three monomers form the asymmetric unit and the crystal symmetry is easy to recognize (***z***-axis vertical). **B**) The unit cell of the $P2_12_12_1$ form is built up by four of the hexamers that are also found in A). Six monomers form the asymmetric unit.

In all crystals, nitrite reductase forms the same tight dimer that allows for the close interaction of hemes 5 and can be considered as the functional form of the protein. This hypothesis is supported by the observation, that concentration of the purified protein strongly facilitates crystal formation, supposedly because dimer formation is promoted at higher protein concentrations.

Furthermore, *S. deleyianum* nitrite reductase crystallizes with three molecules per asymmetric unit in space group $P2_12_12$ and with six molecules per asymmetric unit in space group $P2_12_12_1$ (Table 4). The three molecules of the $P2_12_12$ form build up a hexamer using the crystallographic twofold *z*-axis, and this hexamer corresponds exactly to the one that forms the asymmetric unit in the $P2_12_12_1$ crystal form. This particular arrangement was not observed in *W. succinogenes* nitrite reductase and it is not assumed to be of functional significance, but the interactions between the three dimers in the hexamer might provide an important hint as to where nitrite reductase reacts with other proteins, in particular with its electron donor, NrfH.

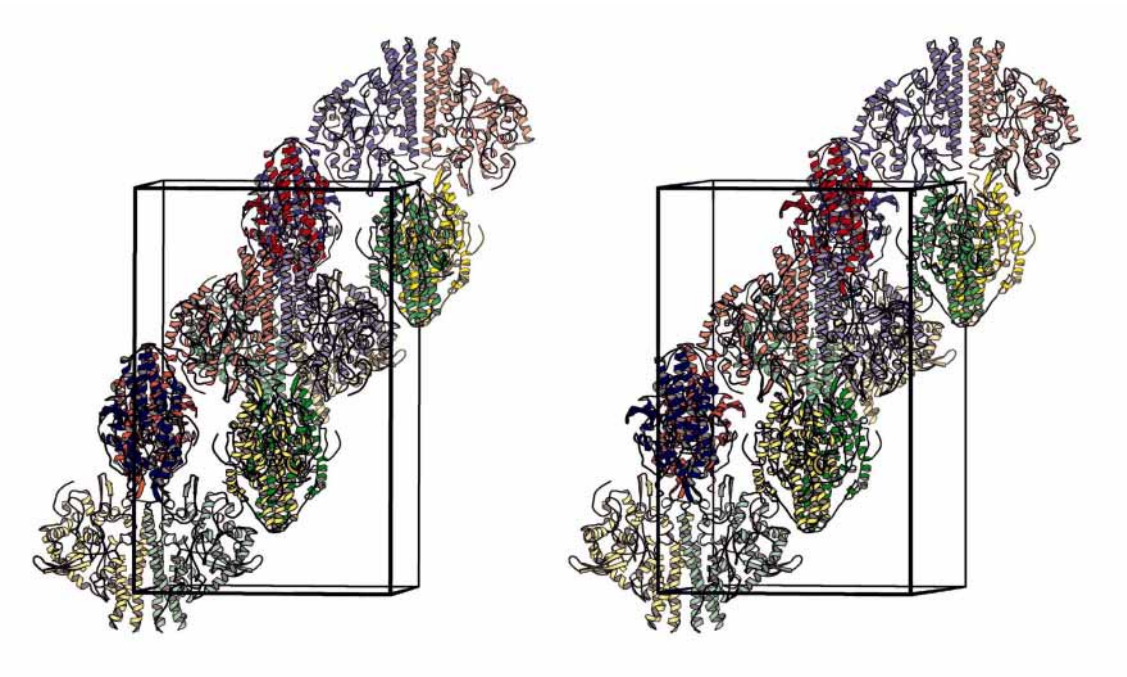

Figure 31: Crystal packing in *W. succinogenes* nitrite reductase crystals of space group $I4_122$. The unit cell holds 16 asymmetric units, each consisting of one monomer.

The crystals of *W. succinogenes* nitrite reductase belong to space group $I4_122$. They hold one molecule per asymmetric unit and the dimer is formed by a crystallographic twofold axis. Two dimers interact rather closely, again with the bottom face as in the *S. deleyianum* crystals, but in a completely different arrangement, rotated by 90° according to the 4_122 symmetry of the crystal. A determining factor for the growth of this crystals was the presence of yttrium ions in the crystallization buffer, and so it is not surprising that several of them could be identified in the structure. Three of these yttrium positions lie exactly between and are ligated by two monomers.

The first one is coordinated by Glu 52 from one monomer and by Asp 444 from another monomer in a bidentate manner as well as by five water molecules (in the most highly resolved structures). The second yttrium is located at the tip of the external loop that precedes the distal histidine ligand of heme 2 (residues 301 through 313), coordinated by Gln 304 in this loop and by Glu 334 and Asp 323 from another monomer. A further ligand of Y^{+3} is a sulfate ion, and in the substrate soaks that were deprivated of sulfate, this ion is missing as well as the yttrium itself, resulting in a slightly different conformation of the loop mentioned. Such a flexible loop could take part in the formation of a complex with NrfH, which is expected to take place in this area of the protein.

The third of the conserved yttrium ions occupies a special position. This is true not only from the crystallographic point of view, as it sits on a twofold symmetry axis in the dimer interface, but also because it is coordinated by Glu 408 and – more importantly – the propionate sidechains of hemes 5 from both monomers. Being in a crucial position for electron conduct between the monomers, a metal in this position might have significant influence on spectroscopic experiments carried out with crystals of nitrite reductase. In the *S. deleyianum* dimer, this position is occupied by a water molecule and there is no indication that the situation *in vivo* should be different in *W. succinogenes*.

A fourth yttrium ion is present in all structures, but is coordinated only by residues from a single monomer. It is located right at the exit of the substrate/product channel, coordinated by the propionate sidechains of hemes 3 and 4 and by the backbone carbonyl oxygen of Pro 99. Further coordination is provided by five water molecules.

In all positions observed, the yttrium ions are coordinated solely by oxygen atoms and the coordination geometry is mostly octahedral, sometimes with a seventh ligand, similar to the situation observed for calcium and with similar bond distances. In spite of this, the addition of calcium ions had no positive effect on crystal growth of *W. succinogenes* nitrite reductase.

5.5 Cytochrome c_3 from *D. desulfuricans* Essex 6

In contrast to the enzyme nitrite reductase, cytochromes c_3 are redox carriers, mediating electron transfer between different oxidoreductases in the periplasm of sufate-reducing bacteria. Their first description dates back to the fifties (Postgate, 1954) and they have been shown to be redox partners of periplasmic hydrogenase (Haladjian *et al.*, 1987; Nivière *et al.*, 1988) as well as of dissimilatory sulfite reductase (Steuber *et al.*, 1994). The coupling to the membraneous quinone pool was suggested to be mediated through interaction with membrane-associated high molecular weight cytochromes like nine-heme cytochrome *c* from *D. desulfuricans* (Matias *et al.*, 1999b).

5.5.1 Crystallization

D. desulfuricans Essex 6 cytochrome c_3 was crystallized in space group $P2_12_12_1$ using sitting drop vapour diffusion and a reservoir solution of 30% PEG 2000 monomethyl ester, 0.2 M ammonium sulfate and 0.1 M sodium acetate at pH 4.6. 2 µl of protein solution (7 $mg \cdot ml^{-1}$) were mixed with 2 µl of the precipitant solution and equilibrated against a buffer reservoir at room temperature. Crystals of up to $1.0 \times 0.1 \times 0.1$ mm^3 and unit cell dimensions

of **a** = 36.37 Å, **b** = 49.39 Å and **c** = 70.99 Å grew within two to three days and diffracted to resolutions better than 2.0 Å using $Cu_{K\alpha}$ radiation.

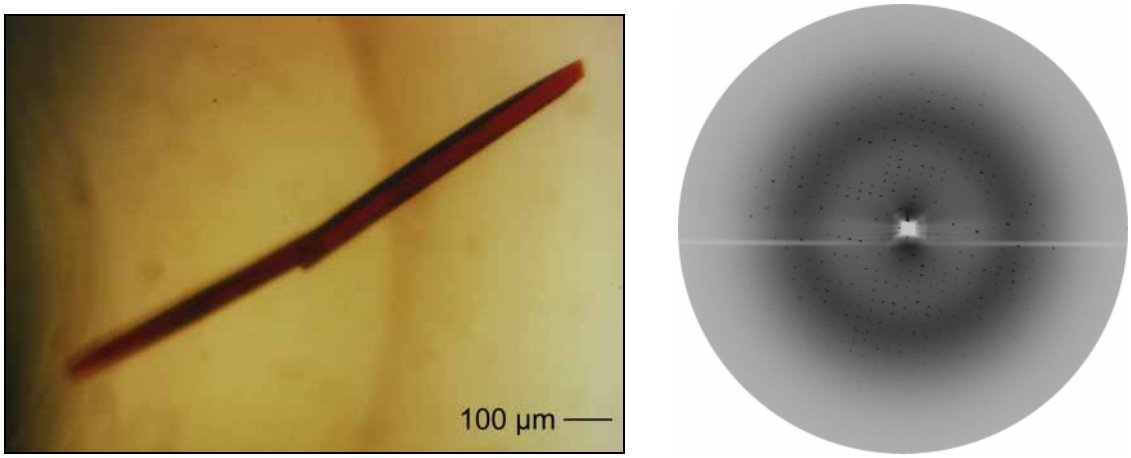

Figure 32: A crystal of *D. desulfuricans* Essex 6 cytochrome c_3 and its diffraction pattern with a roating anode X-ray source. The edge of the detector corresponds to a resolution of 1.95 Å.

The crystals were grown and measured using protein in the oxidized state. A data set with a completeness of 98.4 % to 1.95 Å was collected at room temperature on a Mar Research 2000 image plate detector.

5.5.2 Sequence Determination

The full protein sequence could be obtained from redissolved crystals, limiting the total amount of protein needed for sequencing and structure determination to approximately 1 mg. The mature protein consists of 107 residues, all of which were visible in the electron density. Four binding motives for covalently attached heme groups were present, two of them in the most commonly observed form, C-X_1-X_2-C-H, and the other two with a spacing of four residues in between the two cysteines.

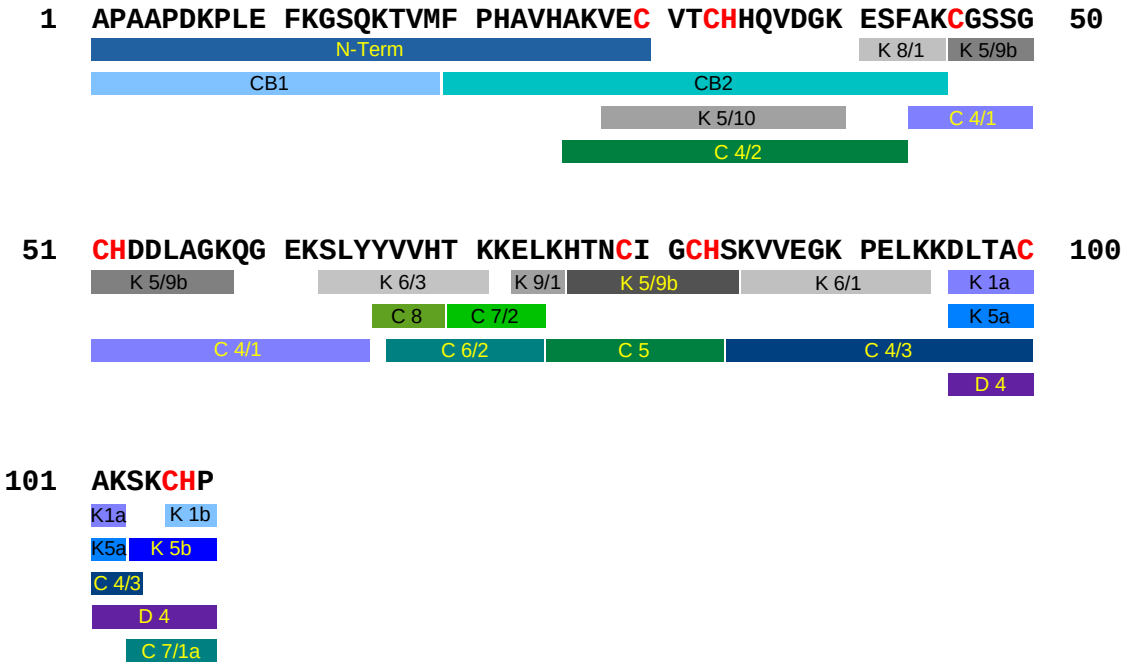

Figure 33: Sequence of cytochrome c_3 from *D. desulfuricans* Essex 6. An overview of the peptidic digest fragments that were sequenced by Edman degradation. N-Term, N-terminal sequence; CB, CNBr peptides; K, C, D, peptides created by cleavage with endoproteinase Lys-C, chymotrypsin and endoproteinase Asp-N, respectively. Numbers denote chromatographic pools. The residues belonging to the *c*-type heme binding motives are marked red.

The known sequences of cytochromes c_3 divide into at least two groups as far as heme binding is concerned. While all sequences have a Cys-X_1-X_2-Cys-His motif for binding hemes 1 and 3 and a Cys-X_1-X_2-X_3-X_4-Cys-His for heme 2 (with the single exception of *D. africanus*; Nørager *et al.*, 1999), the binding mode for heme 4 varies between the two. The effect of all those changes on the structures of these cytochromes is marginal.

It should be noted, that a phenylalanine residue stacked between hemes 1 and 3 (Phe 20 in the sequence of *D. desulfuricans*) is also conserved in all sequences. As it will be discussed below, this residue is also present in several otherwise completely unrelated proteins which have conserved hemes that correspond to heme 1 and heme 3 (Figure 41).

With a total of seventeen lysine residues, most of which are located on the surface of the protein, this cytochrome c_3 belongs to the basic group of c_3's, as reflected in a pI of 8.5 (Steuber, 1996). The sequence-derived molecular mass of 14073 Da (including four hemes) is in good accordance with

the 14070 ± 1 Da determined by MALDI-TOF mass spectrometry (Steuber, 1996).

5.5.3 Structure Solution

Several structures of cytochromes c_3 were known at the time the crystals were obtained, including the one of *D. desulfuricans* ATCC 27774 (Morais *et al.*, 1995), which, at a sequence identity of 84%, was expected to be highly homologous and was thus used as a model for molecular replacement. The program AMoRe (Navaza, 1994) produced a clear solution with a correlation of 72.6 % and a crystallographic *R*-factor of 0.376 for the single molecule in the asymmetric unit.

The model was built with "O" (Jones *et al.*, 1991) and refined using the development version 0.3 of CNS (Brünger *et al.*, 1998) to a final *R*-factor of 0.173 at an R_{free} of 0.228 for 5% of the measured reflections. RMS deviations from ideality were 0.011 Å for bond lengths and 1.47° for bond angles.

5.5.4 Description of the Structure

As a typical member of its class, the protein shows a fold and heme arrangement which is very similar to the one of the other structures solved for cytochrome c_3 to date. These structures are the ones from *Desulfovibrio vulgaris* Miyazaki F (Higuchi *et al.*, 1984), *Desulfovibrio vulgaris* Hildenborough (Matias *et al.*, 1993), *Desulfomicrobium norvegicum* (in a monomeric form; Czjzek *et al.*, 1994a; and in a dimeric form; Czjzek *et al.*, 1994b), *Desulfovibrio desulfuricans* ATCC 27774 (Morais *et al.*, 1995), *Desulfovibrio gigas* (Matias *et al.*, 1996) and *Desulfovibrio africanus* (Nørager *et al.*, 1999).

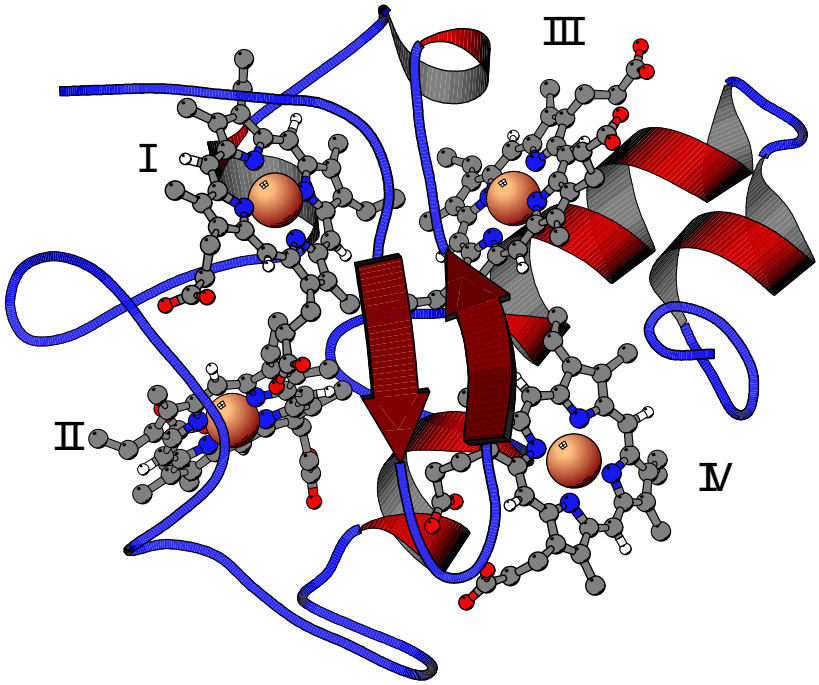

Figure 34: Cytochrome c_3 from *D. desulfuricans* Essex 6. The four heme groups are numbered according to their attachment to the protein chain. The N-terminal end of the chain is close to heme I, the C-terminus is close to heme IV.

In a single compact domain, hemes 1 and 4 as well as hemes 2 and 3 are roughly coplanar while the two pairs they form are in turn almost perpendicular to each other. The mainly α-helical protein folds around those four closely packed hemes, but allows for access to the protein surface for all of them. Midpoint redox potentials for the individual hemes have been determined for several of those proteins and range between –12 and –400 mV, although the range within one species can be considerably smaller. A range of only –210 to –270 mV has been determined for the acidic cytochrome c_3 of *D. africanus* (Pieulle *et al.*, 1996), and a range of –280 to –380 mV for the one of *D. vulgaris* Hildenborough (Mus-Veteau *et al.*, 1992).

It is still a matter of debate how many electrons are actually transported by cytochromes c_3 *in vivo*. For the *D. vulgaris* protein, a coupling to the oxidation of molecular hydrogen has been proposed, with cytochrome c_3 transferring two protons and two electrons at a time through a concerted mechanism described as a "proton thruster" (Louro *et al.*, 1997).

In all structures of basic cytochromes c_3 obtained so far (i.e. all except for the *D. africanus* protein), the surface region where heme IV emerges is surrounded by a patch of lysine residues that induce a net positive charge. Thus this heme group was considered to be the point of interaction with hydrogenase and the entry point for electrons. This hypothesis was confirmed in part by NMR redox titration experiments, which showed that heme IV is the one with the highest redox potential in *D. vulgaris* Hildenborough (Turner *et al.*, 1996), *D. vulgaris* Miyazaki F (Park *et al.*, 1996) and *D. gigas* (Picarra-Pereira *et al.*, 1993). In two other cases however, in *D. desulfuricans* ATCC 27774 (Louro *et al.*, 1996) and *D. norvegicum* (Coutinho *et al.*, 1993), it turned out that heme III was reduced before heme IV.

6 Discussion

6.1 Distribution of the DNRA pathway

With only seven sequences of cytochrome *c* nitrite reductase available to date, a discussion of the distribution of the DNRA pathway in the bacterial kingdom is necessarily limited. Furthermore, it is difficult to discern fermentative from respiratory nitrate dissimilation, only the latter of which is dependent on the *nrf* system. However, the discovery of a *nrf* operon in the bacteroid *P. gingivalis* was surprising, as well as the relationships between different multiheme proteins which, due to the absence of sequence homology, were only recognized on a structural basis.

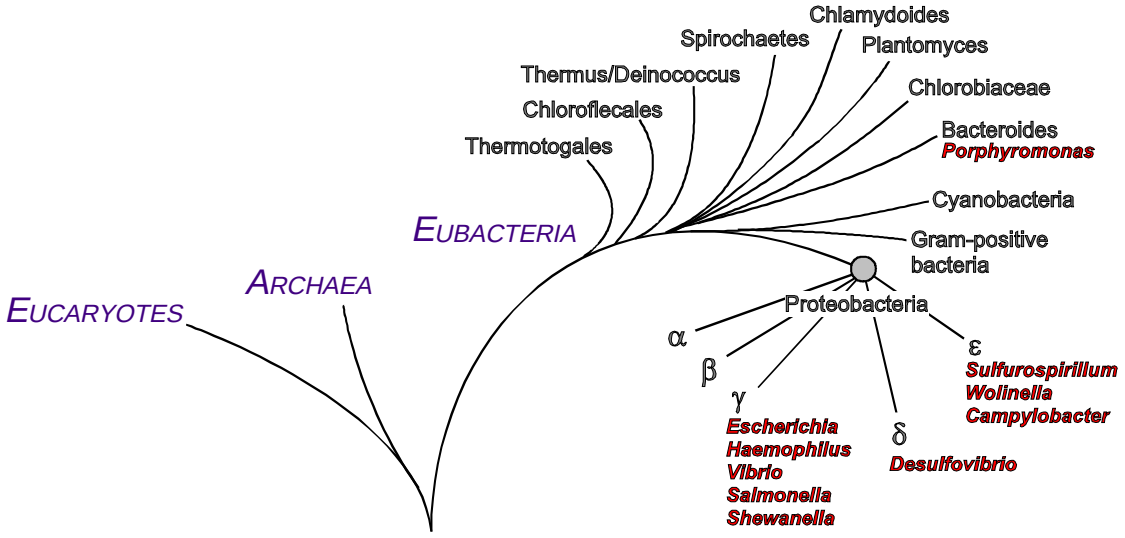

Figure 35: A phylogenetic tree of the Eubacteria based on 16S rRNA sequence homologies (modified after Schlegel, 1992). Dissimilatory cytochrome *c* nitrite reductases are found within the group of proteobacteria (purple non-sulphur bacteria), with the single exception of the bacteroid *P. gingivalis*. Multiheme cytochromes related to nitrite reductase are also found in β-proteobacteria (e.g. *Nitrosomonas*, see 6.3.1, 6.3.2).

All examples of the *nrf* system examined so far fall into the group of proteobacteria, with the expection of *P. gingivalis*. The comparison of heme group arrangements later in this discussion will lead to systems like hydroxylamine oxidase and the NirT/NapC family of cytochromes, but they too were only observed in proteobacteria. One main reason for this is without doubt, that proteobacteria consitute the probably largest, most diverse and best studied group of bacteria. Nevertheless, the exact conservation of heme arrangements in all different kinds of multiheme cytochromes is an indication, that this way of fine-tuning redox potentials might be more ancient still.

6.2 Organization Forms of the *nrf*-Operon

Although the known types of *nrf* operons, *nrfABCDEFG*, *nrfHAIJ* and *nrfHAKLM*, are organized differently, it is possible for both cases to extract three essential elements for the dissimilatory nitrite ammonification system:

- The enzymatic activity, located on the NrfA protein
- A system to connect NrfA to the membraneous quinone pool, made up by NrfBCD in γ-proteobacteria and solely by NrfH in ε-proteobacteria and bacteroides.
- A modified heme transporter to attach the active site heme group with its lysine coordination.

A discussion of these points will help to find the common ground of all those systems in order to present a concise model of the organization of the *nrf* machine.

6.2.1 Nitrite Reductase

The enzymatic activity of nitrite reduction is located on the NrfA protein. A comparison of the available primary sequences of the gene in combination with sequence-based secondary structure predictions strongly suggests, that key features of all those enzymes are strictly conserved throughout all organisms investigated so far. Among those features are not only the number and arrangement of heme groups, the lysine-coordinated active site and the substrate/product channel, but also the long α-helices at the C-terminus of the chain which are essential for dimer formation.

Although it has been shown that NrfA is soluble and active as a monomer, the tight dimer formation in all crystal forms observed as well as the obvious interaction of hemes 5 across the dimer interface and the predicted conservation of the long helical segments in all sequences strongly support the hypothesis, that the physiologically active form of cytchrome *c* nitrite reductase is a dimer.

6.2.2 Quinol Oxidase and Electron Carrier

Electrons for the reduction of nitrite are obtained from the membraneous quinone pool, as it has been shown in the case of *W. succinogenes* (Simon *et al.*, 2000), and as it has furthermore been suggested for systems employing cytochromes of the NapC/NirT family in general (Roldán *et al.*, 1998). Thus the *nrf* system must contain components that can oxidize menaquinone and transfer electrons to NrfA. While this task is performed by a complex system consisting of three genes in the *nrfABCDEFG* operon type, the *nrfHAIJ* and *nrfHAKLM* types only need a single protein, NrfH. Surprisingly, both systems seem completely unrelated except for the fact that electrons are donated to NrfA via a multiheme cytochrome *c*. NrfH is anchored to the membrane by a single transmembrane helix only, while NrfC and NrfD are predicted to form a fully membrane-inserted quinol oxidase com-

plex (Hussain *et al.*, 1994). NrfH on the other hand seems to be a variation of a widespread theme, as cytochromes of the NirT/NapC family are found in a large number of periplasmic oxidoreductase systems, including the other reductase system of the DNRA metabolic pathway, periplasmic nitrate reductase (NapABC). However, all these systems do not use universal quinol-oxidizing cytochromes, but carry their own member of the family in the same operon as the reductase itself. This is a prerequisite to evolve towards interaction specifity and formation of a stable complex that makes diffusion of reaction partners unnecessary, speeding up electron transport by orders of magnitude.

In the γ-proteobacteria, NrfB appears to be a unique type of electron carrier, with known sequence homologies only to membrane-inserted metal reductase systems described for *Shewanella putrefaciens* (Beliaev & Saffarini, 1998). The other two genes however are not unique. The highest homologies to NrfC and NrfD are found for genes in the polysulphide reductase operon of *W. succinogenes*, where they can be expected to play exactly the same role, which is to provide a link to the membraneous quinone pool (Krafft *et al.*, 1995).

6.2.3 Active Site Heme Lyase

For both types of the *nrf* operon, the remaining genes are assumed to participate in the covalent attachment of the active site heme group to the protein chain. This is mainly suggested by the high similarity of those genes to regular heme *c* lyase genes.

To date, three distinct systems of cytochrome *c* biogenesis have been characterized (Kranz *et al.*, 1998). While γ-proteobacteria share the *ccm* (**C**ytochrome ***C*** **M**aturation, (Thöny-Meyer, 1997)) system (system I) with archaea and plant mitochrondria, the group of ε-proteobacteria possesses system II, which they share with chloroplasts, Gram-positive and cyanobacteria. The genes found in both types of the *nrf* operon do correspond to the

respective heme lyase system which is present in the bacteria themselves. As it has been shown for both *E. coli* (Eaves *et al.*, 1998) and *W. succinogenes* (Simon *et al.*, 2000), a deletion of the *nrf* genes *nrfEFG* or *nrfIJ*, respectively, leads to the expression of an inactive NrfA protein in which the active site heme group is missing.

It can be expected that the main difference in the constitutive and the *nrf*-encoded heme lyase systems is the recognition of the binding motif for heme attachment. The regular system will act on a motif Cys-X_n-Cys-His with n = 2 or 4, while the active site heme of NrfA is linked to a motif Cys-X_2-Cys-Lys.

This finding raises the question how those differences in operon types were established in the course of evolution. The high degree of conservation of the NrfA gene in all cases observed leaves little doubt that a functional nitrite reductase is the original system, and that the different operon organizations are a more recent acquisition. Shuffling and exchange of gene arrangements within an operon is a common observation in bacteria, and it might be taken as an indication, that NrfA is more ancient than the separation of heme *c* biogenesis pathways.

The other possible explanation is a horizontal gene transfer, as suggested recently for the whole heme *c* biosynthetic pathway (Goldman & Kranz, 1998). While this is a possibility for NrfA itself, it does not explain the differences in the heme attachment system.

6.2.4 The Nitrite Ammonification Complex

In view of the organization of the *nrf* genes, it seems quite clear how a membrane-associated nitrite reductase complex might be arranged. Although at present, the existence of such a complex remains uncertain. Alternatively, the components are soluble and transfer electrons only when diffusing into proper orientations.

A support for the latter thesis is the observation, that purified NrfA is soluble as a monomer and does effectively catalyze electron transfer from methyl or benzyl viologen to nitrite, as it has been shown for *S. deleyianum* (Schumacher *et al.*, 1994; Schumacher & Kroneck, 1991). On the other hand, the structure shows that almost all hemes groups of nitrite reductase partially extend to the surface of the protein and can thus be accessible for small electron donors *in vitro*. In the oxidative environment of the periplasm of a bacterial cell however, the situation is substantially different. Electrons provided by menaquinol have to be directed specifically to reach their destination. An electron carrier, encoded on the same operon as the reductase, will have to be complementary to it in order to guarantee specific and directed electron transport. From that point on, the next logical step would be to form a stable complex associated to the membrane, making use of the complementarity between quinol oxidase, electron carrier and reductase. Such a complex can be considered as an optimization of the system, especially as a respiratory system can be expected to evolve towards higher effectivity.

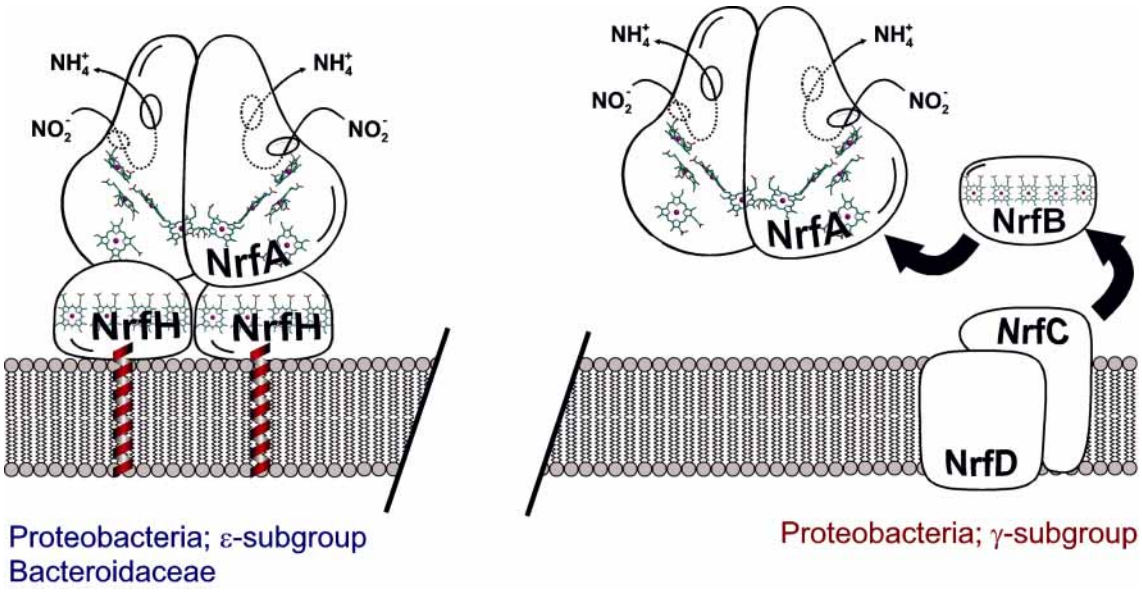

Figure 36: A cartoon model for the Nrf complex. **Left:** The NrfHA complex of ε-proteobacteria and bacteroides has been described in this work. The quinol oxidase NrfH is attached to the membrane *via* a single transmembrane helix and obtains electrons from menaquinone which is mobile within the membrane. Associated to it is the NrfA dimer. **Right:** The NrfABCD complex of γ-proteobacteria. NrfC and NrfD form a membrane-integrated quinol oxidase and NrfB is the electron carrier between this complex and NrfA.

The formation of a membrane-associated complex has been suggested for *S. deleyianum* (Einsle *et al.*, 1998; Schumacher *et al.*, 1997) and it has been found in and purified from *W. succinogenes* (Simon *et al.*, 2000), but it remains unclear whether the same can be expected in the γ-subdivision of proteobacteria.

If the proteins of the *nrfABCDEFG* operon are transcribed in equal ratios, a complex seems more likely than a system consisting of a separate quinol oxidase and a soluble reductase. All known *nrf* operons of γ-proteobacteria show a gap of approximately 70 residues between *nrfA* and *nrfB*, while *nrfB*, *nrfC* and *nrfD* are in line, with their respective start and stop codons overlapping. This led to the suggestion (Hussain *et al.*, 1994), that *nrfB*, *nrfC* and *nrfD* are cotranscribed, while *nrfA* might be expressed at a different, presumably higher level. This hypothesis would speak against the existence of a nitrite reductase complex in the *nrfABCDEFG* system, but there is no biochemical evidence so far from *E. coli*.

6.3 Heme Group Arrangement of Nitrite Reductase

Understanding of the arrangements and interactions of the heme centers of multiheme proteins is still rudimentary. The first structure of a multiheme cytochrome *c* was the small subunit of the photosynthetic reaction center of *Rhodopseudomonas viridis* (Deisenhofer *et al.*, 1984), a tetraheme protein with two diheme units connected through a local twofold symmetry axis. It did not show any similarities to the heme arrangement of the cytochrome c_3 family, whose crystallographic analysis began shortly thereafter (see 5.5). Until today there is a considerable number of structures available and in spite of a high divergence in sequence, molecule size and heme arrangement, common motives begin to emerge. A comparison of the structures presented in this work with the structures of several other cytochromes

is intended to help in working out underlying principles, a task which can only give a crude picture at the present state of knowledge.

6.3.1 Hydroxylamine Oxidoreductase

Hydroxylamine oxidoreductase (HAO) is a trimeric octaheme *c* enzyme that catalyzes the four-electron oxidation of hydroxylamine to nitrite. It was purified and characterized from *Nitrosomonas europaea* (Collins *et al.*, 1993), a nitrifying chemoautotrophic proteobacterium belonging to the β-subdivision. The crystal structure of the protein was solved to a resolution of 2.8 Å (Igarashi *et al.*, 1997) by Multiple Isomorphous Replacement, revealing a novel and complex arrangement of the heme cofactors and a high amount of monomer interaction.

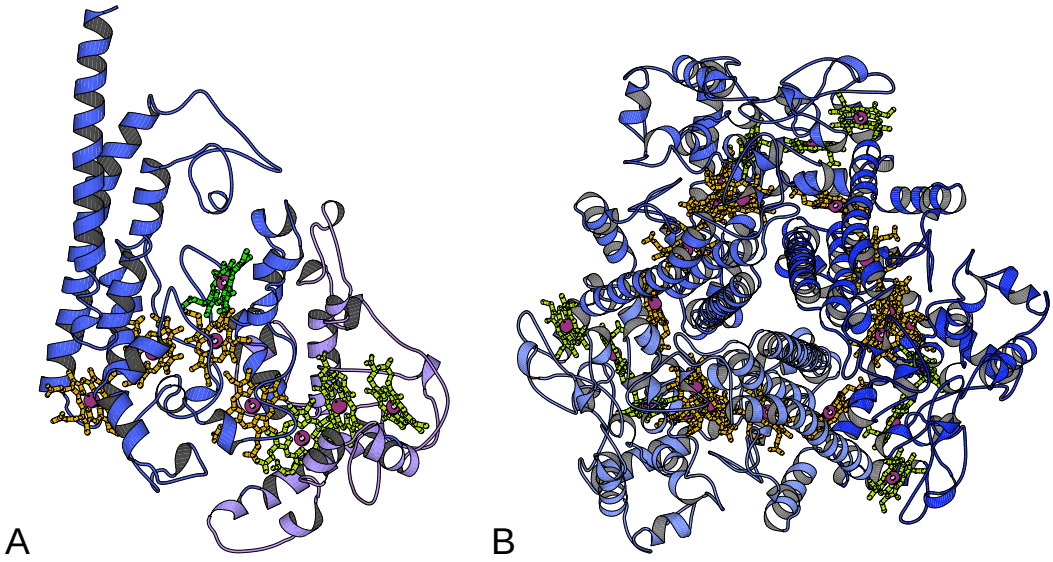

Figure 37: The structure of hydroxylamine oxidoreductase (HAO) from *Nitrosomonas europaea*. **A**) Side view of the single monomer of 67 kDa with eight *c*-type heme groups. The active site heme is depicted in green, and the four other hemes which correspond to nitrite reductase are drawn in orange. **B)** Top view of the cone-shaped HAO trimer, showing the ring of monomers formed by 18 of the 24 heme groups.

Most interestingly, the five hemes of nitrite reductase align to hemes 4 to 8 of HAO with a root-mean-square deviation of 2.00 Å and the three dimer-forming helices *h*22, *h*23 and *h*25 of nitrite reductase (Figure 21) find

their topological equivalents in helices α20, α22/α23 and α24 of HAO. Furthermore, helix *h*18 of nitrite reductase, which runs along the three coplanar hemes, corresponds to helix α15 of HAO. These similarities strongly suggest a distant evolutionary relatedness for both proteins.

The overall setup of both proteins shows remarkable differences. While HAO is a functional trimer, nitrite reductase acts as a dimer. The trimerization of HAO leads to the formation of a ring of eighteen hemes - six from each monomer (Igarashi *et al.*, 1997). The P_{460}-heme is situated above this ring and is close to heme 8 of the adjacent monomer. Heme 1, the active site, does not participate in the formation of the ring. In nitrite reductase heme 5, the topological equivalent of heme 8 in HAO, is the one that interacts over the dimer interface. In both cases the result is the ability to distribute electrons quickly over a larger number of heme centers.

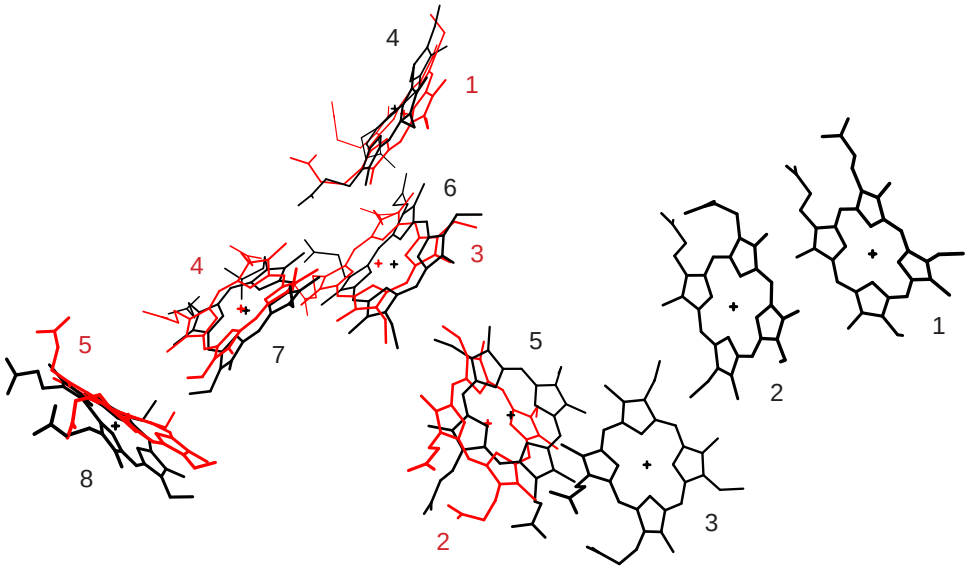

Figure 38: The heme arrangement of nitrite reductase (1-5 in red) and HAO (1-8 in black) with the heme groups numbered according to their attachment to the protein chain. Hemes 1 to 3 of HAO are missing in nitrite reductase, but the remaining five cofactors can be aligned with a total r.m.s. deviation of 2.0 Å.

The corresponding heme groups in both proteins, heme 4 in HAO and heme 1 in nitrite reductase form the active sites of the two enzymes, and both are high-spin hemes with no distal protein ligand (see 6.4.2).

6.3.2 Cytochrome c_{554}

In the pathway of nitrification, electrons that are gained through the oxidation of hydroxylamine by HAO are directly transferred to cytochrome c_{554}, a tetraheme *c* protein of 211 residues (Andersson *et al.*, 1986). The EPR spectra and redox potentials of the heme groups were determined (Arciero *et al.*, 1991), showing that one of the heme groups is high spin, just as in the case of nitrite reductase and HAO. Furthermore, heme-heme interactions were observed, and also a characteristic EPR signal with features at g = 3.85 and g = 9.8, which were assigned to an exchange-coupled pair of a low-spin and a high-spin Fe(III) center (Andersson *et al.*, 1986; Hendrich *et al.*, 1993). These features correspond exactly to the ones observed in nitrite reductase (Schumacher & Kroneck, 1991).

The crystal structure of cytochrome c_{554} was solved recently to a resolution of 2.6 Å (Iverson *et al.*, 1998), revealing a previously unobserved, α-helical protein folding around the four heme centers. In spite of the complete absence of sequence homology, the arrangement of the heme groups bears a clear resemblance to the one of hydroxylamine oxidase, as hemes 1 to 4 of cytochrome c_{554} not only align to hemes 3 to 6 of HAO with a r.m.s. deviation of 0.8 Å, but are also attached to the protein chain in the same order.

A closer look at a superposition of cytochrome c_{554} with HAO showed, that only very few structural elements in the direct vicinity of the hemes were conserved, indicating that the only evolutionarily conserved element is the heme arrangement itself, just as it is found in the case of HAO and nitrite reductase.

As a consequence of the agreement with HAO, hemes 2 to 4 of cytochrome c_{554} also align well with hemes 1 to 3 of nitrite reductase. Thus, heme 2 of cytochrome c_{554} corresponds to the active site hemes of both HAO and nitrite reductase. While the proximal ligand of this heme is a regular histidine as in HAO, it was found to be five-coordinate like in the two enzy-

mes, although the cytochrome has no apparent catalytic activity and the vacant iron site does not seem to be accessible at all (Iverson *et al.*, 1998).

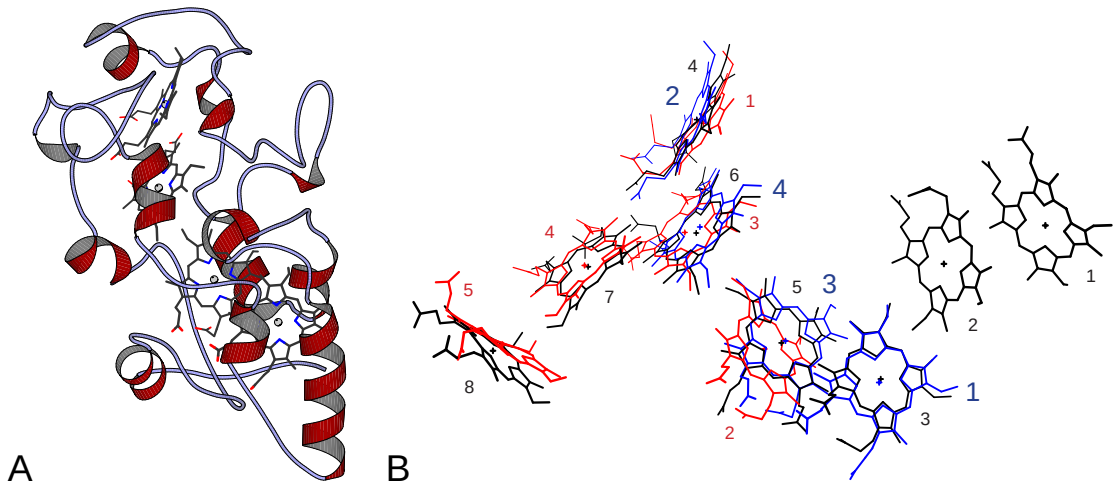

Figure 39: Cytochrome c_{554} from *Nitrosomonas europaea*. **A**) Ribbon plot of the α-helical protein with four *c*-type heme groups. **B**) Superposition of heme groups. The four hemes of cytochrome c_{554} (blue) align very well (r.m.s.d. 0.83 Å) with hemes 3-6 of HAO, and thus also with hemes 1 to 3 of nitrite reductase.

The correlation of heme arrangements in nitrite reductase and cytochrome c_{554} allows to draw conclusions concerning the EPR signals directly from the structure. If the prominent signals at g = 3.85 and g = 9.8 originate from the same heme-heme interaction in both cytochrome c_{554} and nitrite reductase, they can be assigned to the closely stacked hemes 2 and 4 in cytochrome c_{554} or hemes 1 and 3 in nitrite reductase, both of which have an iron-iron distance of 9.3 Å.

6.3.3 Split-Soret Di-heme Cytochrome *c*

"Split-Soret" cytochrome *c* (SSC) from *D. desulfuricans* ATCC 27774 was named after the observation, that upon reduction the Soret band of the UV/vis spectrum of this protein did not only show a maximum at 424 nm, but also a shoulder at 415m. The protein, a homodimer of 26.3 kDa per subunit, carries a total of four heme groups, arranged as two stacked pairs. It has been purified from the soluble fraction of *D. desulfuricans* (Liu *et al.*, 1988), but its physiological function is still unclear.

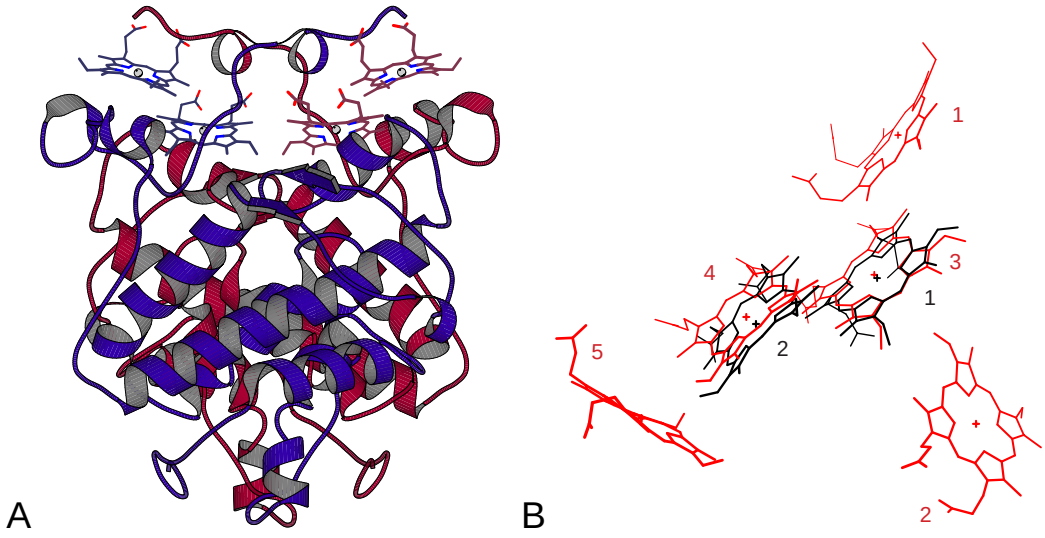

Figure 40: Dimeric di-heme split-Soret cytochrome *c* from *D. desulfuricans* ATCC 27774. The structure shows again an unprecedented protein fold (**A**) with the four heme groups of the dimer located on one extreme side of the molecule. Every heme group in each chain has one histidine ligand from the other chain. **B**) The two hemes of the split-Soret cytochrome monomer align very well with hemes 3 and 4 of nitrite reductase.

The analysis of the primary sequence (DeVreese *et al.*, 1997) showed, that only the C-terminal part resembled other *c*-type cytochromes, while the N-terminal domain, in spite of containing four further cysteines, was predicted to be substantially different. This domain is homologous to a putative protein from the genome sequence of the sulfate-reducing archaeon *Archaeoglobus fulgidus* which does not reduce nitrite, indicating that the split-Soret cytochrome might be involved in sulfate reduction.

At the same time, the structure of the protein was solved by another group without knowledge of the primary structure (Matias *et al.*, 1997), revealing a heme arrangement that is unusual in several ways (Figure 40). All heme groups are exposed to the solvent to a rather high degree. They are located on one side of the protein, attached to the most carboxyterminal part of the chain, while the rest of the protein forms a compact, heme-free domain. All hemes are bis-histidinyl-coordinated, and the distal ligand of each heme is part of the C-terminal extension of the other monomer.

While there is no homology between the folds of SSC and nitrite reductase, the two hemes of SSC align to hemes 3 and 4 of nitrite reductase with

a total r.m.s. deviation of 2.1 Å (Figure 40). As in the other cases presented, distance and angle of the two hemes are strictly conserved.

It should be mentioned that cytochrome *c* nitrite reductase also shows a splitting in the Soret band, visible only in the second derivative of the UV/visible spectrum (Schumacher, 1993), with the main absorption maximum at 419.4 nm and a second peak at 427 nm.

6.3.4 Cytochrome c_3

As mentioned above (see 5.5.4), the heme arrangement is highly conserved in all cytochromes c_3 that have been structurally characterized so far. It has also been noted before, that heme groups 1 and 3 of cytochrome c_3 align well with hemes 3 and 4 of cytochrome c_{554} (Iverson *et al.*, 1998) and also to the heme pairs 2/3, 5/6 and 7/8 of HAO (Nørager *et al.*, 1999).

Thus it is not surprising to find the same homologies with nitrite reductase, where this special heme arrangement is found in the heme pairs 2/3 and 4/5. In the latter it is even possible to locate a conserved phenylalanine residue in nitrite reductase (Phe 410 in the *S. deleyianum* sequence), that corresponds to the one found in all cytochromes c_3 (Figure 41).

It has been suggested that this phenylalanine residue plays an essential role in orienting the heme groups (Pierrot *et al.*, 1982), but the exact conservation of this motif without such a phenylalanine, as it is found in hemes 2/3 of nitrite reductase as well as in HAO and cytochrome c_{554}, rules out this hypothesis. This is consistent with the results of mutational studies in cytochromes c_3, where the replacement of this phenylalanine did not influence the stability of the proteins (Dolla *et al.*, 1999; Saraiva *et al.*, 1996).

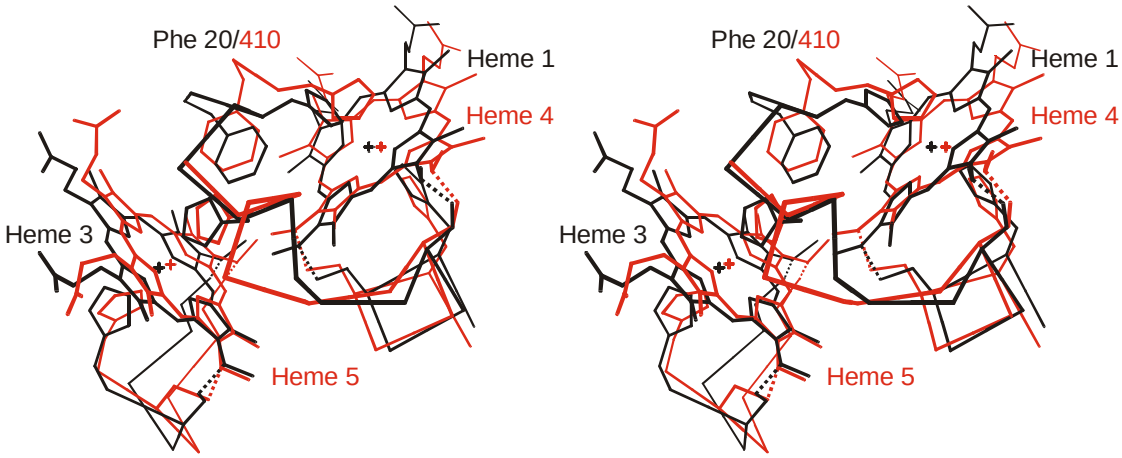

Figure 41: A superposition of the immediate surroundings of hemes 4 and 5 of *S. deleyianum* nitrite reductase (red) with hemes 1 and 3 of *D. desulfuricans* Essex 6 cytochrome c_3 (black). The only conserved protein part apart from the heme binding motives (Cys-X_1-X_2-Cys-His) is the loop containing the two distal histidine ligands of both hemes and a conserved phenylalanine.

Nevertheless the conservation of this residue in the c_3 family as well as in hemes 4/5 of nitrite reductase and hemes 7/8 of HAO is obvious and most likely will influence the redox properties of the system. While the electron transfer rate of the c_3 system does not allow a measurement of mutant and wild type under *in vivo* conditions, nitrite reductase offers the possiblity to accurately monitor the influence of such a mutation on electron transfer to the active site, expressed as a change in nitrite reduction activity. Although there is no feasible expression system for nitrite reductase available yet, this phenylalanine residue will be a prime candidate for mutant studies. It will then be important to overcome one weakness of the activity test, which is that the use of small reductants like dithionite makes it possible to short-cut *in vivo* electron transfer pathways in nitrite reductase. However, this effect should be recognized and can be counteracted, e.g. by using proteins – optimally NrfH – as reducing agents of the enzyme.

6.3.5 Building Blocks for Multiheme Cytochromes

Based on the analysis given above, a model of interaction of the heme groups in different multiheme proteins can be proposed. This model differs substantially from the one given for HAO (Igarashi *et al.*, 1997).

Two core motives of heme-heme interaction are observed in different protein environments:

- The almost perpendicular arrangement of hemes as observed for hemes 1 and 3 of cytochrome c_3, in the following referred to as the CC3 module.
- The parallel and tight stacking interaction with an iron-iron distance between 9 and 10 Å, as it is seen most clearly in the split-Soret cytochrome, in the following referred to as the SSC motif.

Thus nitrite reductase is built up by two CC3-modules (hemes 2/3 and 4/5) that interact via the SSC motif (hemes 3 and 4). HAO then has three such modules (hemes 2/3, 5/6, 7/8) which all interact through SSC motives. In both enzymes, the active site heme group does not form part of this scheme, but it interacts with one of the CC3 modules at a distance and orientation that is similar to the SSC motif (Table 7).

The CC3 module is characterized by an iron-iron-distance ranging between 11.1 Å (cytochrome c_3) and 12.8 Å (*S. deleyianum* nitrite reductase hemes 2/3) and an angle close to 90° between the heme planes. The heme edge to edge distances are around 6.5 Å and the distal histidine ligands are located on the same side of the porphyrin rings, within the module.

The SSC motif on the other hand represents a completely different type of interaction, a stacking arrangement in which the two hemes are almost exactly parallel and related by a local twofold symmetry axis. In the ideal case, realized in the split-Soret cytochrome, in hemes 3 and 4 of nitrite reductase, hemes 6 and 7 of HAO and hemes 1 and 3 of cytochrome c_{554}, this symmetry is kept within a 0.1 Å r.m.s.d. for all porphyrin atoms. Iron-iron

distances range between 9.0 and 9.5 Å and the closest distance of the porphyrin rings, between the CHB atoms of the hemes, is close to or below 4 Å, allowing for direct resonance transfer.

CC3 modules			
	Hemes involved	**Fe – Fe [Å]**	**CHD_1 – CHB_2 [Å]**
cytochrome c_3	1 / 3	11.10	6.66
S. deleyianum nitrite reductase	2 / 3 4 / 5	**A**: 12.83 **B**: 12.84 **C**:12.75 **A**: 11.12 **B**: 11.18 **C**:11.15	**A**: 7.46 **B**: 7.61 **C**:7.50 **A**: 6.35 **B**: 6.65 **C**:6.65
W. succinogenes nitrite reductase	2 / 3 4 / 5	12.56 11.13	7.28 6.49
hydroxylamine oxidoreductase	2 / 3 5 / 6 7 / 8	11.73 11.98 12.07	6.75 7.26 7.43
cytochrome c_{554}	3 / 4	12.17	7.76
SSC motives			
	Hemes involved	**Fe – Fe [Å]**	**CHB_1 – CHB_2 [Å]**
split-Soret cyt.	1 / 2	9.01	3.83
S. del. NiR	3 / 4	**A**: 9.37 **B**: 9.35 **C**:9.28	**A**: 4.03 **B**: 3.88 **C**:3.82
W. succ. NiR	3 / 4	9.49	4.02
hydroxylamine oxidoreductase	1 / 2 3 / 5 6 / 7	9.45 9.18 9.79	4.48 4.13 4.24
cytochrome c_{554}	1 / 3	9.18	4.43
Active sites			
	Hemes involved	**Fe – Fe [Å]**	**$C2D_1$ – $C2D_2$ [Å]**
S. del. NiR	1 / 3	**A**: 9.61 **B**: 9.69 **C**:9.58	**A**: 3.83 **B**: 3.75 **C**:3.82
W. succ. NiR	1 / 3	9.68	3.77
HAO	4 / 6	9.85	3.84
cytochrome c_{554}	2 / 4	9.52	3.68

Table 7: Distances in the characteristic heme-binding motives found in a range of multiheme cytochromes. Three motives are considered, the CC3 module, the SSC motif and the interaction of the active site heme with the others. Details are explained in the text. The data for cytochrome c_3 is taken from the *D. desulfuricans* Essex 6 structure that was solved in this work. For *S. deleyianum* nitrite reductase, three values are given for the three monomers in the asymmetric unit.

A third type of heme-heme-interaction concerns the active site heme groups of nitrite reductase and HAO with their respective closest neighbours. Although hemes 4, 6 and 7 of HAO have been described as a

triplet of stacked hemes (Igarashi *et al.*, 1997), the active site heme does not form a real SSC motif with its neighbour like the ones descibed above. Like in the SSC motif, the active sites hemes are flipped compared to their partners and the iron-iron distance is in the range of 9.5 Å (Table 7). Seen from above however, the two porphyrins are not parallel, but twisted by approximately 45° and the closest distance is not between the CHB atoms, but between the C2D atoms that form part of pyrrole ring D.

In summary, the building principle of both reductases seems to be a distinct arrangement of CC3 modules which are connected via the SSC motif to form an electron conduction system. In the trimer of HAO, nine of these modules form a closed ring, in the nitrite reductase dimer four are linked across the dimer interface. The active site heme groups are positioned such that they can interact with this system although they are not directly part of it.

6.3.6 Other Multiheme Cytochromes

Although only a limited number of multiheme cytochrome structures are available today it is obvious, that the heme arrangements described in the previous paragraphs are more widespread still. The recently described structure of a nonaheme cytochrome *c* from *D. desulfuricans* ATCC 27774 (Matias *et al.*, 1999a) shows similarities to cytochrome c_3 and contains two CC3 modules. A most recently determined structure of a flavocytochrome *c* fumarate reductase, which was solved independently by three different groups from *Shewanella putrefaciens* MR-1 (Leys *et al.*, 1999) and from *Shewanella frigidamarina* NCIMB400 (Bamford *et al.*, 1999; Taylor *et al.*, 1999), also contains four heme groups in an arrangement similar to the one observed in nitrite reductase and HAO. Heme groups 3, 4 and 2 of the flavocytochrome align to hemes 2, 3 and 4 of nitrite reductase, meaning that hemes 2 and 3 form a SSC motif, while hemes 3 and 4 are arranged as a CC3 module.

Moreover, database searches revealed that a presumed outer membrane metal reductase complex, MtrABC from *S. putrefaciens* (Beliaev & Saffarini, 1998) contains two decaheme *c*-type cytochromes, MtrA and MtrC. MtrA exhibits a 34% identity to NrfB from *E. coli* and five of its heme groups can be clearly aligned with the ones from NrfB. NrfB itself has not been discussed much so far, but in analogy to the HAO/cytochrome c_{554} system it can be expected to fall into this same family of multiheme cytochromes.

6.4 Mechanism and Reactivity of Nitrite Reductase

6.4.1 Substrate complexes

The obtained structures of nitrite and hydroxylamine bound to the active site of *W. succinogenes* nitrite reductase provide important information about binding modes and about protein residues involved in substrate binding. Difference electron densities clearly suggest a binding of nitrite via its nitrogen atom (Figure 27). The position of hydroxylamine in the corresponding substrate soak furthermore indicates, which of the nitrogen-oxygen bonds in nitrite is cleaved first (Figure 28). This part of the reaction is analogous to the reaction of cytochrome cd_1, as water can be removed after a single-electron reduction. As seen from the structure of nitrite-bound cytochrome cd_1 (Williams *et al.*, 1997), the oxygen that is obviously the leaving atom in this case is bound to two histidine residues.

A further question that remains is the different binding geometry for both sulfate and nitrite to nitrite reductase from *W. succinogenes* and *S. deleyianum*. In the latter, both the substrate nitrite and the inhibitor sulfate are bound to Tyr 217 and His 282 simultaneously, while in *W. succinogenes* nitrite is bound to His 277 and sulfate to Tyr 218 only. Due to the high similarity of both structures, the active site geometry can hardly account for this difference. Note however, that the nitrite reductase structures from the

two organisms were solved at different pH values, pH 6.8-7.5 for *S. deleyianum* and pH 5.6-5.7 for *W. succinogenes*. As the pK_a value of histidine is around 6.5, it may be possible that the differences observed in both structures originate from protonation (or deprotonation) of the $N_{\varepsilon 2}$ atom of His 282 (277). However it should be considered, that the active site cavity of the enzyme is lined with charged residues that cause a preference for anions and that in this local environment the pK_a of His 282 (277) might differ slightly. Further experiments will be neccessary at this point before a final statement can be made.

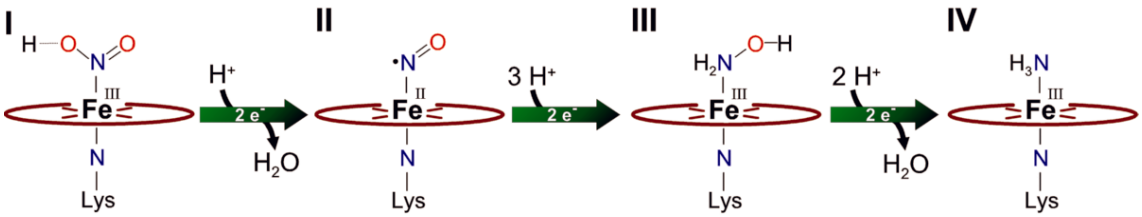

Figure 42: A minimal reaction scheme of cytochrome *c* nitrite reductase. Structure I represents the catalytic heme 1 in the oxidized state with nitrite bound. The Fe^{II}–NO adduct (structure II) has been identified under turnover conditions by rapid freeze EPR spectroscopy, with an intense resonance at g = 2.014, and a hyperfine splitting A^N = 1.55 mT. Structure III shows the hydroxylamine intermediate, after transfer of four electrons. Hydroxylamine is converted to ammonia by nitrite reductase but is not liberated during the reduction of nitrite to ammonia. In the final step ammonia is formed (structure IV) and released as an ammonium cation.

Based on structure and substrate complexes, a minimal reaction scheme for nitrite reductase can be proposed (Figure 42). Nitrite has been shown to bind to the oxidized enzyme (I), and a one-electron reduction step is sufficient to liberate the first oxygen atom as water, taking along the protons from His 282 (277) and possibly from Tyr 217 (218). Transfer of a second electron to the active site heme group will produce an Fe^{II}-NO adduct which has been identified spectroscopically under turnover conditions by rapid freeze EPR, with an intense resonance at g = 2.014 and a hyperfine splitting A^N = 1.55 mT (Stach *et al.*, 2000).

Two further electrons lead to the state of hydroxylamine, which is a known substrate (Schumacher, 1993) and has been characterized crystallo-

graphically. Reaching this point it might be helpful to take a closer look at the reaction of hydroxylamine oxidoreductase.

6.4.2 Nitrite Reductase versus Hydroxylamine Oxidase

The only two multiheme *c* enzymes which are structurally characterized to date are hydroxylamine oxidoreductase and nitrite reductase. In addition to the similarities in heme group arrangement they also catalyze analogous reactions, both involving electron transfer from or to nitrite.

However, while a classical protoporphyrin IX heme with a novel lysine-coordination forms the active site of nitrite reductase, HAO features the P_{460}-type heme with a covalent link between a *meso* CHC of the heme and $C_{\varepsilon 1}$ of a tyrosine residue of an adjacent chain in the functional trimer. The fifth coordinaton position of P_{460} is occupied by a histidine (Figure 43). As HAO functions as an oxidase and nitrite reductase as a reductase, the replacement of histidine by lysine can be expected to raise the redox potential of the heme, generating an electron sink in the system of redox-active cofactors. Furthermore, with a coordinated lysine the symmetric product complex with two sp^3-hybridized nitrogen ligands at heme 1 might add favorably to the overall driving force of the reaction.

The only feature that is strictly conserved between nitrite reductase and HAO, apart from the arrangement of the hemes, is a histidine at the active site at the beginning of a topologically conserved helix: histidine 282 (277) at the beginning of helix *h*18 in nitrite reductase and histidine 268 in helix α15 in HAO. In nitrite reductase this histidine binds the substrate, and its conservation in both proteins suggests a role in the reduction of nitrite to hydroxylamine, or at least in the abstraction of the first oxygen atom in the form of water from nitrite in the reaction sequence of nitrite reductase. This picture is in good accordance to the complexes of *W. succinogenes* nitrite reductase with nitrite and hydroxylamine (see 5.4.5.7).

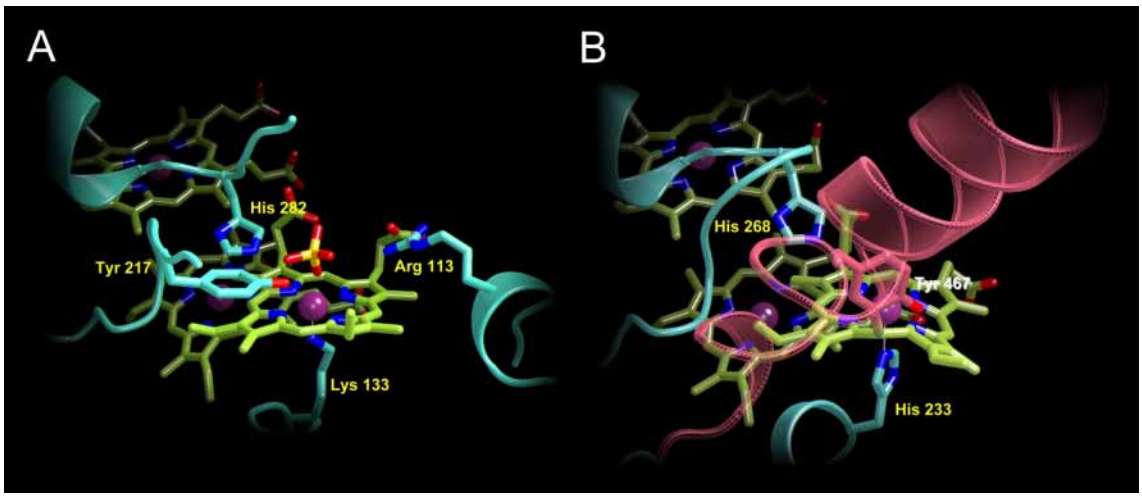

Figure 43: A comparison of the active sites of **A**) *S. deleyianum* nitrite reductase and **B**) hydroxylamine oxidoreductase. Note that the side of the active site channel in nitrite reductase (front) is completely blocked in HAO and vice versa. A single histidine residue (282 in nitrite reductase, 268 in HAO) is conserved, while lysine 133 and tyrosine 217 are unique features of nitrite reductase. Tyrosine 467 in HAO is close to the heme iron, but the position of the O_η atom forbids interaction with any substrate bound to the iron.

While nitrite reductase catalyzes a six-electron reduction, HAO performs a four-electron oxidation. The two-electron step from hydroxylamine to ammonia is only observed in nitrite reductase. Most likely, the features where both active sites differ significantly are involved in this part of the reaction. The main differences are obviously tyrosine residue 217 (218) of nitrite reductase, which binds to the sulfate ion (but not to nitrite in the *W. succinogenes* complex structure), the coordination of lysine 133 (134) to heme 1 and the orientation of its propionate sidechains in nitrite reductase. Conversion of hydroxylamine to ammonia requires the abstraction of an oxygen atom, leaving a bound $NH_2^{\bullet}$ radical, which would then receive an electron plus a proton from tyrosine 217 (218) to yield ammonia and a tyrosyl radical which must persist until a further electron arrives. In HAO, the covalently linked tyrosine 467 comes closer with its oxygen atom (3.7 Å) to the heme iron compared to tyrosine 217 (218) in the sulfate-bound form of nitrite reductase (5.2 Å). However, in HAO the oxygen points away from the iron and forms a rather unfavorable angle for electronic interaction with any iron ligand, whereas in nitrite reductase a simple rotation around the tyrosine's χ_1-angle would bring it much closer to the iron.

7 Danksagung

Die vorliegende Arbeit entstand im Zeitraum von November 1996 bis Dezember 1999 in der Abteilung Strukturforschung am Max-Planck-Institut für Biochemie in Martinsried.

Mein besonderer Dank geht an Prof. Dr. Peter Kroneck, Universität Konstanz, nicht nur für die Überlassung eines reizvollen und faszinierenden Themas und die Betreuung dieser Arbeit, sondern auch und gerade für seine umfangreiche Unterstützung und Föderung, viele gute Ratschläge und exzellente Kommunikation.

Prof. Dr. Robert Huber danke ich für die Übernahme des Koreferats, für sein anhaltendes Interesse an meiner Arbeit und für anregende Diskussionen. Im besonderen schätzte ich die Möglichkeit, mit bester Austattung und in hoher Selbstverantwortlichkeit dem Forscherdrang nachgeben zu können, und dabei stets Unterstützung und Rückhalt zu erfahren.

Bei PD Dr. Albrecht Messerschmidt bedanke ich mich herzlich für die ausgezeichnete Betreuung und Zusammenarbeit, insbesondere bei der Strukturlösung der Nitritreduktase und als Anlaufstelle in kristallographischen Fragen. Aufrichtigen Dank auch dafür, mich im Herbst 1994 als erster auf die Pfade der Strukturbiologie gelockt zu haben.

Prof. Dr. Achim Kröger, Universität Frankfurt, und seinen Mitarbeitern Dr. Jörg Simon, Dr. Oliver Klimmek und Dr. Roland Groß danke ich für die fruchtbare Kooperation bei der Analyse des *nrf*-Operons und für rege Diskussionen über *Wolinella*.

Petra Stach und Klaus Sulger, AG Kroneck, hatten immer noch etwas mehr Protein zum Kristallisieren auf Lager. Vielen Dank auch für die erstklassige experimentelle Zusammenarbeit.

Dr. Hans Bartunik und Gleb Bourenkov, MPG-ASMB Hamburg, danke ich für die ausgezeichnete Verfügbarkeit und Betreuung der Beamline BW6 am DESY. Dr. Karlheinz Mann und Marius Boicu, MPI Martinsried, waren bei Protein- und DNA-Sequenzierungen eine unschätzbare Hilfe.

Ein spezieller Dank für Geduld und Hilfe geht an unsere Sekretärinnen, Renate Rüller und Gina Beckmann, sowie an Werner Dersch und Herbert Fischer, die dem Chaos nach Kräften die Schranken weisen.

Den derzeitigen und ehemaligen Kollegen am MPI Martinsried sei gedankt für eine schöne Zeit, reich an Erfahrungen und Lebensweisheiten: Dr. Markus Deibert, Holger Dobbek, Rupert Lang, Ulrich Rester und Michael Worbs im Schreibzimmer, Dr. Tim Clausen, Stephan Ehlert, Anja Lang, Snezan Marinkovic, Berta Martins, Dr. Pedro Pereira, Dr. Sandra Ribeiro, Dr. Peter Sondermann, Clemens Steegborn und Dr. Markus Wahl im Labor, aber auch Dr. Andreas Bergner, Dr. Jörg Benz, Dr. Lars Ditzel, Dr. Erich Fritsche, Marta Garrido, Stefan Gerhardt, Dr. Michael Groll, Jens Kaiser, Lars Linden, Isabella Pikart, Dr. Stefan Steinbacher und all den anderen, auch der "*next generation*" ...

Ebenso danke ich der gesamten AG Kroneck, besonders Dietmar Abt, Stefanie Foerster, Robert Krieger und Petra Stach für gemeinsame Kristallisiererlebnisse, aber auch Thomas Büchert und Dr. Frank Neese für eine großartige Atmosphäre. Auch bin ich dankbar für gute Freunde, die mich trotz Abwesenheit nicht vergessen haben; Bozana und Martin Gehringer, Michael Schäffauer, Jacqueline Menchini, Andreas Göttlich, Jürgen Happel und André Raquet.

Nicht genug danken kann ich meiner Mutter für Rückhalt, Unterstützung und Geduld trotz großer eigener Sorgen.

... and for almost all the rest, for support, patience and strength, my thanks and my affections go to Susana Andrade.

8 Appendix

8.1 Abbreviations

Å	Ångstrøm; 1 Å = 10^{-10} m
AMO	ammonia monooxygenase
ATP	adenosine-5'-triphosphate
bp	basepair
CTAB	hexadecyl trimethyl ammonium bromide
DEAE	diethyl aminoethyl
Da	Dalton; 1 Da = 1 g·mol^{-1}
DNA	deoxyribonucleic acid
DNRA	dissimilatory nitrate reduction to ammonia
EPR	electron paramagnetic resonance
ESI-MS	Electron spray ionization mass spectrometry
FPLC	fast protein liquid chromatography
HAO	hydroxylamine oxidoreductase
HEPES	N-2-hydroxyethylpiperazine-N'-2-ethanesulfonic acid
ICP-MS	Inductively coupled plasma mass spectrometry
LB	Luria-Bertani medium
MALDI-TOF	Matrix-assisted laser dissorption ionization – time of flight
MES	2-morpholinoethanesulfonic acid
MPD	2-methyl-2,4-pentane diol
N_2OR	nitrous oxide reductase
NaR	nitrate reductase
NiR	nitrite reductase
NOR	nitric oxide reductase
nrf	nitrite reduction with formate
PAGE	polyacrylamide gel electrophoresis
r.m.s.d.	root-mean-square deviation

RNA	ribonucleic acid
SDS	sodium dodecyl sulfate
SSC	Split-Soret cytochrome *c*
Tris	α,α,α-trishydroxymethyl aminomethane
v/v	volume per volume
w/v	weight per volume

Amino Acids

A	Ala	alanine	M	Met	methionine
B	Asx	Asn *or* Asp	N	Asn	asparagine
C	Cys	cysteine	P	Pro	proline
D	Asp	aspartate	Q	Gln	glutamine
E	Glu	glutamate	R	Arg	arginine
F	Phe	phenylalanine	S	Ser	serine
G	Gly	glycine	T	Thr	threonine
H	His	histidine	V	Val	valine
I	Ile	isoleucine	W	Trp	tryptophan
K	Lys	lysine	Y	Tyr	tyrosine
L	Leu	leucine	Z	Glx	Gln *or* Glu

Nucleic Acid Bases

A		adenine	S	G/C	*s*trong
G		guanine	W	A/T	*w*eak
C		cytosine	B	G/C/T	not A
T		thymine	D	A/G/T	not C
R	A/G	pu*r*ine	H	A/C/T	not G
Y	C/T	p*y*rimidine	V	A/G/C	not T
K	G/T	*k*eto group	N	A/G/C/T	a*n*y
M	A/C	a*m*ino group	I	inosine	"wobble" to U/C/A

8.2 Index of Figures

8.3 Index of Tables

9 References

Abou-Jaoudé, A., Chippaux, M. & Pascal, M. C. (1979a). Formate-nitrite reduction in *Escherichia coli* K12. 1. Physiological study of the system. *Eur. J. Biochem.* **95**, 309-314.

Abou-Jaoudé, A., Pascal, M. C. & Chippaux, M. (1979b). Formate-nitrite reduction in *Escherichia coli* K12. 2. Identification of components involved in the electron transfer. *Eur. J. Biochem.* **95**, 315-321.

Abrahams, J. P. & Leslie, A. G. W. (1996). Methods used in the structure determination of bovine mitochondrial F_1 ATPase. *Acta Cryst. D* **52**, 30-42.

Andersson, K. K., Lipscomb, J. D., Valentine, M., Münck, E. & Hooper, A. B. (1986). Tetraheme cytochrome c_{554} from *Nitrosomonas europaea*. Heme-heme interactions and ligand binding. *J. Biol. Chem.* **261**, 1126-1138.

Arciero, D. M., Collins, M. J., Haladjian, J., Bianco, P. & Hooper, A. B. (1991). Resolution of the four hemes of cytochrome c_{554} from *Nitrosomonas europaea* by redox potentiometry and optical spectroscopy. *Biochemistry* **30**, 11459-11465.

Ausubel, F. M., Brent, R., Kingston, R. E., Moore, D. D., Seidman, J. G., Smith, J. A. & Struhl, K. (1990). *Current Protocols in Molecular Biology*, Greene Publishing Associates and Wiley Interscience, New York.

Baikalov, I., Schroder, I., Kaczor-Grzeskowiak, M., Grzeskowiak, K., Gunsalus, R. P. & Dickerson, R. E. (1996). Structure of the *Escherichia coli* response regulator NarL. *Biochemistry* **35**, 11053-11061.

Ballard, A. L. & Ferguson, S. J. (1988). Respiratory nitrate reductase from *Paracoccus denitrificans*. Evidence for two *b*-type haems in the gamma subunit and properties of a water-soluble active enzyme containing alpha and beta subunits. *Eur. J. Biochem.* **174**, 207-212.

Bamford, V., Dobbin, P. S., Richardson, D. J. & Hemmings, A. M. (1999). Open conformation of a flavocytochrome c_3 fumarate reductase. *Nat. Struct. Biol.* **6**, 1104-1107.

Barton, G. J. (1993). ALSCRIPT. A tool to format multiple sequence alignments. *Prot. Engineering* **6**, 37-40.

Barton, L. L., LeGall, J., Odom, J. M. & Peck Jr., H. D. (1983). Energy coupling to nitrite respiration in the sulfate-reducing bacterium *Desulfovibrio gigas*. *J. Bacteriol.* **153**, 867-871.

Beliaev, A. S. & Saffarini, D. A. (1998). *Shewanella putrefaciens mtrB* encodes an outer membrane protein required for Fe(III) and Mn(IV) reduction. *J. Bacteriol.* **180**, 6292-6297.

Bell, A. I., Cole, J. A. & Busby, S. J. (1990). Molecular genetic analysis of an FNR-dependent anaerobically inducible *Escherichia coli* promoter. *Mol. Microbiol.* **4**, 1753-1763.

Bell, A. I., Gaston, K. L., Cole, J. A. & Busby, S. J. (1989). Cloning of binding sequences for the *Escherichia coli* transcription activators, FNR and CRP: location of bases involved in discrimination between FNR and CRP. *Nucl. Ac. Res.* **17**, 3865-3874.

Bergmann, D. J., Arciero, D. M. & Hooper, A. B. (1994). Organization of the *hao* gene cluster of *Nitrosomonas europaea*: genes for two tetraheme *c* cytochromes. *J. Bacteriol.* **176**, 3148-3153.

Berks, B. C., Ferguson, S. J., Moir, J. W. B. & Richardson, D. J. (1995a). Enzymes and associated electron transport systems that catalyse the respiratory reduction of nitrogen oxides and oxyanions. *Biochim. Biophys. Acta - Bioenergetics* **1232**, 97-173.

Berks, B. C., Richardson, D. J., Reilly, A., Willis, A. C. & Ferguson, S. J. (1995b). The *napEDABC* gene cluster encoding the periplasmic nitrate reductase system of *Thiosphaera pantotropha*. *Biochem. J.* **309**, 983-992.

Binnerup, S. J., Jensen, K., Revsbech, N. P., Jensen, M. H. & Sørensen, J. (1992). Denitrification, dissimilatory reduction of nitrate to ammonium, and nitrification in a bioturbated estuarine sediment as measured with ^{15}N and microsensor techniques. *Appl. Env. Microbiol.* **58**, 303-313.

Blackmore, R., Roberton, A. M. & Brittain, T. (1986). The purification and some equilibrium properties of the nitrite reductase of the bacterium *Wolinella succinogenes*. *Biochem. J.* **233**, 547-552.

Blasco, F., Iobbi, C., Giordano, G., Chippaux, M. & Bonnefoy, V. (1989). Nitrate reductase of *Escherichia coli*: completion of the nucleotide sequence of the *nar* operon and reassessment of the role of the alpha and beta subunits in iron binding and electron transfer. *Mol. Gen. Genetics* **218**, 249-256.

Blattner, F. R., Plunkett, G., 3rd, Bloch, C. A., Perna, N. T., Burland, V., Riley, M., Collado-Vides, J., Glasner, J. D., Rode, C. K., Mayhew, G. F., Gregor, J., Davis, N. W., Kirkpatrick, H. A., Goeden, M. A., Rose, D. J., Mau, B. & Shao, Y. (1997). The complete genome sequence of *Escherichia coli* K12. *Science* **277**, 1453-1474.

Blundell, T. L. & Johnson, L. N. (1994). Crystallization of proteins. In *Protein Crystallography* 4. Auflage edit. (Blundell, T. L. & Johnson, L. N., eds.), pp. 59-82. Academic Press Inc., San Diego.

Bokranz, M. J., Katz, J., Schröder, I., Roberton, A. M. & Kröger, A. (1983). Energy metabolism and biosynthesis of *Vibrio succinogenes* growing with nitrate or nitrite as terminal electron acceptor. *Arch. Microbiol.* **135**, 36-41.

Boyington, J. C., Gladyshev, V. N., Khangulov, S. V., Stadtman, T. C. & Sun, P. D. (1997). Crystal structure of formate dehydrogenase H - catalysis involving Mo, molybdopterin, selenocysteine, and an Fe_4S_4 cluster. *Science* **275**, 1305-1308.

Brittain, T., Blackmore, R., Greenwood, C. & Thomson, A. J. (1992). Bacterial nitrite-reducing enzymes. *Eur. J. Biochem.* **209**, 793-802.

Brons, H. J. & Zehnder, A. J. B. (1990). Aerobic nitrite reduction in continuous cultures of *Escherichia coli* E4. *Arch. Microbiol.* **153**, 531-536.

Brünger, A. T. (1992). *X-PLOR Version 3.1. A System for Crystallography and NMR*, Yale University Press, New Haven, CT.

Brünger, A. T., Adams, P. D., Clore, G. M., Delano, W. L., Gros, P., Grosse Kunstleve, R. W., Jiang, J. S., Kuszewski, J., Nilges, M., Pannu, N. S., Read, R. J., Rice, L. M., Simonson, T. & Warren, G. L. (1998). Crystallography and NMR system: A new software suite for macromolecular structure determination. *Acta Cryst. D* **54**, 905-921.

Bullock, W. O., Fernandez, J. M. & Short, J. M. (1987). XL1-Blue: A high efficiency plasmid transforming *recA*$^-$ *E. coli* strain with β-galactosidase selection. *Bio-Techniques* **5**, 376.

Carter Jr., C. W. & Carter, C. W. (1979). Protein crystallization using incomplete factorial experiments. *J. Biol. Chem.* **254**, 12219-12223.

Cole, J. A. (1968). Cytochrome c_{552} and nitrite reduction in *Escherichia coli*. *Biochim. Biophys. Acta* **162**, 356-368.

Cole, J. A. (1988). Assimilatory and dissimilatory reduction of nitrate to ammonia. In *The nitrogen and sulphur cycles* (Cole, J. A. & Ferguson, S. J., eds.), pp. 281-329. Society for General Microbiology, Cambridge University Press.

Cole, J. A. (1990). Physiology, biochemistry and genetics of nitrate dissimilation to ammonia. In *Denitrification in soil and sediments* (Revsbech, N. P. & Sørensen, J., eds.), pp. 57-76. Plenum Press, New York.

Cole, J. A. & Brown, C. M. (1980). Nitrite reduction to ammonia by fermentative bacteria: a short circuit in the biological nitrogen cycle. *FEMS Microbiol. Lett.* **7**, 65-72.

Coleman, K. J., Cornish-Bowden, A. & Cole, J. A. (1978). Activation of nitrite reductase from *Escherichia coli* K12 by oxidized nicotinamide-adenine dinucleotide. *Biochem. J.* **175**, 495-499.

Collaborative Computational Project No. 4. (1994). The CCP4 Suite: Programs for protein crystallography. *Acta Cryst. D* **50**, 760-763.

Collins, M. J., Arciero, D. M. & Hooper, A. B. (1993). Optical spectropotentiometric resolution of the hemes of hydroxylamine oxidoreductase. Heme quantitation and pH dependence of E_m. *J. Biol. Chem.* **268**, 14655-14662.

Costa, C., Moura, I., Teixeira, M., LeGall, J. & Moura, J. J. G. (1993). Spectroscopic characterization of a nitrate reductase isolated from *D. desulfuricans* ATCC 27774. *J. Inorg. Biochem.* **51**, 372-378.

Costa, C., Moura, J. J. G., Moura, I., Wang, Y. N. & Huynh, B. H. (1996). Redox properties of cytochrome *c* nitrite reductase from *Desulfovibrio desulfuricans* ATCC 27774. *J. Biol. Chem.* **271**, 23191-23196.

Coutinho, I. B., Turner, D. L., LeGall, J. & Xavier, A. V. (1993). Characterization of the structure and redox behaviour of cytochrome c_3 from *Desulfovibrio baculatus* by ^{1}H-nuclear-magnetic-resonance spectroscopy. *Biochem. J.* **294**, 899-908.

Crane, B. R., Siegel, L. M. & Getzoff, E. D. (1995). Sulfite reductase structure at 1.6 Å - Evolution and catalysis for reduction of inorganic anions. *Science* **270**, 59-67.

Craske, A. & Ferguson, S. J. (1986). The respiratory nitrate reductase from *Paracoccus denitrificans*. Molecular characterisation and kinetic properties. *Eur. J. Biochem.* **158**, 429-436.

Cromer, D. T. & Liberman, D. (1970). Relativistic calculation of anomalous scattering factors for X-rays. *J. Chem. Phys.* **53**, 1891-8.

Crooke, H. & Cole, J. A. (1995). The biogenesis of *c*-type cytochromes in *Escherichia coli* requires a membrane-bound protein, DipZ, with a protein disulphide isomerase-like domain. *Mol. Microbiol.* **15**, 1139-1150.

Czjzek, M., Payan, F., Guerlesquin, F., Bruschi, M. & Haser, R. (1994a). Crystal structure of cytochrome c_3 from *Desulfovibrio desulfuricans* Norway at 1.7 Å resolution. *J. Mol. Biol.* **243**, 653-667.

Czjzek, M., Payan, F. & Haser, R. (1994b). Molecular and structural basis of electron transfer in tetra- and octa-heme cytochromes. *Biochimie* **76**, 546-553.

Darwin, A., Hussain, H., Griffiths, L., Grove, J., Sambongi, Y., Busby, S. & Cole, J. (1993). Regulation and sequence of the structural gene for cytochrome c_{552} from *Escherichia coli*: not a hexahaem but a 50 kDa tetrahaem nitrite reductase. *Mol. Microbiol.* **9**, 1255-1265.

Darwin, C. G. (1914). The theory of X-ray reflexion. *Phil. Mag.* **27**, 315-333.

Davis, D. J., Frame, M. K. & Johnson, D. A. (1988). Resonance Raman spectroscopy indicates a lysine as the sixth iron ligand in cytochrome *f*. *Biochim. Biophys. Acta* **936**, 61-66.

de Vries, W., Niekus, H. G., Boellaard, M. & Stouthamer, A. H. (1980). Growth yields and energy generation by *Campylobacter sputorum* subspecies *bubulus* during growth in continuous culture with different hydrogen acceptors. *Arch. Microbiol.* **124**, 221-227.

de Vries, W., Niekus, H. G., van Berchum, H. & Stouthamer, A. H. (1982). Electron transport-linked proton translocation at nitrite reduction in *Campylobacter sputorum* subspecies *bubulus*. *Arch. Microbiol.* **131**, 132-139.

Deisenhofer, J., Epp, O., Miki, K., Huber, R. & Michel, H. (1984). X-ray structure analysis of a membrane protein complex. Electron density map at 3 Å resolution and a model of the chromophores of the photosynthetic reaction center from *Rhodopseudomonas viridis*. *J. Mol. Biol.* **180**, 385-398.

DeVreese, B., Costa, C., Demol, H., Papaefthymiou, V., Moura, I., Moura, J. J. & Van Beeumen, J. (1997). The primary structure of the split-Soret cytochrome *c* from *Desulfovibrio desulfuricans* ATCC 27774 reveals an unusual type of diheme cytochrome *c*. *Eur. J. Biochem.* **248**, 445-451.

Dias, J. M., Than, M. E., Humm, A., Huber, R., Bourenkov, G. P., Bartunik, H. D., Bursakov, S., Calvete, J., Caldeira, J., Carneiro, C., Moura, J. J. G., Moura, I. & Romão, M. J. (1999). Crystal structure of the first dissimilatory nitrate reductase at 1.9 Å solved by MAD methods. *Structure* **7**, 65-79.

Dolla, A., Arnoux, P., Protasevich, I., Lobachov, V., Brugna, M., Giudici-Orticoni, M. T., Haser, R., Czjzek, M., Makarov, A. & Bruschi, M. (1999). Key role of phenylalanine 20 in cytochrome c_3 structure, stability and function studies. *Biochemistry* **38**, 33-41.

Drenth, J. (1994). *Principles of Protein X-ray Crystallography*, Springer Verlag, Heidelberg.

Duong, F., Eichler, J., Price, A., Leonard, M. R. & Wickner, W. (1997). Biogenesis of the Gram-negative bacterial envelope. *Cell* **91**, 567-573.

Eaves, D. J., Grove, J., Staudenmann, W., James, P., Poole, R. K., White, S. A., Griffiths, I. & Cole, J. A. (1998). Involvement of products of the *nrfEFG* genes in the covalent attachment of haem *c* to a novel cysteine-lysine motif in the cytochrome c_{552} nitrite reductase from *Escherichia coli*. *Mol. Microbiol.* **28**, 205-216.

Edman, P. & Henschen, A. (1975). Sequence determination. In *Protein sequence determination* 2. Auflage edit. (Needleman S.B., ed.), pp. 232-279. Springer-Verlag, Heidelberg.

Eiglmeier, K., Honore, N., Iuchi, S., Lin, E. C. & Cole, S. T. (1989). Molecular genetic analysis of FNR-dependent promoters. *Mol. Microbiol.* **3**, 869-878.

Einsle, O. (1996). Untersuchungen zur Struktur des Tetrahämproteins Nitritreduktase aus *Sulfurospirillum deleyianum*: Bestimmung der Aminosäuresequenz des Enzyms. Diplomarbeit, Universität Konstanz.

Einsle, O., Schumacher, W., Kurun, E., Nath, U. & Kroneck, P. M. H. (1998). Cytochrome *c* nitrite reductase from *Sulfurospirillum deleyianum* and *Wolinella*

succinogenes. Molecular and spectroscopic properties of the multihaem enzyme. In *Biological Electron Transfer Chains: Genetics, Composition and Mode of Operation* (Canters, G. W. & Vijgenboom, E., eds.), pp. 197-208. Kluwer Academic Press.

Engh, R. A. & Huber, R. (1991). Accurate bond and angle parameters for X-ray protein structure refinement. *Acta Cryst. D* **4**, 392-400.

Enoch, H. G. & Lester, R. L. (1974). The role of a novel cytochrome *b*-containing nitrate reductase and quinone in the in vitro reconstruction of formate-nitrate reductase activity of *E. coli*. *Biochem. Biophys. Res. Comm.* **61**, 1234-1241.

Esnouf, R. M. (1997). An extensively modified version of MolScript that includes greatly enhanced coloring capabilities. *J. Mol. Graph.* **15**, 132-134.

Fleischmann, R. D., Adams, M. D., White, O., Clayton, R. A., Kirkness, E. F., Kerlavage, A. R., Bult, C. J., Tomb, J.-F., Dougherty, B. A., Merrick, J. M., McKenney, K., Sutton, G., FitzHugh, W., Fields, C., Gocayne, J. D., Scott, J., Shirley, R., Liu, L. I., Glodek, A., Kelley, J. M., Weidman, J. F., Philips, C. A., Spriggs, T., Hedblorn, E., Cotton, M. D., Utterback, T. R., Hanna, M. C., Nguyen, D. T., Saudek, D. M., Brandon, R. C., Fine, L. D., Fritchman, J. L., Fuhrman, J. L., Geoghagen, N. S. M., Gnehm, C. L., McDonald, L. A., Small, K. V., Fraser, C. M., Smith, H. O. & Venter, J. C. (1995). Whole-genome random sequencing and assembly of *Haemophilus influenzae* Rd. *Science* **269**, 496-512.

Fontana, A., Veronese, F. M. & Boccu, E. (1973). Reaction of sulfenyl halides with cytochrome *c*. A novel method for heme cleavage. *FEBS Lett.* **32**, 135-138.

Fujita, T. (1966). Studies on soluble cytochromes in enterobacteriaceae. I. Detection, purification and properties of cytochrome c_{552} in anaerobically grown cells. *J. Biochem.* **60**, 204-215.

Fujita, T. & Sato, R. (1966). Studies on soluble cytochromes in enterobacteriaceae. IV. Possible involvement of cytochrome c_{552} in nitrite metabolism. *J. Biochem.* **60**, 691-700.

Fülöp, V., Moir, J. W. B., Ferguson, S. J. & Hajdu, J. (1995). The anatomy of a bifunctional enzyme: structural basis for reduction of oxygen to water and synthesis of nitric oxide by cytochrome cd_1. *Cell* **81**, 369-377.

Godden, J. W., Turley, S., Teller, D. C., Adman, E. T., Liu, M. Y., Payne, W. J. & Le Gall, J. (1991). The 2.3 Å X-ray structure of nitrite reductase from *Achromobacter cycloclastes*. *Science* **253**, 438-442.

Goldman, B. S., Beck, D. L., Monika, E. M. & Kranz, R. G. (1998). Transmembrane heme delivery systems. *Proc. Natl. Acad. Sci.* **95**, 5003-5008.

Goldman, B. S. & Kranz, R. G. (1998). Evolution and horizontal transfer of an entire biosynthetic pathway for cytochrome *c* biogenesis. *Mol. Microbiol.* **27**, 871-873.

Green, D. W., Ingram, V. M. & Perutz, M. F. (1954). The structure of hemoglobin. IV. Sign determination by the isomorphous replacement method. *Proc. Roy. Soc. A* **225**, 287-307.

Gudat, J. C., Shing, J. & Wharton, D. C. (1973). Cytochrome oxidase from *Pseudomonas aeruginosa*. I. Purification and some properties. *Biochim. Biophys. Acta* **292**, 376-390.

Guex, N. & Peitsch, M. C. (1996). Swiss-PdbViewer: A fast and easy-to-use PDB viewer for Macintosh and PC. *PDB Quart. Newslett.* **77**, 7-10.

Haladjian, J., Bianco, P., Guerlesquin, F. & Bruschi, M. (1987). Electrochemical study of the electron exchange between cytochrome c_3 and hydrogenase from *Desulfovibrio desulfuricans* Norway. *Biochem. Biophys. Res. Comm.* **147**, 1289-1294.

Hammann, C. (1994). Kristallographische Untersuchungen an zwei Metalloproteinen: Röntgenkristallographische Strukturaufklärung punktspezifischer Mutanten von Azurin aus *Pseudomonas aeruginosa* und Kristallisation der Nitritreduktase aus *Sulfurospirillum deleyianum*. Diplomarbeit, Universität.

Hanahan, D. (1983). Studies on transformation of *E. coli* with plasmids. *J. Mol. Biol.* **166**, 557-568.

Harker, D. (1956). The determination of the phases of the structure factors on non-centrosymmetric crystals by the method of double isomorphous replacement. *Acta Cryst.* **9**, 1-9.

Hendrich, M. P., Logan, M., Andersson, K. K., Arciero, D. M., Lipscomb, J. D. & Hooper, A. B. (1993). The active site of hydroxylamine oxidoreductase from *Nitrosomonas*: evidence for a new metal cluster in enzymes. *J. Am. Chem. Soc.* **116**, 11961-11968.

Hendrickson, W. A., Smith, J. L., Phizackerley, R. P. & Merrit, E. A. (1988). Crystallographic structure analysis of lamprey hemoglobin from anomalous dispersion of synchrotron radiation. *Proteins* **4**, 77-88.

Hernandez, D., Dias, F. M. & Rowe, J. J. (1991). Nitrate transport and its regulation by O_2 in *Pseudomonas aeruginosa*. *Arch. Biochem. Biophys.* **286**, 159-163.

Hernandez, D. & Rowe, J. J. (1988). Oxygen inhibition of nitrate uptake is a general regulatory mechanism in nitrate respiration. *J. Biol. Chem.* **263**, 7937-7939.

Heukeshoven, J. & Dernick, R. (1985). Simplified method for silver staining of proteins in polyacrylamide gels and mechanism of silver staining. *Electrophoresis* **6**, 103-108.

Higuchi, Y., Kusunoki, M., Matsura, M., Yasuoka, N. & Kakudo, M. (1984). Refined structure of cytochrome c_3 at 1.8 Å resolution. *J. Mol. Biol.* **172**, 109-139.

Hille, R. (1996a). The mononuclear molybdenum enzymes. *Chem. Rev.* **96**, 2757-2816.

Hille, R. (1996b). Structure and function of mononuclear molybdenum enzymes. *J. Biol. Inorg. Chem.* **1**, 397-404.

Hoppe, W. (1957). Die Faltmolekülmethode: eine neue Methode zur Bestimmung der Kristallstruktur bei ganz oder teilweise bekannten Molekülstrukturen. *Acta Cryst.* **10**, 750-751.

Huber, R. (1965). Die automatisierte Faltmolekülmethode. *Acta Cryst.* **19**, 353-356.

Hussain, H., Grove, J., Griffiths, L., Busby, S. & Cole, J. (1994). A seven-gene operon essential for formate-dependent nitrite reduction to ammonia by enteric bacteria. *Mol. Microbiol.* **12**, 153-163.

Igarashi, N., Moriyama, H., Fujiwara, T., Fukumori, Y. & Tanaka, N. (1997). The 2.8 Å structure of hydroxylamine oxidoreductase from a nitrifying chemoautotrophic bacterium, *Nitrosomonas europaea*. *Nat. Struct. Biol.* **4**, 276-284.

Innis, M. A., Myambo, K. B., Gelfand, D. H. & Brow, M. A. D. (1988). DNA sequencing with *Thermus aquaticus* DNA polymerase and direct sequencing of polymerase chain reaction-amplified DNA. *Proc. Nat. Acad. Sci. USA* **85**, 9436-9440.

Iverson, T. M., Arciero, D. M., Hsu, B. T., Logan, M. S. P., Hooper, A. B. & Rees, D. C. (1998). Heme packing motifs revealed by the crystal structure of the tetra-heme cytochrome c_{554} from *Nitrosomonas europaea*. *Nat. Struct. Biol.* **5**, 1005-1012.

Jackson, R. H., Cornish-Bowden, A. & Cole, J. A. (1981). Prosthetic groups of the NADH-dependent nitrite reductase from *Escherichia coli* K12. *Biochem. J.* **193**, 861-867.

Jancarik, J. & Kim, S.-H. (1991). Sparse matrix sampling: a screening method for crystallization of proteins. *J. Appl. Cryst.* **24**, 409-411.

Janick, P. A., Rueger, D. C., Krueger, R. J., Barber, M. J. & Siegel, L. M. (1983). Characterization of complexes between *Escherichia coli* sulfite reductase hemoprotein subunit and its substrates sulfite and nitrite. *Biochemistry* **22**, 396-408.

Jayaraman, P. S., Cole, J. A. & Busby, S. J. (1989). Mutational analysis of the nucleotide sequence at the FNR-dependent *nirB* promoter in *Escherichia coli*. *Nucl. Ac. Res.* **17**, 135-145.

Jones, T. A., Zou, J.-Y., Cowan, S. W. & Kjelgaard, M. (1991). Improved methods for building proteins in electron density maps and location of errors in these models. *Acta Cryst.* **A47**, 110-119.

Jørgensen, K. S. (1989). Annual pattern of denitrification and nitrate ammonification in estuarine sediment. *Appl. Env. Microbiol.* **55**, 1841-1847.

Jüngst, A., Wakabayashi, S., Mastubara, H. & Zumft, W. G. (1991). The *nirSTBM* region coding for cytochrome cd_1-dependent nitrite respiration of *Pseudomonas stutzeri* consists of a cluster of mono-, di- and tetraheme proteins. *FEBS Lett.* **279**, 205-209.

Kaije, S. & Anraku, Y. (1986). Purification of a hexaheme cytochrome c_{552} from *Escherichia coli* K12 and its properties as a nitrite reductase. *Eur. J. Biochem.* **154**, 457-463.

Kendrew, J. C., Dickerson, R. E., Strandberg, B. E., Hart, R. G., Davies, D. R., Phillips, D. C. & Shore, V. C. (1960). Structure of myoglobin; a three-dimensional Fourier synthesis at 2 Å resolution. *Nature* **185**, 422-427.

Ketchum, P. A., Denariaz, G., LeGall, J. & Payne, W. J. (1991). Menaquinol-nitrate oxidoreductase of *Bacillus halodenitrificans*. *J. Bacteriol.* **173**, 2498-2505.

Kleywegt, G. J. (1996). Use of non-crystallographic symmetry in protein structure refinement. *Acta Cryst. D* **52**, 842-857.

Klimmek, O., Kröger, A., Steudel, R. & Holdt, G. (1991). Growth of *Wolinella succinogenes* with polysulfide as terminal acceptor of phosphorylative electron transport. *Arch. Microbiol.* **155**, 177-182.

Krafft, T., Bokranz, M., Klimmek, O., Schroeder, I., Fahrenholz, F., Kojro, E. & Kröger, A. (1992). Cloning and nucleotide sequence of the *psrA* gene of *Wolinella succinogenes* polysulphide reductase. *Eur. J. Biochem.* **206**, 503-510.

Krafft, T., Gross, R. & Kröger, A. (1995). The function of *Wolinella succinogenes psr* genes in electron transport with polysulphide as the terminal electron acceptor. *Eur. J. Biochem.* **230**, 601-606.

Kranz, R., Lill, R., Goldman, B., Bonnard, G. & Merchant, S. (1998). Molecular mechanisms of cytochrome *c* biogenesis - three distinct systems. *Mol. Microbiol.* **29**, 383-396.

Kraulis, P. (1991). MOLSCRIPT: a program to produce both detailed and schematic plots of proteins. *J. Appl. Cryst.* **24**, 946-950.

Kroneck, P. M. H., Beuerle, J. & Schumacher, W. (1992). Metal-dependent conversion of inorganic nitrogen and sulfur compounds. In *Metal ions in biological systems, Volume 28* (Sigel H., S. A., ed.), pp. 455-505. Marcel Dekker Inc., New York.

La Fortelle, E. de, Irwin, J. J. & Bricogne, G. (1997). SHARP: A maximum-likelihood heavy-atom parameter refinement and phasing program for the MIR and MAD methods. *Crystallograph. Comp.* **7**, 1-9.

Laemmli, U. K. (1970). Cleavage of structural proteins during the assembly of the head of bacteriophage T4. *Nature* **227**, 680-685.

Lancaster, J. R., Vega, J. M., Kamin, H., Orme-Johnson, N. R., Orme-Johnson, W. H., Krueger, R. J. & Siegel, L. M. (1979). Identification of the iron-sulfur center of spinach ferredoxin-nitrite reductase as a tetranuclear center, and preliminary EPR studies of mechanism. *J. Biol. Chem.* **254**, 1268-1272.

Laskowski, R. A., MacArthur, M. W., Moss, D. S. & Thornton, J. M. (1993). PROCHECK: A program to check the stereochemical quality of protein structures. *J. Appl. Cryst.* **26**, 283-291.

Leys, D., Tsapin, A. S., H., N. K., Meyer, T. E., Cusanovich, M. A. & Van Beuumen, J. J. (1999). Structure and mechanism of the flavocytochrome *c* fumarate reductase of *Shewanella putrefaciens* MR-1. *Nat. Struct. Biol.* **6**, 1113-1117.

Libby, E. & Averill, B. A. (1992). Evidence that the type 2 copper centers are the site of nitrite reduction by *Achromobacter cycloclastes* nitrite reductase. *Biochem. Biophys. Res. Comm.* **187**, 1529-1535.

Liu, M. C., Costa, C., Coutinho, I. B., Moura, J. J., Moura, I., Xavier, A. V. & LeGall, J. (1988). Cytochrome components of nitrate- and sulfate-respiring *Desulfovibrio desulfuricans* ATCC 27774. *J. Bacteriol.* **170**, 5545-5551.

Liu, M. C. & Peck, H. D. J. (1981). The isolation of a hexaheme cytochrome from *Desulfovibrio desulfuricans* and its identification as a new type of nitrite reductase. *J. Biol. Chem.* **256**, 13159-13164.

Liu, M.-C., Liu, M.-Y., Payne, W. J., Peck Jr., H. D. & LeGall, J. (1983). *Wolinella succinogenes* nitrite reductase: purification and properties. *FEMS Microbiol. Lett.* **19**, 201-206.

Lorenzen, J. P., Kröger, A. & Unden, G. (1993). Regulation of anaerobic respiratory pathways in *Wolinella succinogenes* by the presence of electron acceptors. *Arch. Microbiol.* **159**, 477-483.

Louro, R. O., Catarino, T., Legall, J. & Xavier, A. V. (1997). Redox-Bohr effect in electron/proton energy transduction - Cytochrome c_3 coupled to hydrogenase works as a proton thruster in *Desulfovibrio vulgaris*. *J. Biol. Inorg. Chem.* **2**, 488-491.

Louro, R. O., Pacheco, I., Turner, D. L., LeGall, J. & Xavier, A. V. (1996). Structural and functional characterization of cytochrome c_3 from *D. desulfuricans* ATCC 27774 by ^{1}H-NMR. *FEBS Lett.* **390**, 59-62.

Martinez, S. E., Huang, D., Szczepaniak, A., Cramer, W. A. & Smith, J. L. (1994). Crystal structure of chloroplast cytochrome *f* reveals a novel cytochrome fold and unexpected heme ligation. *Structure* **2**, 95-105.

Massa, W. (1994). *Kristallstrukturbestimmung*, Teubner Studienbücher: Chemie, Stuttgart.

Matias, P. M., Coelho, R., Pereira, I. A. C., Coelho, A. V., Thompson, A. W., Sieker, L. C., Le Gall, J. & Carrondo, M. A. (1999a). The primary and three-dimensional structures of a nine-haem cytochrome *c* from *Desulfovibrio desulfuricans* ATCC 27774 reveal a new member of the Hmc family. *Structure* **7**, 119-130.

Matias, P. M., Frazão, C., Morais, J., Coll, M. & Carrondo, M. A. (1993). Structure analysis of cytochrome c_3 from *Desulfovibrio vulgaris* Hildenborough at 1.9 Å resolution. *J. Mol. Biol.* **234**, 680-699.

Matias, P. M., Morais, J., Coelho, A. V., Meijers, R., Gonzalez, A., Thompson, A. W., Sieker, L., Legall, J. & Carrondo, M. A. (1997). A preliminary analysis of the three-dimensional structure of dimeric di-haem split-Soret cytochrome *c* from *Desulfovibrio desulfuricans* ATCC 27774 at 2.5 Å resolution using the MAD phasing

method - a novel cytochrome fold with a stacked-haem arrangement. *J. Biol. Inorg. Chem*. **2**, 507-514.

Matias, P. M., Morais, J., Coelho, R., Carrondo, M. A., Wilson, K., Dauter, Z. & Sieker, L. (1996). Cytochrome c_3 from *Desulfovibrio gigas* - Crystal structure at 1.8 Å resolution and evidence for a specific calcium-binding site. *Prot. Sci.* **5**, 1342-1354.

Matias, P. M., Saraiva, L. M., Soares, C. M., Coelho, A. V., LeGall, J. & Carrondo, M. A. (1999b). Nine-haem cytochrome *c* from *Desulfovibrio desulfuricans* ATCC 27774: primary sequence determination, crystallographic refinement at 1.8 Å and modelling studies of its interaction with the tetrahaem cytochrome c_3. *J. Biol. Inorg. Chem*. **4**, 478-494.

Matthews, B. W. (1968). Solvent content of protein crystals. *J. Mol. Biol.* **33**, 491-497.

McPherson, A. (1982). *Preparation and analysis of protein crystals*, Wiley & Sons, New York.

McRee, D. E. (1993). *Practical Protein Crystallography*, Academic Press Inc., San Diego.

Meininghaus, M. (1996). Kristallisation zweier Nitritreduktasen: Cytochrom *c* Nitritreduktase aus *Sulfurospirillum deleyianum* und Cytochrom cd_1 Nitritreduktase aus *Thiobacillus denitrificans*. Diplomarbeit, Universität.

Méjean, V., Iobbi-Nivol, C., Lepelletier, M., Giordano, G., Chippaux, M. & Pascal, M. C. (1994). TMAO anaerobic respiration in *Escherichia coli*: involvement of the *tor* operon. *Mol. Microbiol.* **11**, 1169-1179.

Merritt, E. A. & Bacon, D. J. (1997). Raster3D: Photorealistic Molecular Graphics. *Meth. Enzymol.* **277**, 505-524.

Meyer, T. E. & Kamen, M. D. (1982). New perspectives on *c*-type cytochromes. *Adv. Prot. Chem*. **35**, 105-212.

Moir, J. W., Baratta, D., Richardson, D. J. & Ferguson, S. J. (1993). The purification of a cd_1-type nitrite reductase from, and the absence of a copper-type nitrite reductase from, the aerobic denitrifier *Thiosphaera pantotropha*; the role of pseudoazurin as an electron donor. *Eur. J. Biochem*. **212**, 377-385.

Monika, E. M., Goldman, B. S., Beckman, D. L. & Kranz, R. G. (1997). A thioreduction pathway tethered to the membrane for periplasmic cytochromes *c* biogenesis; *in vitro* and *in vivo* studies. *J. Mol. Biol.* **272**, 679-692.

Morais, J., Palma, P. N., Frazão, C., Caldeira, J., LeGall, J., Moura, I., Moura, J. J. G. & Carrondo, M. A. (1995). Structure of tetraheme cytochrome c_3 from *Desulfovibrio desulfuricans* ATCC 27774: X-ray diffraction and electron paramagnetic resonance studies. *Biochemistry* **34**, 12830-12841.

Murillo, F. M., Gugliuzza, T., Senko, J., Basu, P. & Stolz, J. F. (1999). A heme-*c*-containing enzyme complex that exhibits nitrate and nitrite reductase activity from the dissimilatory iron-reducing bacterium *Geobacter metallireducens*. *Arch. Microbiol.* **172**, 313-320.

Murphy, M. E., Turley, S. & Adman, E. T. (1997). Structure of nitrite bound to copper-containing nitrite reductase from *Alcaligenes faecalis*. Mechanistic implications. *J. Biol. Chem*. **272**, 28455-28460.

Murphy, M. J. & Siegel, L. M. (1973). Siroheme and sirohydrochlorin. The basis for a new type of porphyrin-related prosthetic group common to both assimilatory and dissimilatory sulfite reductases. *J. Biol. Chem*. **248**, 6911-6919.

Mus-Veteau, I., Dolla, A., Guerlesquin, F., Payan, F., Czjzek, M., Haser, R., Bianco, P., Haladjian, J., Rapp-Giles, B. J. & Wall, J. D. (1992). Site-directed mutagene-

sis of tetraheme cytochrome c_3. Modification of oxido-reduction potentials after heme axial ligand replacement. *J. Biol. Chem.* **267**, 16851-16858.

Navaza, J. (1994). AMoRe: an Automated Package for Molecular Replacement. *Acta Cryst. A* **50**, 157-163.

Nicholls, A., Bharadwaj, R. & Honig, B. (1993). GRASP - graphical representation and analysis of surface properties. *Biophys. J.* **64**, A166.

Nicholson, D. W. & Neupert, W. (1989). Import of cytochrome *c* into mitochondria: Reduction of heme, mediated by NADH and flavin nucleotides, is obligatory for its covalent linkage to apocytochrome *c*. *Proc. Natl. Acad. Sci.* **86**, 4340-4344.

Nishio, T., Koike, I. & Hattori, A. (1982). Denitrification, nitrate reduction and oxygen consumption in coastal and estuarine sediments. *Appl. Env. Microbiol.* **43**, 648-653.

Nivière, V., Hatchikian, E. C., Bianco, P. & Haladjian, J. (1988). Kinetic studies of electron transfer between hydrogenase and cytochrome c_3 from *Desulfovibrio gigas* electrochemical properties of cytochrome c_3. *Biochim. Biophys. Acta* **935**, 34-40.

Nørager, S., Legrand, P., Pieulle, L., Hatchikian, C. & Roth, M. (1999). Crystal structure of the oxidised and reduced acidic cytochrome c_3 from *Desulfovibrio africanus*. *J. Mol. Biol.* **290**, 881-902.

Otwinowski, Z. & Minor, W. (1996). Processing of X-ray diffraction data collected in oscillation mode. *Meth. Enzymol.* **276**, 307-326.

Page, L., Griffiths, L. & Cole, J. A. (1990). Different physiological roles of two independent pathways for nitrite reduction to ammonia by enteric bacteria. *Arch. Microbiol.* **154**, 349-354.

Park, J. S., Ohmura, T., Kano, K., Sagara, T., Niki, K., Kyogoku, Y. & Akutsu, H. (1996). Regulation of the redox order of four hemes by pH in cytochrome c_3 from *D. vulgaris* Myazaki F. *Biochim. Biophys. Acta* **1293**, 45-54.

Parr, S. R., Barber, D., Greenwood, C. & Brunori, M. (1977). The electron-transfer reaction between azurin and the cytochrome *c* oxidase from *Pseudomonas aeruginosa*. *Biochem. J.* **167**, 447-455.

Paster, B. J., Dewhirst, F. E., Olsen, I. & Fraser, G. J. (1994). Phylogeny of *Bacteroides, Prevotella,* and *Porphyromonas* spp. and related bacteria. *J. Bacteriol.* **176**, 725-732.

Patterson, A. L. (1934). A Fourier series method for the determination of the components of interatomic distances in crystals. *Phys. Rev.* **46**, 372-376.

Perutz, M. F., Rossmann, M. G., Cullis, A. F., Muirhead, H., Will, G. & North, A. C. T. (1960). Structure of haemoglobin; a three-dimensional Fourier synthesis at 5.5 Å resolution, obtained by X-ray analysis. *Nature* **185**, 416-422.

Picarra-Pereira, M. A., Turner, D., LeGall, J. & Xavier, A. V. (1993). Structural studies on *Desulfovibrio gigas* cytochrome c_3 by two-dimensional ^{1}H-nuclear-magnetic-resonance spectroscopy. *Biochem. J.* **294**, 904-915.

Pierrot, M., Haser, R., Frey, M., Payan, F. & Astier, J. P. (1982). Crystal structure and electron transfer properties of cytochrome c_3. *J. Biol. Chem.* **257**, 14341-14348.

Pieulle, L., Haladjian, J., Bonicel, J. & Hatchikian, E. C. (1996). Biochemical studies of the *c*-type cytochromes of the sulfate reducer *Desulfovibrio africanus*. Characterization of two tetraheme cytochromes c_3 with different specificity. *Biochim. Biophys. Acta* **1273**, 51-61.

Pohlschröder, M., Prinz, W. A., Hartmann, E. & Beckwith, J. (1997). Protein translocation in the three domains of life: variations on a theme. *Cell* **91**, 563-566.

Pope, N. R. & Cole, J. A. (1982). Generation of a membrane potential by one of two independent pathways for nitrite reduction by *Escherichia coli*. *J. Gen. Microbiol.* **128**, 219-222.

Postgate, J. R. (1954). Presence of cytochrome in an obligate anaerobe. *Biochem. J.* **56**, 10-14.

Prakhash, O. & Sadana, J. C. (1972). Purification, characterization and properties of nitrite reductase of *Achromobacter fischeri*. *Arch. Biochem. Biophys.* **148**, 614-632.

Rehr, B. & Klemme, J. H. (1986). Metabolic role and properties of nitrite reductase of nitrate-ammonifying marine *Vibrio* species. *FEMS Microbiol. Lett.* **35**, 325-328.

Richardson, D. J., McEwan, A. G., Page, M. D., Jackson, J. B. & Ferguson, S. J. (1990). The identification of cytochromes involved in the transfer of electrons to the periplasmic nitrate reductase of *Rhodobacter capsulatus* and resolution of a soluble nitrate reductase - cytochrome c_{552} redox complex. *Eur. J. Biochem.* **194**, 263-270.

Rodgers, D. W. (1994). Cryocrystallography. *Structure* **2**, 1135-1140.

Roldán, M. D., Sears, H. J., Cheesman, M. R., Ferguson, S. J., Thomson, A. J., Berks, B. C. & Richardson, D. J. (1998). Spectroscopic characterization of a novel multiheme *c*-type cytochrome widely implicated in bacterial electron transport. *J. Biol. Chem.* **273**, 28785-28790.

Rossmann, M. G. & Blow, D. M. (1962). The detection of subunits within the crystallographic asymmetric unit. *Acta Cryst.* **15**, 24-31.

Rost, B. (1996). PHD: predicting one-dimensional protein structure by profile-based neural networks. *Meth. Enzymol.* **266**, 525-539.

Rost, B. & Sander, C. (1993). Prediction of protein structure at better than 70% accuracy. *J. Mol. Biol.* **232**, 584-599.

Rost, B. & Sander, C. (1994). Combining evolutionary information and neural networks to predict protein secondary structure. *Proteins* **19**, 55-77.

Saiki, R. K., Gelfand, D. H., Stoffel, S., Scharf, S. J., Higuchi, R., Horn, G. T., Mullis, K. B. & Erlich, H. A. (1988). Primer-directed enzymatic amplification of DNA with a thermostable DNA polymerase. *Science* **233**, 1076-1078.

Sambrook, J., Fritsch, E. F. & Maniatis, T. (1989). *Molecular Cloning: A laboratory manual*, Cold Spring Harbour Laboratory Press, New York, USA.

Saraiva, L. M., Salgueiro, C. A., LeGall, J., van Dongen, W. M. A. M. & Xavier, A. V. (1996). Site-directed mutagenesis of a phenylalanine residue strictly conserved in cytochromes *c*3. *J. Biol. Inorg. Chem.* **1**, 542-550.

Schiött, T., von Wachenfeldt, C. & Hederstedt, L. (1997). Identification and characterization of the *ccdA* gene, required for cytochrome *c* synthesis in *Bacillus subtilis*. *J. Bacteriol.* **179**, 1962-1973.

Schlegel, H. G. (1992). *Allgemeine Mikrobiologie*. 7th edit, Thieme Verlag, Stuttgart.

Schumacher, W. (1993). Dissimilatorische Reduktion von Nitrat zu Ammoniak. Dissertation, Universität Konstanz.

Schumacher, W., Hole, U. & Kroneck, P. M. H. (1994). Ammonia-forming cytochrome *c* nitrite reductase from *Sulfurospirillum deleyianum* is a tetraheme protein: new aspects of the molecular composition and spectroscopic properties. *Biochem. Biophys. Res. Comm.* **205**, 911-916.

Schumacher, W. & Kroneck, P. M. H. (1991). Dissimilatory hexaheme *c* nitrite reductase of "*Spirillum*" strain 5175: purification and properties. *Arch. Microbiol.* **156**, 70-74.

Schumacher, W. & Kroneck, P. M. H. (1992). Anaerobic energy metabolism of the sulfur-reducing bacterium "Spirillum" 5175 during dissimilatory nitrate reduction to ammonia. *Arch. Microbiol.* **157**, 464-470.

Schumacher, W., Kroneck, P. M. H. & Pfennig, N. (1992). Comparative systematic study of "Spirillum" 5175, *Campylobacter* and *Wolinella* species. Description of "Spirillum" 5175 as *Sulfurospirillum deleyianum*gen. nov., spec. nov. *Arch. Microbiol.* **158**, 287-293.

Schumacher, W., Neese, F., Hole, U. & Kroneck, P. M. H. (1997). Cytochrome *c* nitrite reductase and nitrous oxide reductase: two metallo enzymes of the nitrogen cycle with novel metal sites. In *Transition Metals in Microbial Metabolism* (Winkelmann, G. & Carrano, C. J., eds.), pp. 329-356. Harwood Academic Publishers.

Seitz, H. J. & Cypionka, H. (1986). Chemolithotrophic growth of *Desulfovibrio desulfuricans* with hydrogen coupled to ammonification of nitrate or nitrite. *Arch. Microbiol.* **146**, 63-67.

Shaw, A. L., Hanson, G. R. & McEwan, A. G. (1996). Cloning and sequence analysis of the dimethylsulfoxide reductase structural gene from *Rhodobacter capsulatus*. *Biochim. Biophys. Acta* **1276**, 176-180.

Shaw, D., Rice, D. & Guest, J. (1983). Homology between CAP and FNR, a rgulator of anaerobic respiration in *Escherichia coli*. *J. Mol. Biol.* **166**, 241-247.

Sias, S. R. & Ingraham, J. L. (1979). Isolation and analysis of mutants of *Pseudomonas aeruginosa* unable to assimilate nitrate. *Arch. Microbiol.* **122**, 263-270.

Siddiqui, R. A., Warnecke-Eberz, U., Hengsberger, A., Schneider, B., Kostka, S. & Friedrich, B. (1993). Structure and function of a periplasmic nitrate reductase in *Alcaligenes eutrophus* H16. *J. Bacteriol.* **175**, 5867-5876.

Siegel, L. M., Rueger, D. C., Barber, M. J., Krueger, R. J., Orme-Johnson, N. R. & Orme-Johnson, W. H. (1982). *Escherichia coli* sulfite reductase hemoprotein subunit. Prosthetic groups, catalytic parameters, and ligand complexes. *J. Biol. Chem.* **257**, 6343-6350.

Silvestrini, M. C., Tordi, M. G., Musci, G. & Brunori, M. (1990). The reaction of *Pseudomonas* nitrite reductase and nitrite. A stopped-flow and EPR study. *J. Biol. Chem.* **265**, 11783-11787.

Simon, J., Gross, R., Einsle, O., Kroneck, P. M. H., Kröger, A. & Klimmek, O. (2000). A NapC/NirT-type cytochrome *c* (NrfH) is the mediator between the quinone pool and the cytochrome *c* nitrite reductase of *Wolinella succinogenes*. *Mol. Microbiol.* **35**, 686-696.

Simon, J., Gross, R., Klimmek, O., Ringel, M. & Kröger, A. (1998). A periplasmic flavoprotein in *Wolinella succinogenes* that resembles the fumarate reductase of *Shewanella putrefaciens*. *Arch. Microbiol.* **169**, 424-433.

Smith, P. K., Krohn, R. I., Hermanson, G. T., Mallia, A. K., Gartner, F. H., Provenzano, M. D., Fujimoto, E. K., Goeke, N. M., Olson, B. J. & Klenk, D. C. (1985). Measurement of protein using bicinchoninic acid. *Analyt. Biochem.* **150**, 76-85.

Spiro, S. & Guest, J. R. (1987). Regulation and over-expression of the *fnr* gene of *Escherichia coli*. *J. Gen. Microbiol.* **133**, 3279-3288.

Spiro, S. & Guest, J. R. (1990). FNR and its role in oxygen-regulated gene expression in *Escherichia coli*. *FEMS Microbiol. Rev.* **6**, 399-428.

Stach, P., Einsle, O., Schumacher, W., Kurun, E. & Kroneck, P. M. H. (2000). Bacterial cytochrome *c* nitrite reductase: new structural and functional aspects. *J. Inorg. Biochem.* **in press**.

Steenkamp, D. J. & Peck Jr., H. D. (1980). The association of hydrogenase and dithionite reductase activities with the nitrite reductase of *Desulfovibrio desulfuricans*. *Biochem. Biophys. Res. Comm.* **94**, 41-48.

Steenkamp, D. J. & Peck Jr., H. D. (1981). Proton translocation associated with nitrite respiration in *Desulfovibrio desulfuricans*. *J. Biol. Chem.* **256**, 5450-5458.

Steuber, J. (1996). Molecular and kinetic properties of desulfoviridin, the dissimilatory ferrocytochrome c_3:sulfie oxidoreductase from *Desulfovibrio desulfuricans* Essex 6. Dissertation, Universität.

Steuber, J., Cypionka, H. & Kroneck, P. M. H. (1994). Mechanism of dissimilatory sulfite reduction by *Desulfovibrio desulfuricans*: purification of a membrane-bound sulfite reductase and coupling with cytochrome c_3 and hydrogenase. *Arch. Microbiol.* **162**, 255-260.

Sun, G., Sharkova, E., Chesnut, R., Birkey, S., Duggan, M. F., Sorokin, A., Pujic, P., Ehrlich, S. D. & Hulett, F. M. (1996). Regulators of aerobic and anaerobic respiration in *Bacillus subtilis*. *J. Bacteriol.* **178**, 1374-1385.

Taylor, P., Pealing, S. L., Reid, G. A., Chapman, S. K. & Walkinshaw, M. D. (1999). Structural and mechanistic mapping of a unique fumarate reductase. *Nat. Struct. Biol.* **6**, 1108-1112.

Thauer, R. K., Jungermann, K. & Decker, K. (1977). Energy conservation in chemotrophic anaerobic bacteria. *Bacteriol. Rev.* **41**, 100-180.

Thöny-Meyer, L. (1997). Biogenesis of respiratory cytochromes in bacteria. *Microbiol. Mol. Biol. Rev.* **61**, 337 ff.

Tiedje, J. M. (1988). Ecology of denitrification and dissimilatory nitrate reduction to ammonia. In *Biology of anaerobic microorganisms* (Zehnder, A. J. B., ed.), pp. 179-244. John Wiley & Sons Inc., New York.

Tong, L. & Rossman, M. G. (1990). The locked rotation function. *Acta Cryst. A* **46**, 783-792.

Turner, D. L., Salguiero, C. A., Catarino, T., LeGall, J. & Xavier, A. V. (1996). NMR studies of cooperativity in the tetraheme cytochrome c_3 from *Desulfovibrio vulgaris*. *European Journal of Biochemistry* **241**, 723-731.

Tyson, K. L., Bell, A. I., Cole, J. A. & Busby, S. J. (1993). Definition of nitrite and nitrate response elements at the anaerobically inducible Escherichia coli *nirB* promoter: interactions between FNR and NarL. *Mol. Microbiol.* **7**, 151-157.

Ubbink, M., Campos, A. P., Teixeira, M., Hunt, N. I., Hill, H. A. & Canters, G. W. (1994). Characterization of mutant Met100Lys of cytochrome c_{550} from *Thiobacillus versutus* with lysine-histidine heme ligation. *Biochemistry* **33**, 10051-10059.

van't Riet, J., Stouthamer, A. H. & Planta, R. J. (1968). Regulation of nitrate assimilation and nitrate respiration in *Aerobacter aerogenes*. *J. Bacteriol.* **23**, 122-134.

Watson, J. D. & Crick, F. H. (1953). Molecular structure of nucleic acids. A structure for deoxyribose nucleic acid. *Nature* **171**, 737-740.

Widdel, F. (1986). Growth of methanogenic bacteria in pure culture with 2-propanol and other alcohols as hydrogen donor. *Appl. Env. Microbiol.* **51**, 1056-1062.

Williams, P. A., Fülöp, V., Garman, E. F., Saunders, N. F. W., Ferguson, S. J. & Hajdu, J. (1997). Haem-ligand switching during catalysis in crystals of a nitrogen-cycle enzyme. *Nature* **389**, 406-412.

Williams, R. J. P. (1990). Bioinorganic chemistry: Its conceptual evolution. *Coord. Chem. Rev.* **100**, 573-610.

Wimpenny, J. W. T. & Cole, J. A. (1967). The regulation of metabolism in facultative bacteria. III. The effect of nitrate. *Biochim. Biophys. Acta* **148**, 233-242.

Woese, C. R. (1987). Bacterial evolution. *Microbiol. Rev.* **51**, 221-271.

Xie, Z. & Merchant, S. (1996). The plastid-encoded *ccsA* gene is required for heme attachment to chloroplast *c*-type cytochromes. *J. Biol. Chem.* **271**, 4632-4639.

Yamanaka, T., Kijimoto, S. & Okunuki, K. (1963). Biological significance of *Pseudomonas* cytochrome oxidase in *Pseudomonas aeruginosa*. *J. Biochem.* **53**, 416-421.

Yamanaka, T. & Okunuki, K. (1963). Crystalline *Pseudomonas* cytochrome oxidase. *Biochim. Biophys. Acta* **67**, 379-393.

Zarowny, D. P. & Sanwal, D. B. (1963). Characterization of an NADH specific NO_2^- reductase from *E. coli* K12. *Can. J. Microbiol.* **9**, 531-539.

Zumft, W. G. (1997). Cell biology and molecular basis of denitrification. *Microbiol. Mol. Biol. Rev.* **61**, 533-546.

10 *Curriculum vitae* and List of Publications

Personal Data

Name:	Oliver Florian Einsle
born:	8. 11. 1970 in Konstanz

Education

1996 – 1999	Ph.D. studies at the MPI für Biochemie, Martinsried.
1996	Diploma Thesis "*Untersuchungen zur Struktur des Tetrahämproteins Nitritreduktase aus Sulfurospirillum deleyianum: Bestimmung der Aminosäuresequenz des Enzyms*" at the MPI für Biochemie, Martinsried.
1991 – 1996	Studies of Biology at Universität Konstanz
1990 – 1991	Alternative service at the *Haus am Briel* home for mentally challenged people, Konstanz.
1990	Abitur, Alexander-von-Humboldt-Gymnasium, Konstanz.

Courses and Working Experience

1997 European Science Foundation Workshop on Molecular Recognition in Metalloproteins, Sevilla, Spain.

1998 EU-ESF Advanced Course "Chemistry of Metals in Biological Systems", Louvain-la-Neuve, Belgium.

1999 TMR Summer School "Structure and Function of Metalloproteins", Oeiras, Portugal.

Conference Presentations

1996 **Nath, U., Kurun, E., Einsle, O., Schumacher, W. & Kroneck, P. M. H.**; Biochemical and spectroscopic studies on the soluble tetraheme cytochrome *c* nitrite reductase; 3rd European Conference on Bioinorganic Chemistry (EUROBIC 3), Noordwijkerhout, The Netherlands.

1998 **Einsle, O., Foerster, S., Mann, K.-H., Fritz, G., Messerschmidt, A. & Kroneck, P. M. H.**; The crystal structure of cytochrome c_3 from *Desulfovibrio desulfuricans* strain Essex 6 at 1.95 Å resolution; DFG-Symposium, Bosen, Germany.

1998 **Einsle, O., Messerschmidt, A. & Kroneck, P. M. H.**; Cloning, sequencing and preliminary crystallization results of cytochrome *c* nitrite reductase from *Sulfurospirillum deleyianum*; VAAM-Frühjahrstagung, Frankfurt, Germany.

1998 **Einsle, O. & Messerschmidt, A.**; Iron and copper proteins in electron transport: Crystal structure analysis of plantacyanin and cytochrome c_3; EU-ESF Advanced Course "Chemistry of Metals in Biological Systems", Louvain-la-Neuve, Belgium.

1998 **Einsle, O., Messerschmidt, A., Huber R. & Kroneck, P. M. H.**; The crystal structure of cytochrome *c* nitrite reductase from *Sulfurospirillum deleyianum* solved by multiple wavelength anomalous dispersion methods; TMR Summer School "Structure and Function of Metalloproteins", Oeiras, Portugal

1999 **Einsle, O., Stach, P., Messerschmidt, A., Huber R. & Kroneck, P. M. H.**; The 1.9 Å crystal structure of dissimilatory cytochrome *c* nitrite reductase from *Sulfurospirillum deleyianum* solved by multiple wavelength anomalous dispersion methods; VAAM-Frühjahrstagung, Göttingen, Germany.

1999 **Einsle, O., Stach, P., Messerschmidt, A., Huber R. & Kroneck, P. M. H.**; The structure of cytochrome *c* nitrite reductase from *Sulfurospirillum deleyianum*: Nature's machinery for the six-electron reduction of nitrite to ammonia; Symposium of the Volkswagen Foundation on Electron Transfer in Biological Systems, Konstanz, Germany.

1999 **Einsle, O.**; The X-ray structure of pentaheme cytochrome *c* nitrite reductase from *Sulfurospirillum deleyianum*; European Research Conference on Chemistry of Metals in Biological Systems, Tomar, Portugal.

1999 **Einsle, O., Messerschmidt, A., Stach, P., Huber R. & Kroneck, P. M. H.**; Crystal structure of cytochrome c nitrite reductase from *Sulfurospirillum deleyianum*; 9th International Conference on Bioinorganic Chemistry (ICBIC 9), Minneapolis, USA.

Publications

Einsle, O. (1996). Untersuchungen zur Struktur des Tetrahämproteins Nitritreduktase aus *Sulfurospirillum deleyianum*: Bestimmung der Aminosäuresequenz des Enzyms. Diplomarbeit, Universität Konstanz.

Einsle, O., Schumacher, W., Kurun, E., Nath, U. & Kroneck, P. M. H. (1998). Cytochrome *c* nitrite reductase from *Sulfurospirillum deleyianum* and *Wolinella succinogenes*. Molecular and spectroscopic properties of the multihaem enzyme. In *Biological Electron Transfer Chains: Genetics, Composition and Mode of Operation* (Canters, G. W. & Vijgenboom, E., eds.), pp. 197-208. Kluwer Academic Press.

Einsle, O., Messerschmidt, A., Stach, P., Bourenkov, G. P., Bartunik, H. D., Huber, R. & Kroneck, P. M. H. (1999) Structure of cytochrome *c* nitrite reductase. *Nature* **400**, 476-480.

Einsle, O., Messerschmidt, A., Stach, P., Huber, R. & Kroneck, P. M. H. (1999) Crystal structure of cytochrome *c* nitrite reductase from *Sulfurospirillum deleyianum*. *J. Inorg. Biochem*. **74**, 121.

Simon, J., Gross, R., Einsle, O., Kroneck, P. M. H., Kröger, A. & Klimmek, O. (2000) A NapC/NirT-type cytochrome *c* (NrfH) is the mediator between the quinone pool and the cytochrome *c* nitrite reductase of *Wolinella succinogenes*. *Mol. Microbiol.* **35**, 686-696.

Stach, P., Einsle, O., Schumacher, W., Kurun, E. & Kroneck, P. M. H. (2000). Bacterial cytochrome *c* nitrite reductase: new structural and functional aspects. *J. Inorg. Biochem*. **in press**.

Fritz, G., Steuber, J., Büchert, T., Foerster, S., Einsle, O., Behrens, A. & Kroneck, P. M. H. (2000) Metalloproteins in sulfate-reducing bacteria. *FEMS Microbiol. Rev.* **in press**.

Einsle, O., Mehrabyan, Z., Nalbandyan, R. & Messerschmidt, A. (2000) Crystal structure of plantacyanin, a basic blue cupredoxin from spinach. **submitted**.

Einsle, O., Foerster S., Mann, K.-H., Fritz, G., Messerschmidt, A. & Kroneck, P. M. H. (2000) Spectroscopic investigation, reactivity and structure determination of the tetraheme cytochrome c_3 from *Desulfovibrio desulfuricans* Essex 6. **in preparation**.

Einsle, O., Stach, P., Messerschmidt, A., Huber, R. & Kroneck, P. M. H. (2000) Crystal structure of cytochrome *c* nitrite reductase from *Wolinella succinogenes* at 1.6 Å resolution. **in preparation**.